Cochlear Neuropathy: Detection using envelope following responses and Impacts on central auditory coding

by

Luke A. Shaheen

B.S. Electrical Engineering
Northeastern University, 2009

SUBMITTED TO
THE HARVARD-MIT DIVISION OF HEALTH SCIENCES AND TECHNOLOGY
IN PARTIAL FULFILLMENT OF THE REQUIREMENTS FOR THE DEGREE OF

DOCTOR OF PHILOSOPHY
IN SPEECH AND HEARING BIOSCIENCE AND TECHNOLOGY
AT THE
MASSACHUSETTS INSTITUTE OF TECHNOLOGY

SEPTEMBER 2016

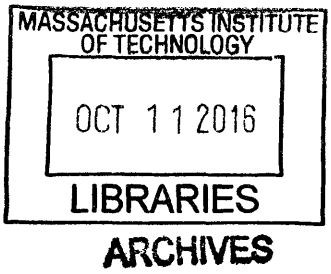

Signature of Author: Signature redacted

Luke A. Shaheen
Harvard-MIT Division of Health Sciences and Technology
July 1, 2016

Certified by: Signature redacted

M. Charles Liberman, Ph.D.
Thesis Supervisor
Director, Eaton-Peabody Laboratory, Massachusetts Eye & Ear Infirmary
Harold F. Schuknecht Professor of Otology and Laryngology, Harvard Medical School

Accepted by: Signature redacted

Emery Brown, MD, PhD
Director, Harvard-MIT Division of Health Sciences and Technology
Professor of Computational Neuroscience and Health Sciences and Technology

Cochlear Neuropathy: Detection using envelope following responses and Impacts on central auditory coding

by

Luke A. Shaheen

Submitted to the Harvard-MIT Division of Health Sciences and Technology
on July 1, 2016 in partial fulfillment of the requirements
for the degree of Doctor of Philosophy in
Speech and Hearing Bioscience and Technology

Abstract

Nearly all information about the acoustic environment is conveyed to the brain by auditory nerve (AN) fibers. While essential for hearing, these fibers may also be the most vulnerable link in the auditory pathway: moderate noise exposure can cause loss of AN fibers without causing hair cell damage or permanent threshold shift. This neuropathy is undetectable by standard clinical examination, but post-mortem evidence suggests that it is widespread in humans. Its impact on suprathreshold hearing ability is likely profound, but is not well understood.

An essential tool for evaluating the impact of neuropathy is a non-invasive test useable in humans. Since noise-induced neuropathy is selective for high-threshold AN fibers, where phase locking to envelopes is particularly strong, we hypothesized that the envelope following response (EFR) might be a more sensitive measure of neuropathy than the more traditional auditory brainstem response (ABR). We compared ABRs and EFRs in mice following a neuropathic noise exposure. Changes to EFRs were more robust: the variance was smaller, thus inter-group differences were clearer.

Neuropathy may be the root cause of a number of deficits that can occur in listeners with normal audiograms, such as speech discrimination in noise and ability to use envelope cues. We searched for neural correlates of these deficits in the mouse auditory midbrain following exposure. Consistent with reductions in EFRs, synchronization to envelopes was impaired. Neural detectability of tones in background noise was impaired, but only for cases when noise level changed every 600 milliseconds. When noise level changed every minute, responses were equal to those of unexposed mice, implicating changes to adaptation. In quiet, tone-evoked rate-level functions were steeper, indicating that neuropathy may initiate a compensatory response in the central auditory system leading to the genesis of hyperacusis. In sum, we found compensatory effects on coding in the midbrain beyond the simple direct effects expected by peripheral neuropathy.

Thesis supervisor: M. Charles Liberman, Ph.D.

Title: Harold F. Schuknecht Professor of Otology and Laryngology, Harvard Medical School

Table of Contents

Figure Reference

General Introduction

The mammalian auditory system interprets the acoustic environment with remarkable sensitivity and range. From the quietest sounds to the loudest, hearing extends over a dynamic range of 120 dB (Viemeister, 1988). Humans maintain fine discrimination of level differences (~1 dB) across this range, and can discriminate frequency differences as low as .1% at moderate and high intensities (Wier et al., 1977; Viemeister, 1983; Florentine et al., 1987). Furthermore, the system is superbly impervious to noise; young humans can pick out and discriminate context-free speech streams at a signal to noise ratio of 0 dB relative multi-talker babble (Plomp and Mimpen, 1979; Dubno et al., 1984), a feat that, despite decades of work, has yet to be matched by machine algorithms (Sroka and Braida, 2005; Benzeghiba et al., 2007).

Auditory perception is supported by specializations in both cochlear and neural anatomy. Insight into the distinct role of these two components can be gleaned by studies of pathology. Acoustic overexposure can cause a variety of insults to the cochlea, including outer hair cell (OHC) stereocilia damage, OHC loss, and inner hair cell (IHC) damage and loss (Liberman et al., 2010). Damage to OHCs reduces their ability to amplify auditory signals, causing elevated thresholds and impaired frequency selectivity (Liberman and Dodds, 1984). At more moderate noise exposure levels, OHC morphology and function and initially altered, but recover completely, generally by 1-2 weeks post-exposure. However, it is now clear that such exposures are not benign, and can cause loss of at least 50% of the synapses between IHCs and auditory nerve (AN) terminals, followed by a slow degeneration of AN cell bodes and central axons, without causing permanent threshold elevations (Kujawa and Liberman, 2009). Elderly humans with normal audiometric thresholds often exhibit perceptual deficits in understanding speech in noise, perhaps due to difficulty using both fine structure and temporal envelope cues (Harris et al., 2009; Clinard et al., 2010; King et al., 2014; summarized in Plack et al., 2014). While numerous studies have identified changes in the central nervous system that could be responsible for these deficits, they may also be caused, or perhaps triggered, by cochlear neuropathy. However, a robust test for neuropathy has yet to be devised, and so its impact on hearing is as of yet unknown. The aims of this thesis were two: 1) to evaluate the utility of the envelope following response as a non-invasive method for quantifying neuropathy, and 2) to identify changes in midbrain auditory coding following neuropathy, with the hope that any changes found may ultimately be used to predict impacts of neuropathy on auditory perception.

In guinea pigs, noise-induced neuropathy is selective for high-threshold, low-spontaneous rate fibers (Furman et al., 2013). Since phase locking to envelopes is particularly strong in these fibers (Joris and Yin, 1992), I hypothesized that the envelope following response (EFR) might be a more sensitive non-invasive measure of neuropathy than the more traditional auditory brainstem response (ABR). In Chapter 1, I compare ABRs and EFRs in mice following a neuropathic noise exposure. Changes to EFRs were more robust: the variance was smaller, thus inter-group differences were clearer. I further explored principles that can be used to optimize the EFR for detection of neuropathy, and found that best separation of control and exposed groups was

achieved with a high modulation frequency and moderate levels.

While the neural consequences of acoustic overexposure have been studied for decades, most exposures used have caused both hair cell and neural damage. Based on anatomical, physiological and behavioral evidence, I hypothesized that cochlear neuropathy alone may cause neural hyperactivity, impaired coding of signals in noise, and impaired coding of envelopes. These hypotheses were tested by comparing single- and multi-unit responses in the inferior colliculus of mice with noise-induced neuropathy with those of age-matched controls. Consistent with reductions in EFRs, synchronization to envelopes was impaired. Neural detectability of tones in background noise was impaired, but only for cases when noise level changed every 600 milliseconds. When noise level changed every minute, responses were equal to those of unexposed mice, implicating changes to adaptation. In quiet, tone-evoked rate-level functions were steeper, indicating that neuropathy may initiate a compensatory response in the central auditory system leading to the genesis of hyperacusis. In sum, we found a combination of both positive and negative changes to coding in the midbrain, some of which as likely direct effects of neuropathy, and some of which could be due to central compensation.

Chapter 1

Towards a diagnosis of cochlear neuropathy with envelope following responses

Luke A. Shaheen, Michelle D. Valero, and M. Charles Liberman

ABSTRACT

Listeners with normal audiometric thresholds can still have suprathreshold deficits, for example, in the ability to discriminate sounds in complex acoustic scenes. One likely source of these deficits is cochlear neuropathy, a loss of auditory nerve (AN) fibers without hair cell damage, which can occur due to both aging and moderate acoustic overexposure. Since neuropathy can affect up to 50% of AN fibers, its impact on suprathreshold hearing is likely profound, but progress is hindered by lack of a robust non-invasive test of neuropathy in humans. Reduction of suprathreshold auditory brainstem responses (ABRs) can be used to quantify neuropathy in inbred mice. However, ABR amplitudes are highly variable in humans, and thus more challenging to use. Since noise-induced neuropathy is selective for AN fibers with high thresholds, and because phase locking to temporal envelopes is particularly strong in these fibers, the envelope following response (EFR) might be a more robust measure. We compared EFRs to sinusoidally amplitude-modulated tones and ABRs to tone-pips in mice following a neuropathic noise exposure. EFR amplitude, EFR phase-locking value, and ABR amplitude were all reduced in noise-exposed mice. However, the changes in EFRs were more robust: the variance was smaller, thus inter-group differences were clearer. Optimum detection of neuropathy was achieved with high modulation frequencies and moderate levels. Analysis of group delays was used to confirm that the AN population was dominating the responses at these high modulation frequencies. Application of these principles in clinical testing can improve the differential diagnosis of sensorineural hearing loss.

INTRODUCTION

Moderate noise exposure can cause a rapid loss of synapses between cochlear hair cells and auditory nerve (AN) terminals, followed by a slow degeneration of AN cell bodies and central axons (Kujawa and Liberman, 2009; Lin et al., 2011). This neuropathy can occur without damage to hair cells, and despite full recovery of thresholds for distortion-product otoacoustic emissions (DPOAEs) and auditory brainstem responses (ABRs). In normal ears, from 10 - 30 AN fibers synapse on each inner hair cell (IHC), depending on species and cochlear location (Liberman et al., 1990; Maison et al., 2013b) and these fibers can be divided into functional subgroups based on spontaneous discharge rate (SR) and sensitivity to sound (Liberman, 1978). The SR distribution is bimodal, with roughly 40% in the low-rate peak (SR < about 18 spikes/second) and 60% in the high-rate peak. Single-fiber recordings in guinea pig suggest that noise-induced neuropathy is selective for high-threshold, low-SR fibers, and that the remaining low-threshold, high-SR fibers exhibit normal responses (Furman et al., 2013). This helps explain why noise-induced cochlear neuropathy can have no discernible effect on ABR thresholds, which must rely only on high-SR fiber responses since low-SR fibers are unresponsive at low stimulus levels (Liberman, 1978).

Post-mortem studies suggest that AN primary degeneration may be widespread in humans (Makary et al., 2011), but it is currently undetected by routine clinical examination. Work in animals shows that more than 80% of the AN fiber population can be silenced without shifting behavioral thresholds for tones in quiet, so long as the outer hair cell (OHC) amplifier is intact (Lobarinas et al., 2013). The impact of such primary neural degeneration on suprathreshold hearing ability is likely profound, but not well understood. A prerequisite for diagnosing this "hidden hearing loss" is a robust test for neuropathy suitable for use in humans. In animal studies, changes in suprathreshold amplitudes of ABR wave I are well correlated with cochlear neuropathy, so long as the cochlear amplifier is undamaged (Kujawa and Liberman, 2009).

However, the envelope following response (EFR), the far-field response to an amplitude-modulated tone (Rickards and Clark, 1972; Campbell et al., 1977; Kuwada et al., 1986), may provide a more robust metric of neuropathy than ABR. Human studies have documented a strong correlation between EFR threshold and ABR threshold (Stapells et al., 1987; Johnson and Brown, 2005; D'haenens et al., 2009). The EFR, and related measures such as the steady-state response to synthetic vowels, have also been investigated at suprathreshold levels: reduced responses in listeners with normal audiograms have been associated with deficits detecting signals in noise (Dimitrijevic et al., 2004), using temporal cues (Ruggles et al., 2011), and in modulation and interaural-time-delay thresholds (Bharadwaj et al., 2015). One possible cause of these deficits may be partial cochlear neuropathy of the sort documented histologically in noise-exposed animals (Kujawa and Liberman, 2009; Furman et al., 2013; reviewed in Bharadwaj et al., 2014) and aging animals (Sergeyneko et al. 2013).

To the extent that they are dominated by AN fibers, EFRs might be particularly sensitive to noise-induced neuropathy, because low-SR AN fibers show greater synchronization than high-SR fibers to sinusoidally amplitude-modulated (SAM) tones (Joris and Yin, 1992), especially at

moderate-to-high stimulus levels (**Fig 1.1B**). In contrast, ABRs are evoked by transient stimuli and dominated by onset responses, which are relatively small in low-SR fibers (Rhode and Smith, 1985; Taberner and Liberman, 2005; Fig. 1A). Thus, the low-SR contribution to the ABR is disproportionately low (Bourien et al., 2014). In addition, phase information can be extracted from EFRs, and measures of phase-locking value (PLV) might be more robust to human anatomical variations (Gorga et al., 1988; Nikiforidis et al., 1993) that complicate amplitude measures in both electrophysiological tests.

In this study, we compare EFRs and ABRs in mice with selective low-SR neuropathy after noise exposure. We contrast this etiology with one affecting all SR groups: mutant mice lacking the BK channel, the large-conductance K^+ channel expressed in hair cells and AN fibers (Skinner

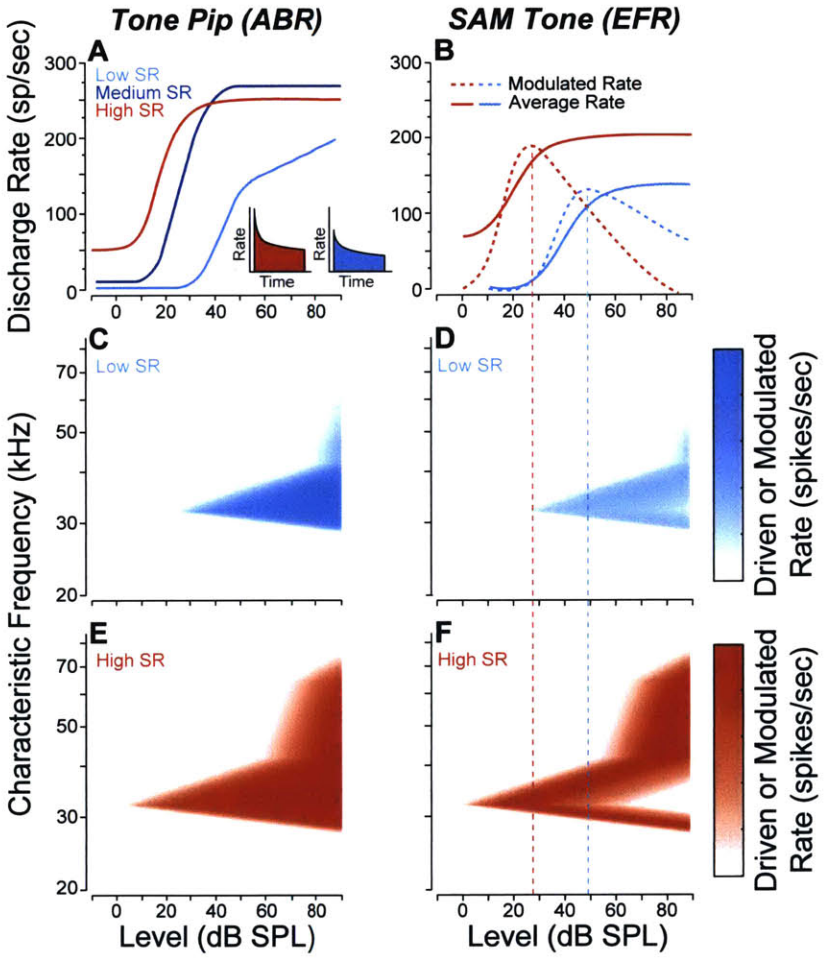

Figure 1.1. Schematics of AN responses according to SR group. **A,** Rate-vs.-level functions for high- medium- and low-SR fibers to tone bursts at the characteristic frequency (Liberman, 1978). The insets show post-stimulus time histograms of the response to a moderate-level tone burst: onset rates are higher in the high-SR fiber than in the low-SR fiber (Taberner and Liberman, 2005). **B,** Responses to SAM tones in high- vs. low-SR fibers expressed as average rate and modulated rate. Responses are to carrier tones at the characteristic frequency, amplitude modulated at 100 Hz (Joris and Yin 1992). **C-F,** Simulated response of mouse low- (**C,D**) and high-SR fibers (**E,F**) to a 32 kHz tone (**C,E**) and 32 kHz SAM tone (**D,F**). Depth of shading indicates rate (**C,E**) and modulated rate (**D,F**) as indicated in the scale at the right.

et al., 2003; Hafidi et al., 2005). In this model, OHC function is normal, but AN fiber firing rates are decreased regardless of SR (Oliver et al., 2006), due to an increase in the IHC time constant, which decreases spike synchronization at stimulus onset, and an increase in the AN refractory period, which directly affects maximum rate.

EFR amplitude and PLV were reduced in both noise-exposed and BK knockout (KO) mice, as was the amplitude of ABR wave I. However, the two pathologies caused different patterns of reduction vs. stimulus level in ways consistent with the different subgroups of AN fibers affected. We found an optimum range of EFR modulation frequencies where sensitivity to AN loss is maximal (~1 kHz), below which responses are increasingly dominated by a mixture of sources, and above which responses are dominated by hair cell potentials. In both models, the EFR data outperformed the ABR data with respect to the sensitivity and specificity for the detection of pathology.

METHODS

Animals and groups: Male CBA/CaJ mice were exposed awake and unrestrained to octave-band noise (8-16 kHz) for 2 hrs, within a cage suspended directly below the horn of the loudspeaker in a small, reverberant chamber. Noise calibration to target SPL was performed immediately before each exposure session. Control mice were of the same age, gender, and strain, but were not exposed to the noise. Three different groups were used, each with their own age-matched controls; Group 1a – exposed to 98 dB SPL at 8 wks of age, (4 control, 5 exposed), Group 1b – also exposed to 98 dB SPL at 8 wks (6 control, 6 exposed), and Group 2 – exposed to 99 dB SPL at 16 wks (8 control, 10 exposed). Both histology and physiology were conducted 2 wks after noise exposure.

Heterozygous breeding pairs of the mutant mouse line with targeted deletion of the gene for the alpha subunit of the BK_{Ca} channel were obtained from the laboratory of origin (Meredith et al., 2004). This same line has been used previously for studies on the role of the BK_{Ca} channel in the inner ear (Pyott et al., 2007; Maison et al., 2013a). The mice were maintained on an FVB/NJ background. Offspring of the heterozygous paternal stock were bred and genotyped in-house to produce homozygous null animals and wildtype littermates. Physiology was conducted at 6-8 weeks of age and included 5 control and 5 KO mice of mixed genders. The comparison here was between wild-type and KO mice; none of these mice were noise-exposed.

In one experiment, electrophysiology was conducted during application of ouabain to the round window niche in order to cause unilateral cochlear neuropathy (Lang et al., 2011; Yuan et al., 2014). After anesthetization (see below) the pinna was removed and a retroauricular incision was made. The underlying muscles and facial nerve were separated by blunt dissection to expose the middle compartment of the bulla, and the round window niche was exposed through a small opening. Ouabain (1–2 µl, 1 mM in distilled water) was applied to the round window membrane for 20 min using a 10 µl Hamilton syringe, and then wicked off and exchanged for a fresh solution

every 20 min for 4 total applications.

All procedures were approved by the Institutional Animal Care and Use Committee of the Massachusetts Eye and Ear Infirmary.

Physiology: Mice were anesthetized with ketamine (100 mg/kg i.p.) and xylazine (20 mg/kg i.p). Recordings were conducted in an acoustically and electrically shielded room held at 30° C. Custom LabVIEW and MATLAB software controlling National Instruments 24-bit digital input/output boards generated all stimuli and recorded all responses. Stimuli were presented using a custom acoustic assembly containing two electrostatic drivers (CUI CDMG15008-03A) and an electret condenser microphone (Knowles FG-23329-P07). The assembly was calibrated with a ¼-inch Bruel and Kjaer condenser microphone. All stimuli were presented unilaterally to the left ear, with the mouse on its right side, and the acoustic assembly just above the ear canal. In-ear calibrations were performed at the onset of each experiment.

DPOAEs were recorded in response to two tones f_1 and f_2, each presented to separate speakers to reduce system distortion (frequency ratio f_2/f_1 = 1.2, and level difference $L_1 = L_2 + 10$ dB). DPOAE response was measured at $2f_1$-f_2 by Fourier analysis of the ear-canal sound pressure waveform. Stimulus duration was 1.6 seconds at each level combination (L_2 varied from 20 to 80 dB SPL in 5 dB steps). Threshold was defined as the interpolated f_2 level producing a DPOAE of 5 dB SPL.

Both ABR and EFR were recorded differentially with subdermal needle electrodes with the common ground at the base of the tail; four different electrode configurations were used (**Fig 1.2**). The first two configurations were used after a dorsal-ventral incision at the intertragal notch of the ipsilateral pinna to allow direct visualization of the eardrum. Following the incision, electrode pairs were placed both (1) vertex (positive electrode) to ipsilateral pinna, with the latter just caudal to the intertragal notch, and (2) contralateral pinna (positive) to ipsilateral pinna, with both electrodes caudal to the intertragal notch. This configuration pair was used for Group 1. In Group 1a the pinna electrode was just caudal to the intertragal notch, which is the standard position used

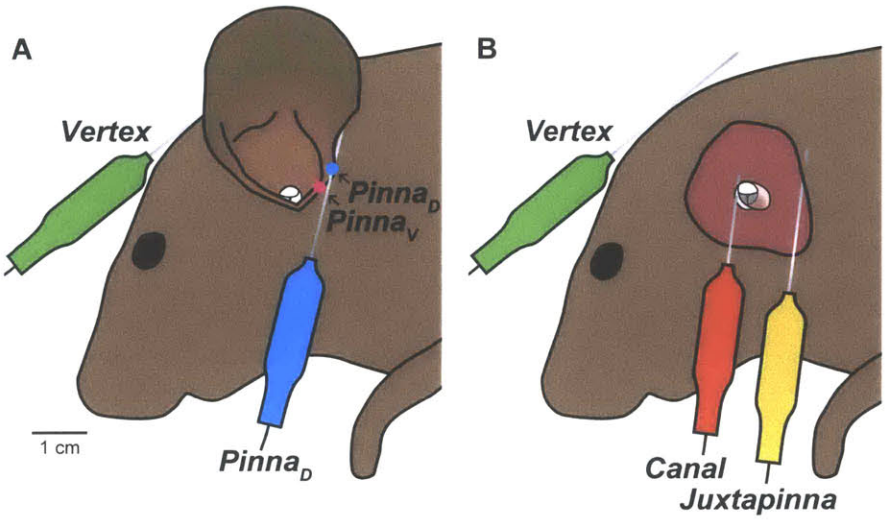

Figure 1.2. Schematic of electrode configurations. **A**, Intact-pinna configurations: vetex to pinna$_D$ shown, vertex to pinna$_V$ location illustrated by magenta dot. For pinna to pinna configurations the positive (green) electrode was placed in an identical location on contralateral side (not shown). **B**, Removed-pinna configurations: vertex to ear canal, vertex to juxta-pinnal skin.

by our lab (Vertex - $Pinna_D$). In Group 1b, the pinna electrode was placed slightly more ventral along the antitragus in order to increase the early ABR waves (Vertex – $Pinna_V$). The second two configurations were used after removing the entire pinna and surrounding skin (8-10 mm posterior to the tympanic ring) to access the bulla and round window. Following that, electrodes were placed both (3) vertex (positive) to ipsilateral ear canal, with the latter through the rostral edge of the severed ear canal, and (4) vertex (positive) to ipsilateral juxta-pinnal skin, with the latter through the cut edge of the skin posterior to the ear canal. This configuration was used for Group 2. Responses were measured simultaneously from each configuration pair.

Responses were amplified 10,000X using two Grass P511 amplifiers with a 0.3-3 kHz passband for ABR, and a 0.03-30 kHz passband for EFR. ABRs were evoked with 5-msec. tone-pips with 0.5 msec. $\cos^2$ rise–fall presented in alternating polarity at a rate of 40/s. Tone-pip frequencies were 11.3 or 32 kHz. Trials where the response amplitude exceeded 15 µV were rejected; 512 artifact-free trials of each polarity were averaged to compute ABR waveforms. Threshold was defined by blinded visual inspection of the stacked waveforms as the lowest level at which a reproducible peak or trough appears, which usually occurs one level-step below that at which peak-to-peak amplitude begins to grow. EFR stimuli were 30-sec. SAM tones using 100% modulation depth and carrier frequencies (f_cs) of 11.3 kHz or 32 kHz. Modulation frequency (f_m) ranged from 400 Hz to 1990 Hz. EFR amplitude was measured at f_m using Fourier analysis. To minimize system distortion, the carrier tone was presented using one of the speakers and the two sidebands using the other. Postmortem measurements demonstrated that this approach eliminated distortion for stimulus levels up to 90 dB SPL. In the mouse, the quadratic difference tone distortion product at f_m (generated by interaction of the carrier and either sideband) falls outside the range of hearing for all f_ms used (up to 2 kHz), so it should not influence results. Cubic difference tones were measureable at $f_c + nf_m$ for n = {-4,-3,-2, +2}, but since their amplitude was always at least 50 dB lower than that of the stimulus tones, contribution to the EFR was minimal. EFR group delay was calculated for each individual by 1) measuring the phase at f_m by Fourier analysis, 2) unwrapping using MATLAB's *unwrap*, 3) fitting a line to each consecutive trio of points to find the local slope

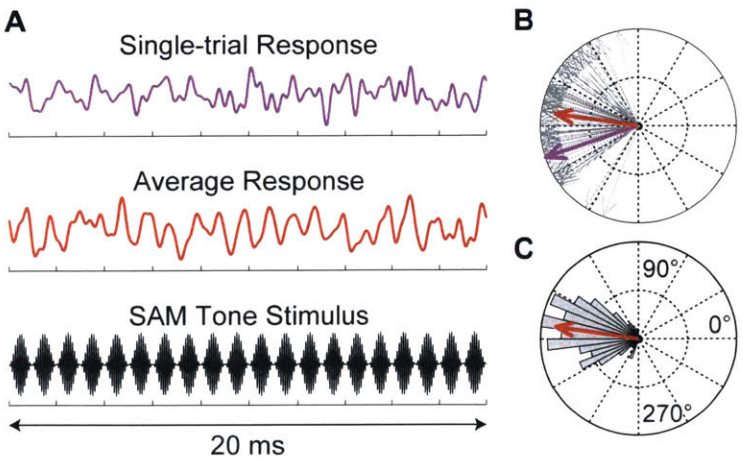

Figure 1.3. EFRs were recorded in response to a 30-sec. continuous SAM tone, a 20 ms sample of which is shown in **A**, along with a typical single-trial and average response. To compute EFR phase-locking value (PLV), the 30-sec. response was split into 100-ms 'trials' and the phase of each trial (**B**, thin-line vectors) was computed. The phase for the single trial in **A** is shown is color coded to match. For clarity, only 100 trials are shown in **B**; Grey bars in **C** show a histogram of all 300 trials. All 300 single-trial phases were vectorially summed to compute the PLV (**B** and **C,** thick red line).

(group delay), and 4) smoothing with a three-point moving average. Modulation sampling was sufficiently fine (30 or 60 Hz steps) to unambiguously unwrap phase (see **Fig 1.5E-G**). EFR PLV (Dobie and Wilson, 1989; Zhu et al., 2013) was calculated by 1) breaking the 30-sec. continuous record into 300 100-msec. 'trials' (**Fig 1.3A**, top panel), 2) measuring the phase of each trial at f_m by Fourier analysis (**Fig 1.3B**, thin lines), and 3) computing the magnitude of the vector average of all phases, assigning each vector equal amplitude (**Fig 1.3B,C**, thick red line). 'Trials' where voltage exceeded 15 μV were rejected as artifact. A 'trial' length of 100 msec. was chosen because it yielded a good signal-to-noise ratio for all data presented in this paper, for other datasets a different length may be necessary. Under this protocol, PLV ranges from 0 (random phase) to 1 (each 'trial' having identical phase).

Cochlear Immunostaining and Innervation Analysis: Mice were perfused transcardially with 4% paraformaldehyde. Cochleas were decalcified, dissected into half-turns and incubated in primary antibodies: 1) mouse (IgG1) anti-CtBP2 from BD Biosciences at 1:200 and 2) mouse (IgG2) anti-GluA2 from Millipore at 1:2000. Primary incubations were followed by 60-min incubations in species-appropriate secondary antibodies. Cochlear lengths were obtained for each case, and a cochlear frequency map computed using a custom ImageJ plugin (http://www.masseyeandear.org/research/otolaryngology/investigators/laboratories/eaton-peabody-laboratories/epl-histology-resources/) that translates cochlear position into frequency according to the published map for the mouse (Müller et al., 2005; Taberner and Liberman, 2005). Confocal z-stacks from each ear were obtained using a glycerol-immersion objective (N.A. = 1.4) and 3.17X digital zoom on a Leica TCS SP5 confocal. Synapses in the IHC area were counted using Amira (Visage Imaging) to find the xyz coordinates of all the ribbons (CtBP2-postiive puncta), and custom re-projection software was then used to assess the fraction of ribbons with closely apposed glutamate-receptor patches (i.e. GluA2 puncta).

Statistical Analysis: Statistical testing was performed in MATLAB, using the *anova*, *ranova*, and *multicompare* functions for ANOVA, repeated-measures ANOVA, and post-hoc tests. When statistically significant interactions were identified, post hoc two-sample t-tests were performed using a Holm–Bonferroni correction for multiple comparisons.

RESULTS

Noise-induced Synaptic Loss after Reversible Noise-Induced Threshold Shift

We titrated the sound level of an octave-band noise (8-16 kHz) such that a 2-hr exposure would produce a large temporary threshold shift (1 day post-exposure) but minimal permanent threshold shift (2 wks post-exposure). For DPOAEs and ABRs, peak threshold shift at 24 hrs. post-exposure was ~ 40 - 50 dB (data not shown). By 2 wks post-exposure, DPOAE thresholds were not significantly elevated at any test frequencies except for at 45 kHz, where thresholds were elevated by 5-20 dB, depending on group (**Fig 1.4A**). ABR thresholds, measured at 11.3 and

32 kHz, were not significantly elevated in any groups (**Fig 1.4B**). Consistent with the observation that overall noise vulnerability decreases with age from 8 to 16 wks (Kujawa and Liberman, 2006), complete threshold recovery was observed in the mice exposed at 16 wks of age (**Fig 1.4A,B** Group 2). The high-frequency threshold shifts in the 8-wk exposure group were associated with scattered loss of OHCs in the extreme basal regions of the cochlea (**Fig 1.4C**). While no significant differences were found in OHC loss between the animals exposed at 8 wks and those exposed at 16 wks, a trend toward more loss and a larger threshold shift suggest greater damage to OHC

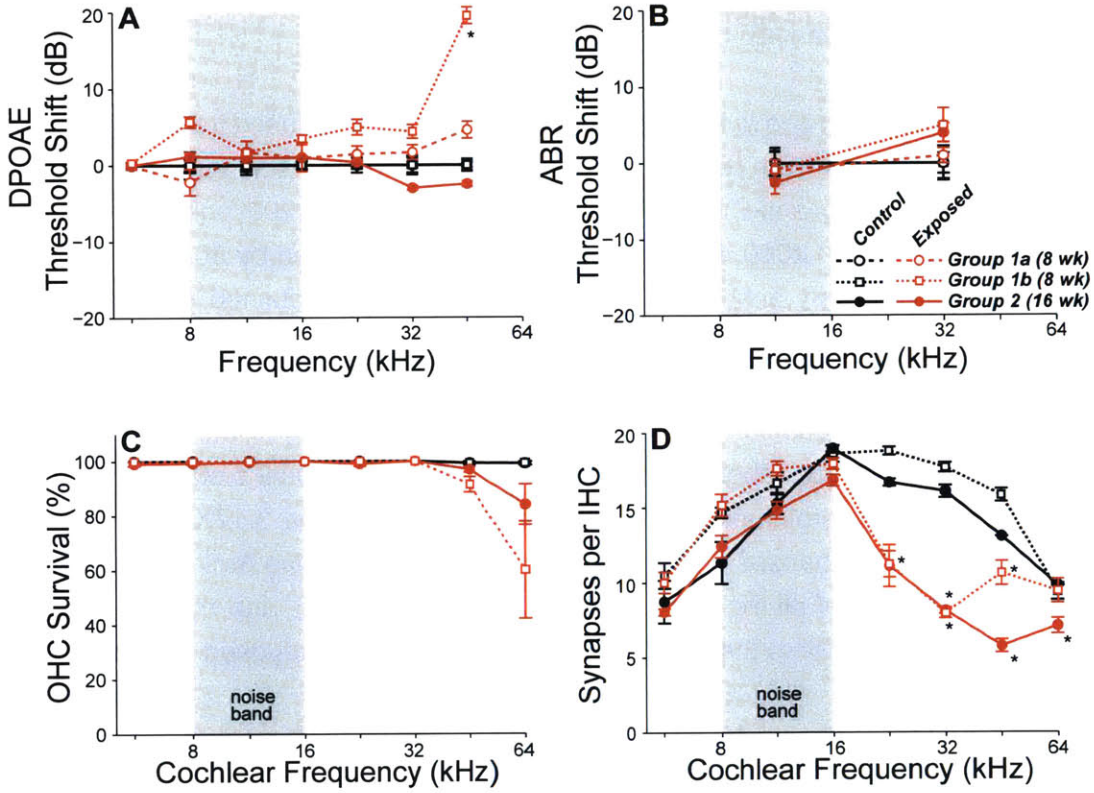

Figure 1.4. Noise-exposure causes permanent synaptic loss with minimal permanent threshold shift. **A,B,** Mean DPOAE thresholds (**A**) and ABR thresholds (**B**) for each of three different groups, normalized to their own age-matched controls: Group 1a – exposed to 98 dB SPL at 8 wks of age (4 control, 5 exposed), Group 1b – exposed to 98 dB SPL at 8 wks (6 control, 6 exposed), and Group 2 – exposed to 99 dB SPL at 16 wks (8 control, 10 exposed). **C,** OHC survival in control (black) and exposed (red) mice. **D,** Counts of pre-synaptic ribbons and post-synaptic glutamate receptors show loss of AN synapses on inner hair cells throughout the basal half of the cochlea. For histology (**C&D**), a subset of Group 2 was used (3 control, 5 exposed), all ears were used in Group 1a and Group 1b. **A,** There were no significant effects of exposure on DPOAE thresholds by two-way repeated-measures ANOVA for group 1a and group 2: $F_{(1,42)} = 0.01$ $p = 0.91$ and $F_{(1,102)} = 0.05$ $p = 0.83$. For group 1b the effect of exposure was significant (interaction between frequency and exposure condition $F_{(6,60)} = 5.97$, $p < 0.001$). **B,** There were no significant effects of exposure on ABR thresholds: group 1a: $F_{(1,7)} = 0.00$ $p = 1$, group 1b: $F_{(1,10)} = 1.24$ $p = 0.29$, group 2: $F_{(1,16)} = 0.33$ $p = 0.57$. **C,** While the effect of exposure was significant (interaction $F_{(14,84)} = 3.07$, $p < 0.01$), there were no significant pairwise comparisons after Bonferroni-Holm correction. **D,** There was a significant interaction between frequency and exposure group for both Group 1b ($F_{(7,63)} = 16.56$, $p < 0.001$) and Group 2 ($F_{(7,35)} = 8.26$, $p < 0.001$). Stars indicate significant paired differences ($p<0.01$ or better) between exposed and corresponding control.

function in the 8 wk group. There were no significant IHC losses in any ears (effect of exposure by two-factor repeated-measures ANOVA for group 1b and group 2: $F_{(1,63)} = 0.21$ $p = 0.66$ and $F_{(1,35)} = 0.01$ $p = 0.94$).

While noise-exposure minimally affected cochlear thresholds, histological analysis clearly demonstrated loss of AN synapses (**Fig 1.4D**). Each mammalian AN fiber contacts one IHC via a single synaptic terminal, with a single active zone, seen in the electron microscope as apposed pre- and post-synaptic plaques of membrane thickening, with a prominent pre-synaptic ribbon surrounded by a halo of synaptic vesicles (Liberman, 1980; Stamataki et al., 2006). At the light-microscopic level, we can count the synapses between AN fibers and IHCs by immunostaining pre-synaptic ribbons and post-synaptic glutamate receptors using antibodies against a ribbon protein (CtBP2: Khimich et al., 2005) and an AMPA-type glutamate receptor subunit (GluR2: Matsubara et al., 1996). In control mice, the number of synapses per IHC varies with cochlear location, with a peak of ~18 synapses/IHC in the middle of the cochlear spiral (**Fig 1.4D**). Noise-exposure caused significant synaptic loss throughout much of the basal half of the cochlea, with maximum losses occurring 1½ to 2 octaves above the noise-exposure band (**Fig 1.4D**). At the 32 kHz region the mean loss of synapses was 53% (Group 1b) and 50% (Group 2). Prior work has shown that this synaptic loss is permanent, and followed by a delayed degeneration of spiral ganglion neurons (Kujawa and Liberman, 2009).

EFR measures in noise-exposed ears: effects of modulation frequency

EFRs were recorded 2 wks after noise exposure in response to 30-sec. continuous SAM tones. We placed the carrier frequencies at 32 kHz (**Fig 1.5B,D,F,H**) and 11.3 kHz (**Fig 1.5A,C,E,G**) to probe cochlear regions with and without neuropathy, respectively (**Fig 1.4D**). We varied modulation frequency from 400 to 1400 Hz to probe responses from different portions of the ascending auditory pathways. With ABRs, contributions from different auditory centers are, at least partially, separated in time (Melcher and Kiang, 1996). With EFRs, responses from different nuclei are, at least partially, separated by modulation frequency: more peripheral neurons (e.g. AN) dominate at high modulation frequencies, whereas more rostral neurons (e.g. inferior colliculus) dominate at low modulation frequencies (Rickards and Clark, 1972; Herdman et al., 2002; Kuwada et al., 2002). In exposed animals, EFR amplitudes were reduced by up to 55% in response to the carrier frequency probing the neuropathic region (32 kHz), but unchanged for the non-neuropathic region (11.3 kHz). For the 32 kHz carrier, the maximum differences in amplitude were seen at higher modulation frequencies (near 1000 Hz), consistent with the idea that AN fibers contribute a larger portion of the response at these higher frequencies than more central auditory nuclei. We computed EFR PLV from the same data (see Methods). Changes in PLV mirrored the changes in EFR amplitude (**Fig 1.5C,D**).

To better understand the generators of the EFR in mouse, we calculated group delay from the slope of the phase-vs.-modulation-frequency function (**Fig 1.5E-H**; See Methods). For a single generator, group delay is equivalent to the latency of that generator. Group delay becomes complicated when two sources contribute, but can still be informative near the amplitude peaks,

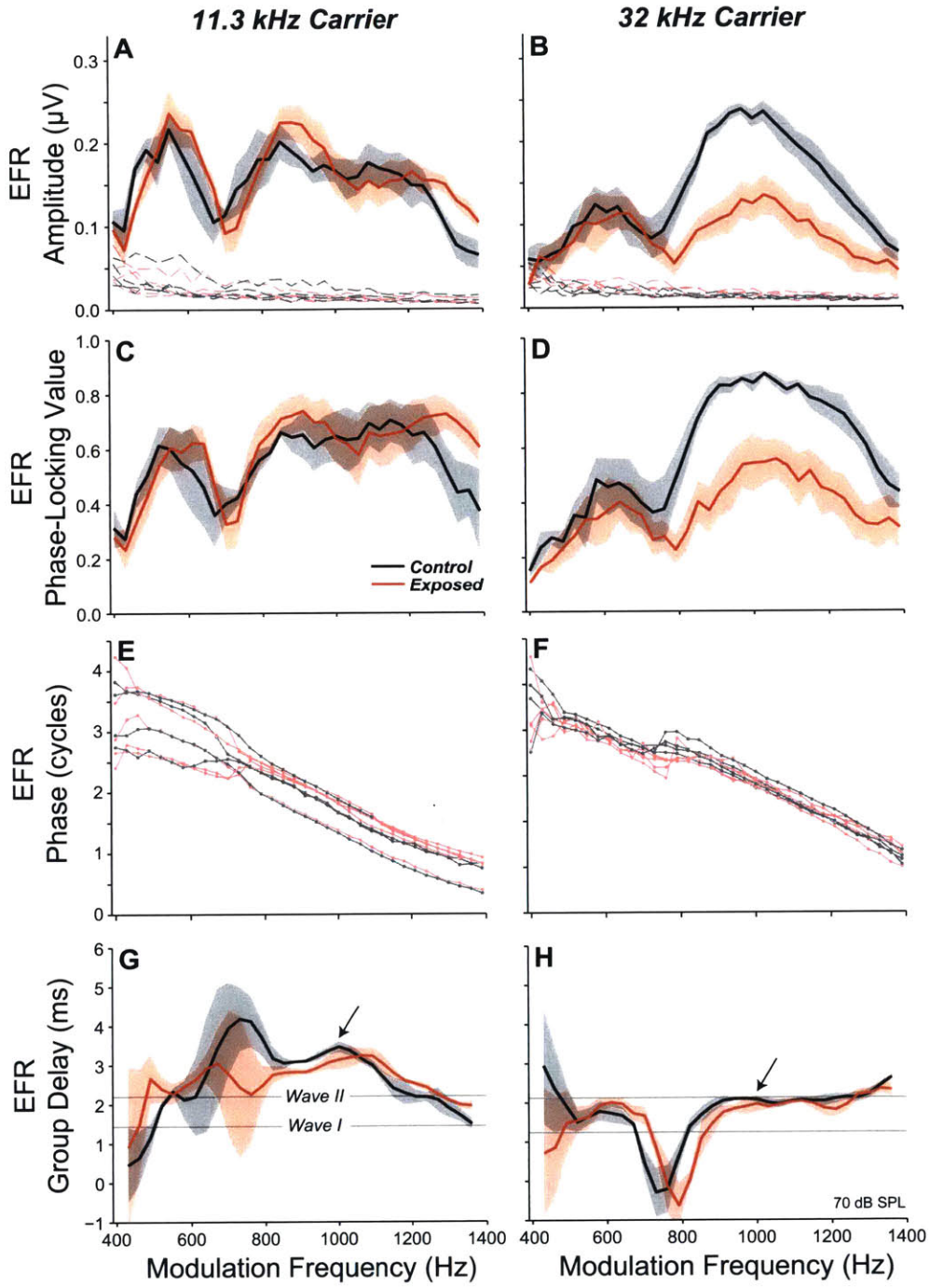

Figure 1.5. Cochlear neuropathy reduces EFR amplitudes and phase-locking values (PLVs). **A-D,** EFR amplitude (**A,B**) and EFR PLV (**C,D**) were decreased in the noise-exposed group for 32 kHz carriers (**B,D**: $F_{(1,231)} = 6.21$, $p = 0.041$; $F_{(1,231)} = 5.75$, $p = 0.048$), but not for 11.3 kHz carriers (**A,C**: $F_{(1,231)} = 0.32$, $p = 0.59$; $F_{(1,231)} = 0.18$, $p = 0.68$). **E,F,** EFR phase, unwrapped for each individual and shifted by an integer number of cycles for best alignment in the 1 to 1.4 kHz range. **G,H,** EFR group delays, computed as the slope of phase-vs.-modulation-frequency functions on an individual basis (see Methods). Horizontal lines show ABR peak latencies measured at 70 dB SPL, the same level used for the SAM tone response shown here. Thin dashed lines show individual noise floors (A and B only), thin solid lines show individual responses (E and F), and thick lines and shaded areas show group means ± SEMs. Data are from Group 1a, recorded using the vertex to $pinna_D$ electrode configuration.

where group delay is equal to a weighted sum (by their amplitudes) of the two sources (Shera and Bergevin, 2012). Consistent with traveling wave delays in the cochlea, 11.3 kHz carriers (**Fig 1.5G**) gave rise to longer group delays than 32 kHz carriers (**Fig 1.5H**) at the 1-kHz modulation frequency (arrows). The difference in group delays (3.1 vs. 2.0 = 1.1 ms) was significantly larger than that observed in ABR peak I latency (1.44 vs. 1.24 = 0.2 ms; two-sided paired t-test $t_{(8)} = 3.44$, $p = 0.009$). The difference in first-spike latency of mouse AN fibers at these two CF regions is intermediate (3.0 vs 2.5 = 0.5 ms; Fig. 4.5, Taberner, 2005). EFR group delay was unchanged following noise-exposure except at amplitude minima (**Fig 1.5G,H**), suggesting little shift in the locus of the neuronal groups dominating the responses. Large swings in group delay near amplitude minima do not necessarily indicate a change in generators, as phase-vs.-frequency gradients can be complicated when multiple sources destructively interfere (see Discussion).

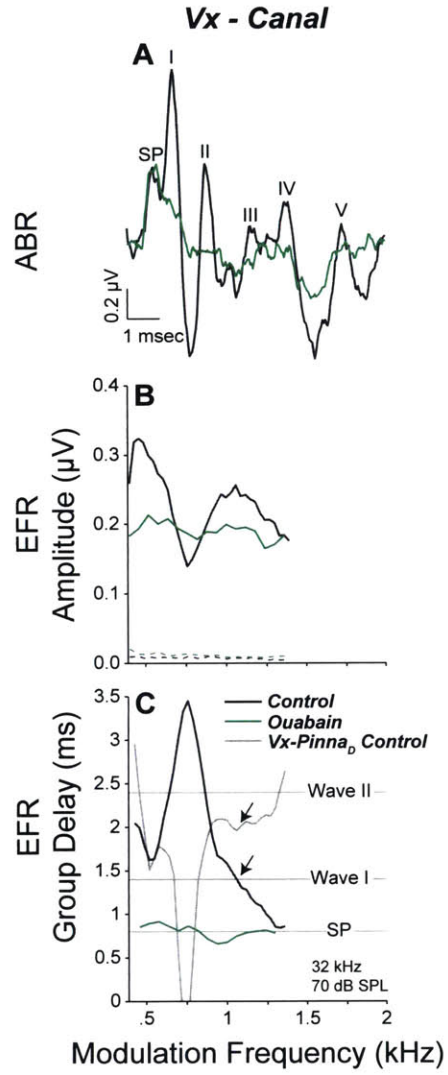

Figure 1.6. Acute ouabain-induced neuropathy reveals hair cell contributions to ABRs and EFRs. **A,** ABR waveforms in response to 70 dB SPL, 32 kHz tone-pips. **B,C,** EFR amplitude and group delay in response to a 32 kHz carrier at 70 dB SPL. Horizontal lines in **C** show ABR peak latencies. In all panels, responses are shown before (black) and after (green) cochlear neuropathy induced by ouabain application to the round window. Data are obtained using the vertex to ear canal electrode configuration in an 8 wk mouse. Grey line in panel **C** replots control vertex to pinna$_D$ mean group delay from Fig 1.5H.

Effects of electrode placement on EFR measures: determining sources

The EFRs in Figure 5 were recorded with a vertex to pinna electrode configuration (see Methods), similar to that used in clinical settings (Hall, 2006). However, noise-induced cochlear neuropathy may be more robustly detected by electrode configurations that increase the relative contributions from peripheral generators, such as electrodes on the tympanic membrane or round window niche as used in electrocochleography (Schwaber and Hall, 1990). To mimic these configurations in the mouse, we removed the pinna and placed the negative electrode through the cartilage of the ear canal, leaving the positive electrode at the vertex. This increased the amplitude of wave I and revealed a short-latency shoulder on wave I (**Fig 1.6A**), which is the analog of the summating potential (SP) recorded on the round window, reflecting summed receptor potentials from IHCs (Durrant et al., 1998; Yuan et al., 2014). Contributions of IHCs and AN fibers were also increased in the EFRs, as group

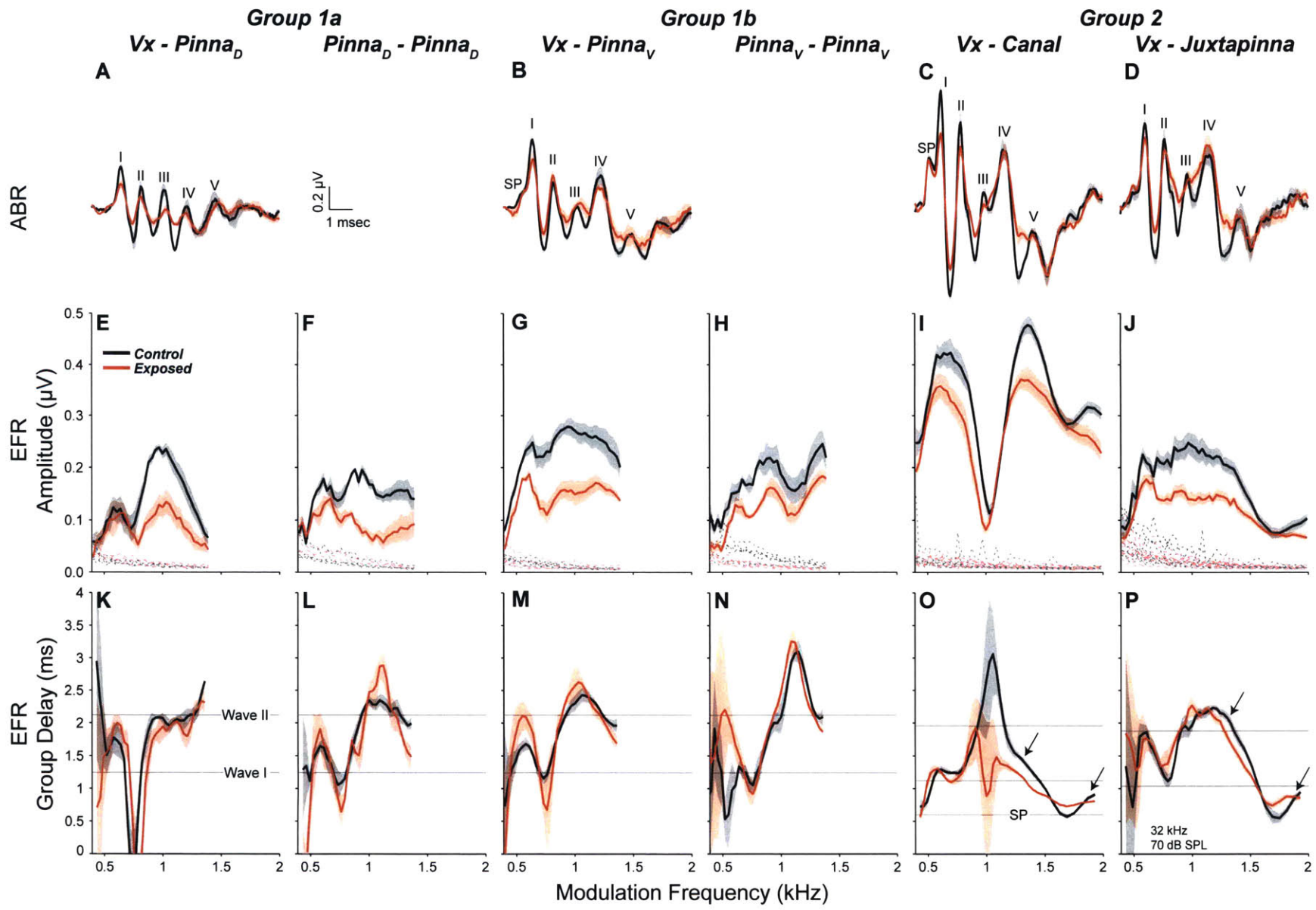
Group 1a
Vx - Pinna$_D$
Pinna$_D$ - Pinna$_D$
Group 1b
Vx - Pinna$_V$
Pinna$_V$ - Pinna$_V$
Group 2
Vx - Canal
Vx - Juxtapinna
A
B
C
D
ABR
I
II
III
IV
V
SP
0.2 µV
1 msec
E
F
G
H
I
J
Control
Exposed
EFR Amplitude (µV)
K
L
M
N
O
P
EFR Group Delay (ms)
Wave II
Wave I
SP
32 kHz
70 dB SPL
Modulation Frequency (kHz)

Figure 1.7. Effects of electrode configuration on EFRs and ABRs. **A-D,** Mean ABR waveforms in response to 70 dB SPL, 32 kHz tone-pips. **E-J,** Mean EFR amplitudes and **K-P**, mean group delays in response to 32 kHz carriers at 70 dB SPL. Horizontal lines **(K-P)** show ABR peak latencies; SP latency is shown only when a clear local maxima is found. Because ABRs were not recorded for the pinna to pinna configuration, latencies (**L,N**) are from vertex to pinna data. Thin dashed lines (**E-J**) show individual noise floors, thick lines and shaded areas in all panels show group means ± SEMs. Wave I amplitude was significantly increased by a slight change in the location of the pinna electrode (**A** vs. **B**; two-way repeated-measures ANOVA: $F_{(1,17)} = 10.17$, $p = 0.005$). For Group 2, group delay was significantly affected by electrode configuration (**O** vs. **P**; three-way repeated-measures ANOVA: $F_{(1,231)} = 6.20$, $p = 0.02$, significant pairwise effect of electrode configuration at 1330 Hz (arrows), $p = 0.002$).

---

delays around 1 kHz (the amplitude peak) were shorter than those measured with the vertex to pinna configuration (**Fig 1.6C,** black line vs. grey line). Due to destructive interference between multiple sources, large group delay excursions around amplitude minima are not close to the latency of either source. Therefore, the large reversal of group delays around 750 Hz does not indicate a sudden change in the source of the EFRs at this frequency.

To validate the use of group delay to infer EFR generators, we made measurements in one mouse before and after inactivating AN responses, without affecting hair cell function, by round-window application of ouabain, a blocker of a neural-specific Na/K ATPase (Azarias et al., 2013; Obrien et al., 1994; Schmiedt et al., 2002). Ouabain effectively eliminated all ABR waves except those from pre-synaptic sources, i.e. the SP (**Fig 1.6A,** green line). Both EFR functions flattened, consistent with a transformation from multiple interacting sources to a single, short-latency source (**Fig 1.6B,C**). Since EFR group delay was approximately equal to SP latency (0.8 ms), the post-ouabain EFR is likely generated by the IHCs: the SAM tone is similar to a series of rapid tone bursts, in response to which IHC receptor potentials fluctuate at the envelope frequency.

To determine if the vertex to ear canal configuration provides a more robust indicator of cochlear neuropathy, we measured ABRs and EFRs from two electrode configurations in one group of control and noise-exposed ears after completely removing the pinna: 1) vertex to cartilaginous ear canal (**Fig 1.7C,I,O)** vs. (2) vertex to juxta-pinnal skin (**Fig 1.7D,J,P**; see Methods). EFR amplitudes were reduced by the neuropathy for both configurations, but dependence on modulation frequency was more complex in the vertex to ear canal configuration, suggesting greater constructive and destructive interference among multiple generators. At 1330 Hz modulation, the locus of the amplitude peak for the vertex to ear canal configuration, group delay was significantly shorter than for the vertex to juxtapinna configuration (**Fig 1.7O** vs. **7P**), suggesting a greater contribution from peripheral generators, as confirmed by the relative heights of the early ABR waves (**Fig 1.7C** vs. **7D**). At the highest modulation frequencies group delays for both configurations fell below 1 msec., indicating that responses were dominated by hair cell potentials.

As a fourth electrode configuration, we measured from ipsilateral pinna to contralateral pinna, thinking that this symmetrical placement ought to emphasize AN and cochlear nucleus contributions over those from higher auditory centers such as the inferior colliculus, given that the peripheral structures are more asymmetrically located with respect to the two electrodes (Ping et al., 2007). In two series of exposed and control ears, responses were simultaneously recorded

from vertex to pinna (**Fig 1.7A,E,K,B,G,M**) and pinna to pinna (**Fig 1.7F,L,H,N**). Group delays were not generally shorter for the pinna to pinna configuration, perhaps because even the lowest modulation frequencies tested may still be too high for colliculus neurons, which respond poorly when modulation frequencies exceed 400 Hz (Joris et al., 2004, Fig. 9).

In Group 1b the pinna electrode was placed slightly more ventral along the antitragus. Perhaps because this decreased the distance to the cochlea, this configuration resulted in a significantly larger SP and wave I amplitude with respect to Group 1a (**Fig 1.7A** vs. **7B**). Along with this small change in ABR, we observed increased EFR amplitudes and shorter group delays at low modulation frequencies (**Fig 1.7E,K** vs. **7G,M**), consistent with EFR contributions from AN responses throughout the modulation frequency range tested.

To more directly assess the effects of electrode configuration and modulation frequency on the detection of cochlear neuropathy, we computed amplitude ratios for responses measured in exposed vs. control ears. As shown in **Fig 1.8C**, amplitudes were reduced over a broad range of modulation frequencies in most electrode configurations. Surprisingly, although the vertex to ear canal configuration showed the largest AN contributions (as seen in the ABR), this configuration was the least effective in yielding consistent EFR amplitude reductions over a wide range of modulation frequencies (**Fig 1.8C**, purple line). Since the ability to separate two groups depends not only on the means, but also their variability, we calculated effect size (Hedge's g), the difference in means divided by the pooled standard deviation (Hentschke and Stüttgen, 2011). As shown

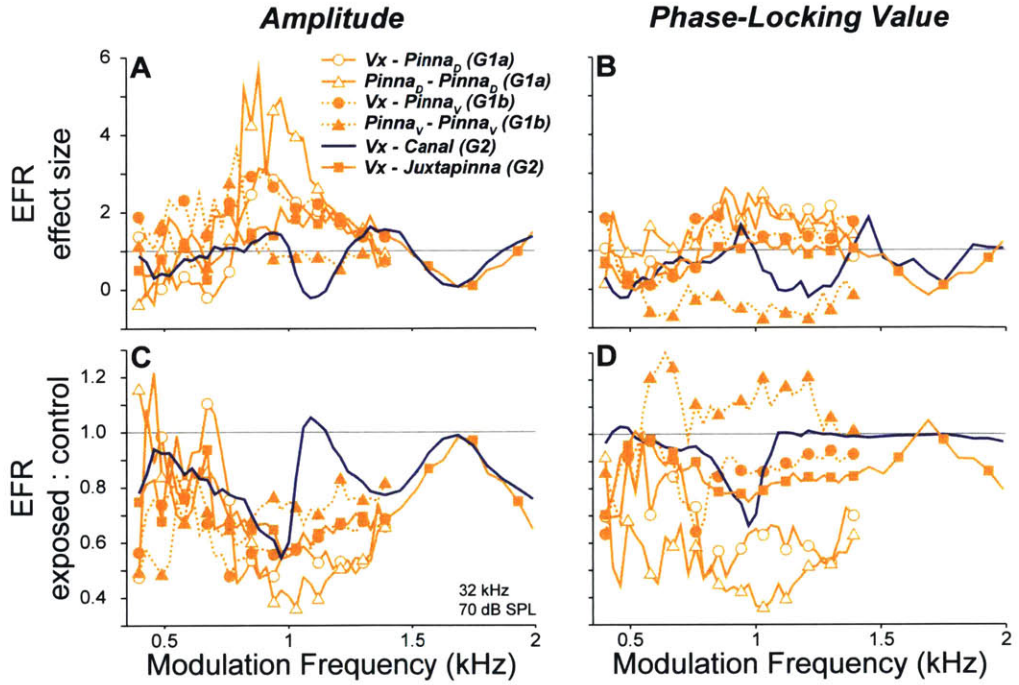

Figure 1.8. EFR amplitudes (**A,C**) and phase-locking values (**B,D**) are most sensitive to cochlear neuropathy for modulation frequencies near 1 kHz. **A,B,** The effect size (Hedge's g; (Hentschke and Stüttgen, 2011)) is the difference in group means (control vs. exposed) divided by the square root of the weighted sum of group variances. Higher values indicate greater separation of the two groups. **C,D,** Ratio between control and exposed means. Data in all panels are for the 32 kHz carrier at 70 dB SPL. Key in A applies to all panels.

in **Fig 1.8A**, effect size exceeded one standard deviation over a broad frequency range for the vertex to pinna, pinna to pinna, and vertex to juxtapinna configurations, but not for the vertex to ear canal configuration (orange lines vs. purple line). With EFRs, detection of neuropathy using an electrode configuration more sensitive to cochlear sources may be detrimental, as AN reductions due to neuropathy are diluted by hair cell potentials, which are unchanged. For such configurations, choice of modulation frequency becomes critical.

Ratio and effect size computed from PLVs were similar to those of amplitude, but effect size reached lower maximum values (**Fig 1.8 B,D**). In cases where signal-to-noise-ratio (SNR) was very high (Vx-Canal, see **Fig 1.8I**), PLVs became saturated and were therefore less useful for detecting neuropathy (**Fig 1.8B,D,** purple line). In the pinna to pinna configuration of Group 1b, noise floors were higher in some control animals (**Fig 1.7H**). This caused the two groups to have similar SNRs, and thus PLVs, so effect size was small (**Fig 1.8D,** filled triangles). PLVs appear not to be useful in high-SNRs conditions such as these, but may be helpful in situations where SNR is poor.

EFR amplitude reductions were minimal at low modulation frequencies (below ~600 Hz) for all configurations and groups (**Fig 1.8C**). If EFR at high modulation frequencies is dominated by more peripheral sources (i.e. hair cells and AN fibers), and by more central sources (e.g. inferior colliculus) at lower modulation frequencies (Kuwada et al., 2002), these data could be reflecting an amplified central auditory response in the face of peripheral response reductions after trauma (Gu et al., 2012; Schaette, 2014). This speculation is supported by the ABR data (**Fig 1.9**): while noise exposure significantly decreased the amplitudes of waves I, II, and III, waves IV and V were unaffected. Data in Figure 9 are for the vertex to pinna configuration of Group 1a. For Group 2, waves III and V were too small to measure in individual cases, but the trend towards less reduction in later waves can be seen in the mean waveforms: wave I ratios 0.66 & 0.70 vs. wave IV/V ratios 0.98 & 1.08 for Figure 7C and D, respectively. However, wave I and wave IV/V were equally reduced in Group 1b (0.68 vs. 0.69; **Fig 1.7B**). This difference could be due to the mild threshold shift observed in that group (**Fig 1.4A**).

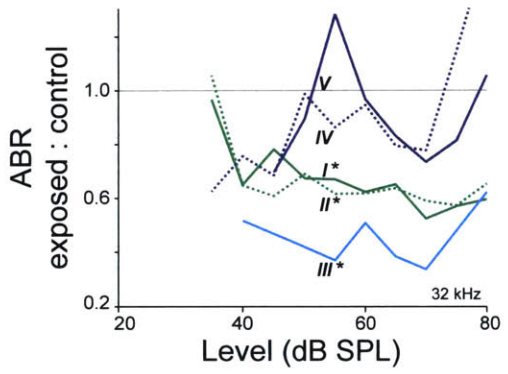

Figure 1.9. Amplitude ratios between control and noise-exposed groups for each of the five ABR waves suggest central compensation. ABR waves were identified using a derivative-based peak-finding algorithm, and are measured peak-to-trough. Data are from Group 1a, recorded using the vertex to pinna$_D$ electrode configuration. There was a significant interaction between wave and exposure by a three-way repeated-measures ANOVA: $F_{(4,35)} = 3.19$, $p = 0.025$. Significant exposed:control differences for each wave are indicated by stars: [I,II,III,IV,V], p = [0.004, 0.015, 0.002, 1, 1].

EFR measures in noise-exposed ears: effects of stimulus level

We recorded amplitude-vs.-level functions for ABR and EFR at a variety of modulation frequencies for all three groups of noise-exposed mice. For brevity, only responses from the vertex to pinna configuration (Group 1a) are shown in **Fig 1.10,** but they are representative of all three groups. ABR wave I (**Fig 1.10A,B**) showed the behavior expected based on prior studies of noise-induced neuropathy in mice (Kujawa and Liberman, 2009): i.e. a fractional reduction of response amplitudes at 80 dB SPL comparable to the fractional loss of synapses in the appropriate cochlear region.

To examine the level dependence of noise-induced changes in EFR, we used the modulation frequency producing the largest responses in controls: 820 Hz for the 11.3 kHz carrier and 1000

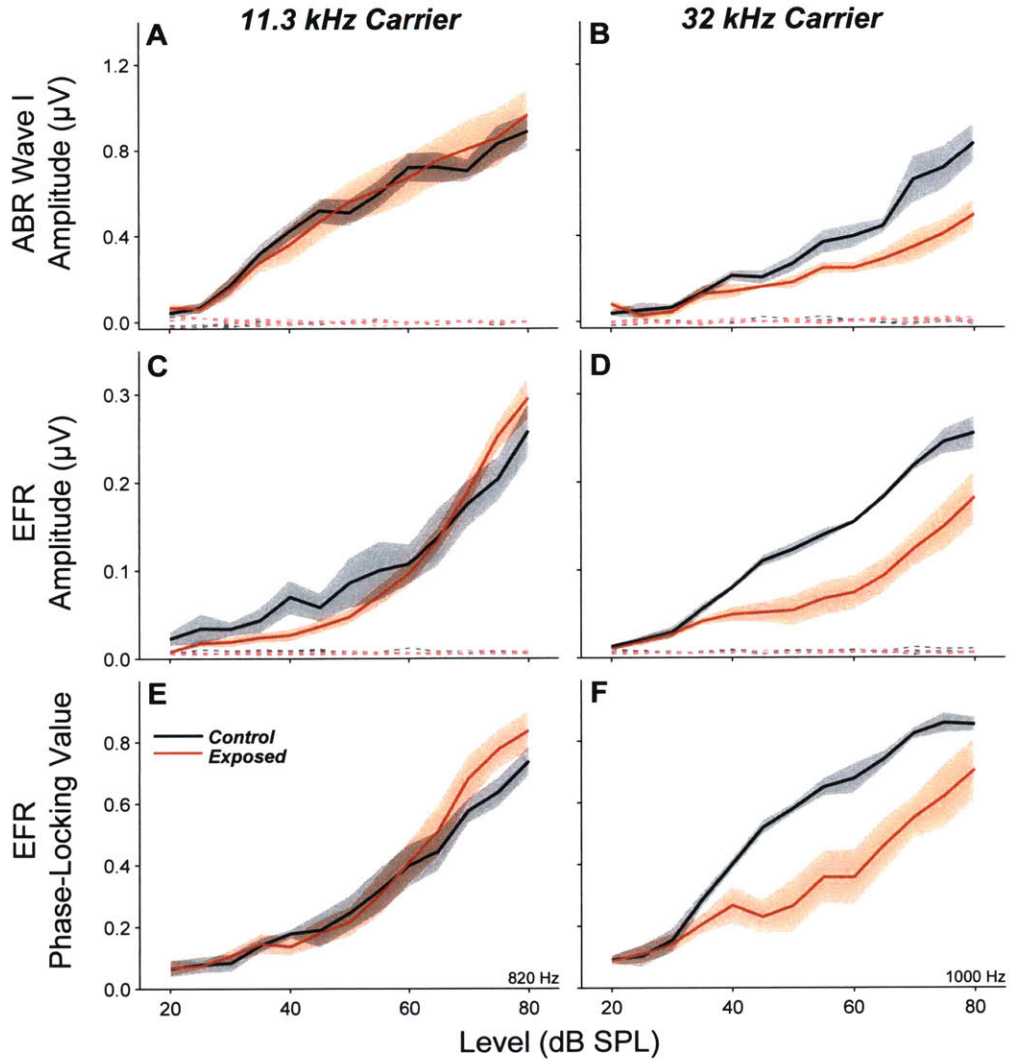

Figure 1.10. After neuropathic noise, changes in EFR amplitude (**C,D**) and phase-locking values (**E,F**) were more robust than changes in ABR Wave I amplitude (**A,B**). EFR data were measured at the modulation frequency producing the largest response in normal mice: 820 Hz for the 11.3 kHz carrier and 1000 Hz for the 32 kHz carrier (see Fig 1.4). ABR wave I amplitude was measured peak to following trough. Thin dashed lines show individual noise floors, and thick lines and shaded areas show group means ± SEMs. Data are from Group 1a, recorded using the vertex to $pinna_D$ electrode configuration.

Hz for the 32 kHz carrier (**Fig 1.5A,B**). The EFR data (**Fig 1.10C,D**) showed the same trends as seen in the ABR, however, the noise-induced changes in EFR were more robust: the scatter was smaller, and the inter-group difference were clearer. Changes to EFR PLV were similar to changes in EFR amplitude. This phase-locking measure may be particularly useful when signal-to-noise is poor (Zhu et al., 2013).

To more quantitatively assess the separability of control vs. noise-exposed groups in EFRs and ABRs, we calculated amplitude ratio and effect size as a function of level (**Fig 1.11**). Several general trends are seen regardless of electrode configuration. First, as suggested from the mean data, the effect sizes are higher with EFRs than with ABRs at all but the highest sound pressure levels, where EFRs become less affected by neuropathy, while effects on ABRs increase (**Fig 1.11, A-F**). This tendency likely reflects the fact that AN synchrony to amplitude-modulated tones rises with sound pressure level to a peak and then falls, whereas rate response to pure tones rises to saturation and does not decline with further level increases.

The second general trend emerging from the effect size and ratio data (**Fig 1.11**) is that effects of neuropathy are minimal on both ABR and EFR at low sound levels. This trend is consistent with the idea that the noise damage is selective for fibers with low SRs and higher thresholds (Furman et al., 2013): since they don't normally contribute to either EFRs or ABRs at near-threshold levels, their loss does not affect the amplitudes of either.

Thirdly, it is important to consider the effects of modulation frequency. Across all electrode configurations, the most robust intergroup differences were seen with modulation frequencies between 820 and 1330 Hz. Using a higher modulation frequency, e.g. 1810 Hz, was less robust

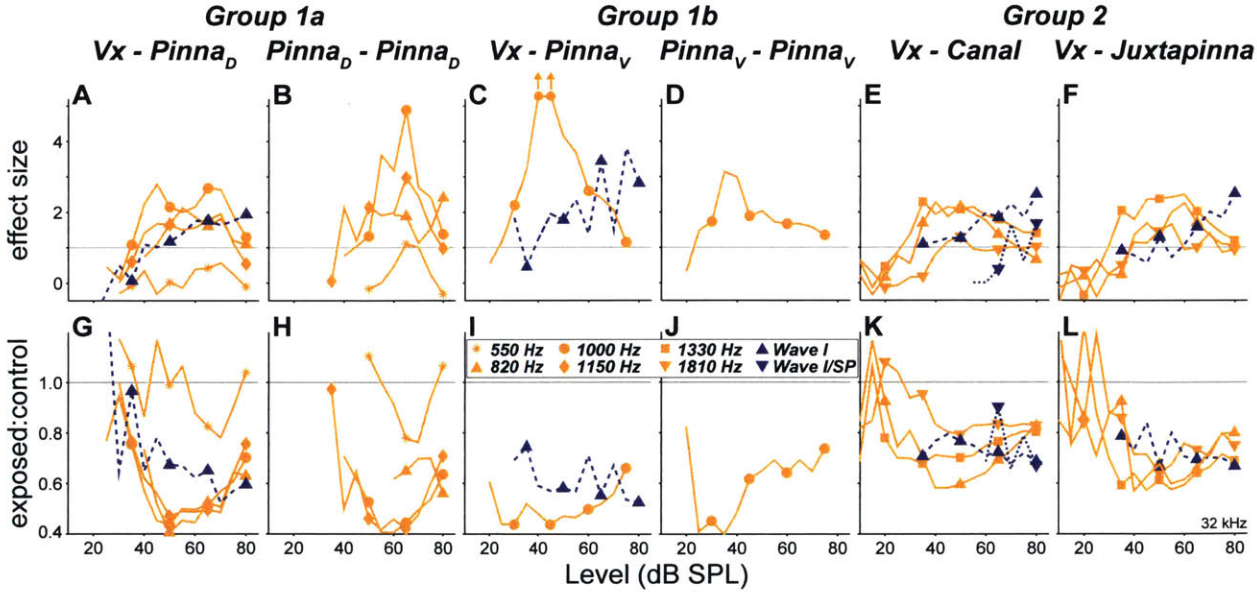

Figure 1.11. EFR is a more powerful measure of cochlear neuropathy than ABR, and effect sizes are largest at moderate SPLs. **A-F,** Effect sizes (Hedge's g) for pairwise comparison between each noise-exposed group and its respective controls for both ABR (purple) and EFR (orange) measures. **G-L,** Simple ratios for the same pairwise comparisons shown in **A-F**. For clarity, only levels at which mean responses were one standard deviation above the mean noise floor are displayed. Key applies to all panels. Up-arrows in **C** show that the effect sizes were off-scale: 7.01 and 7.03 at 40 and 45 dB SPL, respectively.

in detecting neuropathy, presumably because at such a high frequency, the hair cell contributions begin to dominate the responses. EFRs were also less useful at low modulation frequencies, e.g. 550 Hz (**Fig 1.11A,B,G,H**), perhaps due to a larger contribution from more central generators, less affected by neuropathy due to central compensation (**Fig 1.9**).

Lastly, choice of electrode configuration also affected the maximum effect size. Separation was best for the Group 1a pinna to pinna configuration (**Fig 1.11B**), despite a lack of AN dominance evidenced in the group delays (**Fig 1.7M**). Effect sizes were not as high in Group 1b (**Fig 1.11D**), suggesting that small differences in electrode location can strongly affect the results (see also **Fig 1.7F** vs. **7H**). The electrode configuration chosen to maximize contributions from the AN (vertex to ear canal) did not produce maximal effect sizes (**Fig 1.11E**), although response amplitudes were increased (**Fig 1.7I**). This presumably reflects the fact that the proximity of the ear canal to the cochlea increases the size of the hair cell contributions as well as the AN contributions. These sources are separable in ABRs, so the increased AN signal increases effect size. Since they are mixed in EFRs, hair cell potentials decrease effect size since they are not altered by the neuropathy.

There were no differences in mean SP amplitude between control and neuropathic groups, indicating no hair cell dysfunction (see waveforms in **Fig 1.7C**). Intra-subject variability in ABR amplitudes caused by slight differences in anatomy or electrode placement might affect SP and wave I equally. Therefore, we wondered if normalizing wave I amplitude by SP in each case could improve the ability to detect neuropathy. However, effect sizes calculated from the wave I : SP ratio were lower than those for wave I alone (**Fig 1.11E** downward- vs. upward-pointing triangles). Analysis of the individual waveforms revealed that SP and wave I amplitudes were not correlated within each group (data not shown).

In one of our noise-exposed groups, neuropathy was accompanied by high-frequency threshold shift and OHC loss at the basal end of the cochlea (**Fig 1.4**, Group 1b). Since clinical cases with OHC damage superimposed on cochlear neuropathy are likely to be common, it is useful to compare it with cases of pure neuropathy. Unlike in Group 1a (**Fig 1.11G**), amplitudes in exposed ears were reduced even at low SPLs (**Fig 1.11I**). If this reduction were due to a substantial loss of both low- and *high*-SR fibers, ratios would further decrease as SPL increases to moderate levels due to the decreased low-SR contribution. Since ratios do not decrease, EFR changes are likely the result of a combination of hair cell dysfunction and low-SR fiber loss. Due to low inter-subject variability, EFR effect size was very high, peaking to 7.0 at 45 dB SPL (**Fig.11C**).

EFR and ABR variability due to anatomical variation might be minimized by within-subject normalization. In humans, correlations between EFR amplitude and psychophysical performance are improved by using the slope of the EFR amplitude vs. modulation-depth function (Bharadwaj et al., 2015). Transforming the data in Figure 11 into slope-vs.-level functions significantly improved (decreased) exposed:control ratios (mean 0.45, $t_{(20)} = 3.17$, $p = 0.005$), but did not significantly enhance effect sizes (two-sided paired t-test, $t_{(20)} = 1.05$, $p = 0.31$). Normalization may have been ineffective because anatomical variation in genetically identical mice is smaller than in humans,

and therefore may not be a substantial source of variability.

For all groups and electrode configurations, neuropathic effects on EFR amplitude decrease at high levels, while effects on ABR increase (**Fig 1.11,** bottom). This is likely due to differences in AN responses to SAM tones vs. tone-pips. Whereas responses to tone-pips saturate at 10 to 20 dB above threshold, modulated rate to SAM tones peaks around 30 dB above threshold, then decreases with increasing level (**Fig 1.1A** vs. **B**). Thus, as sound level increases, the proportion of the EFR generated by fibers with CFs at the carrier frequency decreases (**Fig 1.1D,F**). Above the low-SR modulated rate peak (~50 dB SPL, vertical dashed blue line), basal spread of excitation causes the high-SR contribution to increase, and the impact of low-SR loss is reduced. Since the low-SR response to tone pips does not decrease at high levels, the impact of low-SR loss on the ABR increases at high levels (**Fig 1.1C,E**). Furthermore, the neuropathy at the base of the cochlea (64 kHz) is less pronounced than at the carrier frequency (32 kHz; **Fig 1.4D**), thus the overemphasis of EFRs on off-CF contributions further reduces its detection power at high levels.

EFR measures in BK-knockout ears

We compared the low-SR specific noise-induced neuropathy with a model affecting all SR groups equally: mice with targeted deletion of the large-conductance, Ca^{2+}-activated K^+ channel (BK). These KO mice show lower sound-evoked discharge rates, for all SR groups, without any significant alterations in OHC function, as demonstrated by normal DPOAEs (Oliver et al. 2006). As seen in the control CBA/CaJ mice used in the noise experiments, the FVB/NJ control mice from the BK KO strain show amplitude-vs.-modulation-frequency functions with two broad peaks, one at ~500 Hz and a second at ~1000 Hz (**Fig 1.12**). In the KO mice, as expected, EFR amplitude (**Fig 1.12A,B**) and PLV (data not shown) were significantly reduced at both 11.3 and 32 kHz carrier frequencies. Furthermore, the BK deletion caused an EFR reduction across all tested modulation frequencies, perhaps because the BK channel is also expressed in neurons

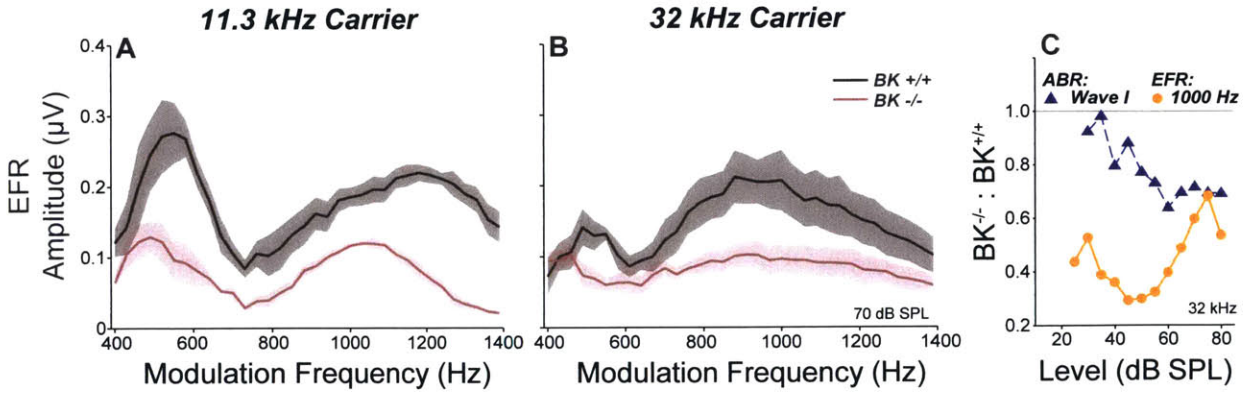

Figure 1.12. BK channel knockout decreases EFR amplitudes over a wide range of carrier frequencies, modulation frequencies, and levels. **A,B,** Mean EFR amplitudes (±SEMs) for 11.3 kHz (**A**) and 32 kHz carriers (**B**) at 70 dB SPL in BK knockout mice ($BK^{-/-}$) and wildtype controls ($BK^{+/+}$). There was a main effect of exposure by three-way repeated-measures ANOVA: $F_{(1,16)} = 27.1$, $p < 0.001$ and significant paired effects at both 11.3 ($p < 0.001$) and 32 kHz ($p = 0.011$). **C,** Mean EFR amplitude ratios as a function of stimulus level for the 32-kHz carrier at 1-kHz modulation. All responses were measured using the vertex to $pinna_D$ electrode configuration.

throughout the central auditory pathways (Sausbier et al., 2006).

We measured EFR amplitude-vs.-level functions at the same modulation frequencies used in the noise experiments (820 for 11.3 kHz and 1000 Hz for 32 kHz). EFR amplitude and PLV (not shown) were both reduced as in noise-induced neuropathy. However, in contrast to the results seen after noise, the response reduction in the BK KO mice occurred even at stimulus levels just above threshold (**Fig 1.12C**). Reductions continued to increase up to 50 dB SPL, consistent with a deficit in all SR groups without any hair cell dysfunction (contrast with **Fig 1.11I**, where reductions are present at threshold, but do not increase with level). While EFR amplitude reductions were greater than in noise-exposed mice, ABR wave I amplitude reductions were smaller. There are three possible reasons for this difference: (1) BK deletion causes a larger decrease in AN steady-state rate than in onset rate (Oliver et al., 2006), (2) although IHC time constants are increased in BK KOs, many AN fibers have normal onset rates and first-spike latencies (Oliver et al., 2006), and (3) unlike ABR wave I, the EFR contains contributions from central auditory neurons, which likely also express BK.

DISCUSSION

Contributions of low- vs. high-SR fibers to ABR vs. EFR: insight from single-fiber studies

Single-fiber recordings suggest that the noise-induced cochlear neuropathy observed in the present study is selective for the subset of AN fibers with low SR and high threshold (Furman et al., 2013). By "low SR" we mean the fiber groups initially characterized in cat as "low" and "medium" SR, i.e. the low-rate peak of the bimodal distribution of SRs, which includes ~40% of the AN population. Although neuropathy was detected by both ABR and EFR, the changes in EFRs were more robust (**Fig 1.11**). The differences between the tests can be understood based on known differences in the responses of high- vs. low-SR fibers to the different stimuli used to generate these auditory evoked potentials; i.e. short tone bursts for ABR vs. continuous amplitude-modulated tones for EFR.

As schematized in **Fig 1.1A**, the ratio of peak to steady-state rate is higher in high-SR fibers than low-SR fibers (~3.5 vs. ~2.5 in mice, Taberner and Liberman, 2005). Since the ABR is dominated by onset responses, the contribution of low-SR fibers to ABR wave I is smaller than their relative numbers (~40% of the population) would predict. Recordings after selective damage by ouabain administration indicate that fibers with the lowest SRs (< 1 sp/sec) contribute little to ABR wave I amplitude (Bourien et al., 2014).

A second important factor is the SR-related difference in response synchrony (**Fig 1.1B**). AN responses to amplitude-modulated tones can be quantified in terms of their average rate and synchronization index, i.e. the extent to which spikes are phase-locked to a periodic stimulus (Joris and Yin, 1992; Cooper et al., 1993). Although the maximum modulated rate (the amplitude of the period histogram at the modulation frequency) of low-SR fibers can be lower than their high-SR counterparts, the maximum synchronization index (0.5*modulated rate/average rate)

is typically higher, because there are fewer spontaneous (and therefore non-stimulus-locked) spikes in the response. Theoretically, EFR amplitude is proportional to the modulated rate of contributing neurons. Thus, when average rates are comparable (i.e. at moderate-to-high levels), the enhanced synchrony of the low-SR fibers makes their EFR contribution larger than their relative numbers would predict.

Low-SR thresholds to pure tones and SAM tones are 10-20 dB higher than for their high-SR counterparts (Joris and Yin, 1992; **Fig 1.1B**). Therefore, loss of low-SR fibers should affect neither ABR nor EFR amplitudes until stimulus levels exceed ~30 dB SPL. This prediction is confirmed by the amplitude ratios between normal and neuropathic mice plotted vs. stimulus level (**Fig 1.11, bottom**). However, it seems that even a small amount of threshold shift causes amplitude reduction at low stimulus levels, masking the low-SR specificity of the neuropathy (**Fig 1.4A**, Group 1b). Correspondingly, EFR reduction is visible in BK KO mice even at the lowest stimulus levels (**Fig 1.12**), consistent with impairment in responses from all SR types (Oliver et al., 2006). A detailed model incorporating a continuous distribution of SR and CF would be able to incorporate EFR changes across multiple stimulus conditions, perhaps revealing more sensitive techniques to pinpoint the etiology of sensorineural hearing loss.

Generators of the EFR

Neurons throughout the auditory pathway can follow the envelope of amplitude-modulated sounds and therefore can theoretically contribute to the EFR (Kuwada et al., 2002). Unlike ABRs, the different cellular generators of EFRs are not separable in the time-domain response. However, evidence suggests that different generators dominate the response at different modulation frequencies. The high-frequency limit of phase-locking to modulation frequency decreases as the signal ascends the auditory pathway (see complete reference list in Fig. 9 of Joris et al., 2004). Spiral ganglion neurons exhibit a lowpass modulation transfer function (MTF) with a cutoff frequency around 1 kHz for high-CF neurons. Cochlear nucleus neurons are more heterogeneous: bushy cell MTFs are also lowpass, with cutoff frequencies only slightly lower than the AN, while stellate and octopus MTFs vary, trending from lowpass to bandpass as level increases, with cutoff frequencies generally lower than those of bushy cells (Frisina et al., 1990). Inferior colliculus and auditory cortex neurons, on the other hand, have upper cutoff frequencies around 400 Hz and 60 Hz respectively. Therefore, at the highest modulation frequencies, EFRs should be dominated by the AN and cochlear nucleus, while at lower modulation frequencies responses could be generated by several sources. Consistent with these predictions, anesthesia or sleep reduces EFR amplitudes at low modulation frequencies only (Pethe et al., 2001; Kuwada et al., 2002; Parthasarathy and Bartlett, 2012), and lesions of the inferior colliculus reduce EFRs at 20-200 Hz modulation frequencies (Tsuzuku, 1993; Kiren et al., 1994).

EFR group delay, i.e. the slope of the phase-vs.-modulation-frequency function (**Fig 1.5G,H 7, bottom**), can be used to infer the underlying generators. Kuwada et al (2002) reported that each successive peak in rabbit EFR MTFs had a shorter group delay, suggesting a progression

from central to peripheral sources with increasing modulation frequency. Here, group delays decreased above 1500 Hz to closely match the SP wave of the ABR indicating domination by IHC receptor potentials (Durrant et al., 1998). Eliminating AN (and central auditory) activity via ouabain confirmed this hypothesis (**Fig 1.6**); EFR group delay indicated that only one source remained. However, even in intact animals, group delay varied little with modulation frequency below 1500 Hz, as reported by others (Pauli-Magnus et al., 2007), and the small changes observed were in the unexpected direction (shorter for lower frequencies).

The use of group delay to infer latency becomes complicated when multiple sources with different latencies are contributing. The addition of two sources with different latencies results in an amplitude function that fluctuates with modulation frequency and yields a delay equal to a weighted sum (by their amplitudes) of the two source delays at amplitude peaks (Shera and Bergevin, 2012). Addition of more than two sources, as is generally the case in EFRs, further complicates the interpretation.

According to our effect-size analysis, modulation frequencies near 1 kHz produced the most robust detection of low-SR neuropathy (**Fig 1.8**). The decreased effect of neuropathy at lower modulation frequencies may reflect increased contribution from higher centers with less prominent noise-induced response reductions, possibly due to changes in "central gain" as suggested by prior studies of noise damage (Gu et al., 2012; Robertson et al., 2013; Schaette, 2014) and by present ABR data (**Fig 1.9**). The decreased effect of neuropathy on EFRs at higher modulation frequencies may reflect an increased contribution of hair cells, which have an even higher corner frequency than the AN (Kidd and Weiss, 1990; Greenwood and Joris, 1996). For most electrode configurations, the group delay near 1 kHz modulation frequency was 2 ms, i.e. similar to the latency of ABR peak II (**Fig 1.7, top**), which according to lesion studies in the cat, is generated by bushy cells of the cochlear nucleus (Melcher and Kiang, 1996). As argued above, such a group delay is not inconsistent with contributions from both AN and cochlear nucleus. While stellate cells contribute little to the ABR, since their modulation phase-locking is much better than that of bushy cells and AN fibers (Frisina et al., 1990), their EFR contribution may be more substantial. However, since 1 kHz is above the upper cutoff frequency of most stellate cells, using a high modulation frequency may isolate the response to AN fibers and bushy cells.

EFRs should be most sensitive to cochlear neuropathy when using an electrode configuration that elicits a response dominated by the AN. As expected, placing an electrode closer to the cochlea increased the AN response in the ABR (**Fig 1.7C**). However, increased SPs indicated that this configuration also increased the hair cell response, which is unaffected by noise-induced primary neural degeneration. This complicated the EFR MTF, reducing in a complex way the range of modulation frequencies sensitive to the cochlear neuropathy (**Fig 1.8A,** purple line). Placing the electrode farther from the ear canal produced smaller overall signal amplitudes, but smoother MTFs (**Fig 1.7A,B,D**). Although group delays indicated significant contributions from sources central to the AN, the effect size analysis suggested that the pinna-to-pinna configuration is the most sensitive to noise-induced cochlear neuropathy (**Fig 1.8**). Indeed, this configuration

might be expected to minimize the contribution of the symmetrically positioned inferior colliculus, and to maximize the contribution of asymmetrically positioned peripheral generators.

Detecting low-SR synaptopathy in humans

The number of AN fibers per hair cell decreases with age in both mice and humans (Makary et al., 2011; Sergeyenko et al., 2013), perhaps due to accumulated noise exposure. Indeed, Individuals with a history of noise exposure, despite normal audiometric thresholds, have poorer EFRs (Plack et al., 2014; Bharadwaj et al., 2015), which may be caused by low-SR neuropathy. ABR and EFR amplitudes are reduced in aged rats, but ABR reductions are greater than predicted by changes in EFRs (Parthasarathy et al., 2014). In the present study, effects of neuropathic noise were level-dependent; at high levels, reduction was greater in ABRs than EFRs, at moderate levels, reduction was greater in EFRs (**Fig 1.11**). As discussed above, these changes are consistent with AN single-unit responses. Further exploration of the utility of ABR and EFR in teasing apart changes due to aging vs. noise-exposure *per se* requires measurements using the same species and electrode configurations.

While a decrease in ABR or EFR amplitudes can be used to detect low-SR neuropathy in mice, in humans the amplitudes of these evoked responses are highly variable, at least partially because of heterogeneity in head size, tissue resistance and electrode placement: thus, diagnosis will be more difficult (Gorga et al., 1988; Nikiforidis et al., 1993). In humans, correlations between EFR amplitudes and perceptual measures can be improved by within-subject normalization (Bharadwaj et al., 2015). In the present dataset, intergroup differences were not improved by a slope transformation, possibly due to the relatively low inter-subject anatomical variations in genetically identical mice. ABR amplitudes are also more variable in outbred guinea pigs than in mice, however they can be used for detecting cochlear neuropathy after normalizing by pre-exposure amplitudes (Furman et al., 2013). This type of normalization may also be possible in some clinical scenarios.

The present study was motivated, in part, by the idea that EFR phase measures might be more robust to heterogeneity-induced amplitude variability. Noise-induced neuropathy caused similar reductions in PLV and amplitude (**Figs 1.5,1.10**), but PLV effect size was lower, indicating that amplitude is a more robust indicator of neuropathy in this case. However, since PLVs may be more reliable than amplitudes when signal-to-noise is poor (Zhu et al., 2013), they may be especially useful in clinical settings where extensive averaging is not possible.

Under optimized parameters, EFRs are more sensitive to neuropathy than ABRs. These optimal parameters succeed because they bias responses toward peripheral neural generators while minimizing contributions from hair cells. Optimal modulation frequency is near the high-frequency cutoff of peripheral generators (~1 kHz here) and ideal electrode configuration is one that increases ABR wave I without increasing SP. In humans, using a high modulation frequency may be especially important because it minimizes the contribution from higher centers where responses are influenced by learning (Anderson et al., 2013; Strait and Kraus, 2014) and arousal levels (Kuwada et al., 2002). While responses can be measured in humans at modulation frequencies

as high as 1 kHz, amplitudes are low. It is not yet clear what constitutes the best compromise. Due to differences in anatomy, optimal parameters differ between species. EFR group delay can be used to estimate EFR generators, and determine these parameters. Application of these principles in humans will improve detection of neuropathy, leading to a more refined diagnosis of sensorineural hearing loss.

ACKNOWLEDGMENTS

We thank Leslie Liberman for expert assistance in cochlear immunostaining, and Yanbo Yin and Mingjie Tong for their assistance in the ouabain experiment. We thank Andrea Meredith for providing the BK knockout mice.

Chapter 2

Effects of neuropathy on spontaneous and evoked activity in the inferior colliculus

Luke A. Shaheen and M. Charles Liberman

ABSTRACT

Tinnitus and hyperacusis are life-disrupting perceptual abnormalities that are often preceded by acoustic overexposure. Animal models of overexposure have provided a tentative link between behavioral changes suggestive of these abnormalities and neural correlates: elevated spontaneous rates (SRs) and elevated evoked responses. Prior work has focused on changes in central auditory structures; thus, the required degree of cochlear damage, if any, is unclear. While tinnitus and hyperacusis can occur in humans with normal audiometric thresholds, a recent discovery that moderate noise overexposure can cause cochlear nerve damage without threshold elevation opens the possibility that cochlear neuropathy may be required for the genesis of these perceptual pathologies. We tested this hypothesis by recording responses in the mouse inferior colliculus (IC) following a bilateral, neuropathic noise exposure. SRs were not increased in mice recorded while awake, or under anesthesia. Furthermore, contrary to prior work, SRs were also unaffected by more intense, or unilateral exposures. These results indicate the neither neuropathy nor hair cell loss are sufficient to cause elevated SRs in the IC. Since evidence of a correspondence between IC SR elevation and tinnitus is weak, it remains possible that neuropathy may be involved in the genesis of tinnitus. Tone-evoked rate-level functions at the characteristic frequency (CF) were steeper following the neuropathic exposure, specifically in the region of maximal neuropathy. Furthermore, responses to off-CF tones indicated a reduction in sideband inhibition. Both changes were especially pronounced in mice recorded while awake. These findings align with a previous demonstration of elevated acoustic startle in neuropathic mice, and indicate that neuropathy may initiate a compensatory response in the central auditory system leading to the genesis of hyperacusis.

INTRODUCTION

Tinnitus, the perception of sound when no sound is physically present, is often preceded by an episode of acoustic overexposure (Eggermont and Roberts, 2004). Acoustic overexposure can cause increased spontaneous rates (SRs) across the auditory pathway, including in the ventral and dorsal cochlear nucleus (DCN), inferior colliculus (IC) and auditory cortex (Brozoski et al., 2002; Bauer et al., 2008; Seki and Eggermont, 2003). Since overexposed animals have been inferred to have a tinnitus-like percept by behavioral tests, hyperactivity is hypothesized to be a neural correlate of tinnitus (Brozoski et al., 2002; Longenecker and Galazyuk, 2011). However, the relationship between neuronal hyperactivity and a tinnitus-like percept is not straightforward: in animals given identical noise exposure the number displaying a reduction in the gap-induced prepulse inhibition (PPI) of the acoustic startle reflex, indicating a tinnitus like-percept, ranges from 50 to 80%. While SRs in the DCN are elevated only in animals with reduced PPI (Dehmel et al., 2012; Koehler and Shore, 2013; Li et al., 2013), SRs in the IC and auditory cortex are elevated regardless of PPI (Engineer et al., 2011; Coomber et al., 2014; Ropp et al., 2014). Furthermore, DCN ablation before noise exposure prevents the emergence of a tinnitus-like percept as assessed by conditioned suppression, the same ablation performed 3-5 months after noise exposure has no effect (Brozoski and Bauer, 2005; Brozoski et al., 2012). Hyperactivity in the IC follows a similar pattern: cochlear ablation up to four weeks post-exposure causes a return of spontaneous rates to control levels, but ablation eight or more weeks post-exposure does not (Mulders and Robertson, 2009, 2011).

It is not clear how much cochlear damage, if any, is necessary to cause hyperactivity. Although threshold shift is a primary risk factor in humans (Roberts et al., 2010), tinnitus can occur without threshold shifts (Gu et al., 2010, 2012; Schaette and McAlpine, 2011). Elevated SRs and behavioral evidence for tinnitus have also been observed in animals where acoustic overexposure caused little to no permanent threshold shift (Bauer et al., 2008; Koehler and Shore, 2013). Moderate noise exposures that do not cause hair cell damage or permanent threshold shift can cause a loss of synapses between cochlear hair cells and auditory nerve (AN) terminals, followed by a slow degeneration of AN cell bodies and central axons (Kujawa and Liberman, 2009). Such a cochlear neuropathy would not be apparent in an audiogram, but may be detected by reductions in evoked response amplitudes such as the auditory brainstem response (ABR) and envelope-following response (Bharadwaj et al., 2015; Shaheen et al., 2015). Since tinnitus patients with normal thresholds have reduced ABR wave I amplitudes, it is possible that these individuals have some cochlear neuropathy.

Hyperacusis, an intolerance to high-level sounds, often co-occurs with tinnitus and like tinnitus, is often preceded by an episode of acoustic overexposure (Kreuzer et al., 2012). In humans with hyperacusis, sound-evoked MRI responses are increased in the auditory midbrain, thalamus, and cortex (Gu et al., 2010). In animal models, acoustic overexposure can result in elevated evoked responses in the ascending auditory pathways (Salvi et al., 1990; Cai et al., 2009; Auerbach et al., 2014). Since hyperacusis can occur in humans with normal audiograms, but is often associated

with acoustic overexposure, cochlear neuropathy may be a necessary catalyst in the generation of hyperacusis.

Most prior work on noise-induced central hyperactivity has not paid close attention to the condition of hair cells and/or cochlear nerve fibers, nor the possible correlations between peripheral pathology and central physiology. While identically-exposed animals develop behavioral evidence of tinnitus at rates ranging from 30 to 70% (Engineer et al., 2011; Dehmel et al., 2012; Li et al., 2013; Rüttiger et al., 2013), these studies did not determine whether variability is related to differences in peripheral insult or central compensation. We tested if both spontaneous and sound-evoked hyperactivity are caused by cochlear neuropathy per se by measuring responses in the IC of mice exposed to noise calibrated to induce cochlear neuropathy with minimal hair cell loss, and to more intense noise that caused both neuropathy and hair cell loss. Exposure-induced peripheral pathologies were carefully quantified using a combination of cochlear histology and physiology. Spontaneous rates were not increased in either group relative to controls, indicating that neither cochlear neuropathy nor hair cell loss is sufficient to cause increased spontaneous rates in the IC. However, tone-evoked rate-level functions were steeper following exposure, specifically in the region of maximal cochlear neuropathy, suggesting that neuropathy plays a role in hyperacusis.

METHODS

Animals and groups: Seven week-old male CBA/CaJ mice were exposed awake and unrestrained to octave-band noise (8-16 kHz) for 2 hrs, within a cage suspended directly below the horn of the loudspeaker in a small, reverberant chamber. Noise calibration to target SPL was performed immediately before each exposure session. Control mice were of the same age, gender, and strain, but were not exposed to the noise. Two groups of mice were used to measure IC responses while awake: 1) control (8 mice) and 2) exposed at 98 dB SPL (6 mice). Three groups of mice were used to measure IC responses under anesthesia: 1) control (13 mice), 2) exposed at 98 dB SPL (10 mice) and 3) exposed at 103 dB SPL (6 mice). An additional three groups of mice were exposed unilaterally while under ketamine (100 mg/kg i.p.) and xylazine (20 mg/kg i.p) anesthesia in a closed sound field using a Realistic 40-1377 speaker (RadioShack, Ft. Worth, TX). Exposures were conducted in an acoustically and electrically shielded room held at 30° C, and a stable anesthetic plane was maintained by 1/3 initial dose booster of both Ketamine and Xylazine every 40 minutes. To minimize exposure to the contralateral ear, mice were exposed on their side and saline-soaked cotton balls were placed in their contralateral ear. These three groups were exposed to: 1) 101 dB SPL (2 mice), 2) 103 dB SPL (2 mice), and 3) 104 dB SPL (2 mice) and used to measure IC responses under anesthesia.

All procedures were approved by the Institutional Animal Care and Use Committee of the Massachusetts Eye and Ear Infirmary.

Preparation for Anesthetized IC recordings: A single session was conducted in each animal, occurring 1-3 weeks post-exposure. Mice were anesthetized with ketamine (100 mg/kg i.p.)

and xylazine (20 mg/kg i.p) with boosters administered as needed. Surgical procedures and recordings were conducted in an acoustically and electrically shielded room held at 30° C. Prior to surgery, DPOAEs and ABRs were measured as described below. Then, the pinnae were removed bilaterally to allow for closed-field acoustic stimuli to be presented using two custom acoustic assemblies, each containing two electrostatic drivers (CUI CDMG15008-03A) and an electret condenser microphone (Knowles FG-23329-P07). The assemblies were calibrated with a ¼-inch Bruel and Kjaer condenser microphone and in-ear calibrations were performed at the onset of each experiment.

A small craniotomy was made over the central nucleus of the inferior colliculus using a scalpel. The dura mater was left intact and covered with high viscosity silicon oil. Recordings were made using a 16-channel, single-shank silicon probe (25 or 50 µm contact separation, 177 μm^2 contact area; NeuroNexus Technologies). Electrodes were inserted dorso-ventrally, along the tonotopic axis, and advanced using a micropositioner (Kopf 607-C). While the central nucleus of the IC is easy to visualize in mice, electrode placement was confirmed by the tonotopic organization and sharp frequency tuning.

Preparation for Awake IC recoding: Two to five days following noise exposure, mice were anesthetized with ketamine and xylazine. The skin overlying the frontal and parietal portions of the skull was retracted and a titanium headplate was affixed to the skull using acrylic bonding material to allow for head-fixed recordings (C&B MetaBond, Parkell). Buprenorphine (0.1 mg/kg s.c.) and meloxicam (0.03 mg/kg s.c.) were given and animals were allowed to recover for at least 48 hours. Recording sessions began as soon as one week post-exposure and continued until three weeks post-exposure; each session lasted up to three hours. One to nine (median 3) recording sessions were conducted in each mouse. At the onset of each session mice were anesthetized with isoflurane in oxygen (2%, 2L/min). In the first session a craniotomy was made over the IC as in the anesthetized recordings. A ring around the craniotomy site was formed using a UV cure resin and the craniotomy was filled with high viscosity silicon oil. The same craniotomy was used in subsequent sessions. Cyanoacrylate was used to affix a 1.8 mm rigid plastic tube to each ear canal. Anesthesia was discontinued and the mouse was transferred to the recording apparatus, where it was head fixed but free to run on a freely rotating 22-cm diameter turntable beneath its feet. The ear tubes were coupled to the acoustic assemblies for closed field sound delivery and in-ear calibration was performed. DPOAEs were monitored throughout the session to ensure that the acoustic environment remained constant. Animals were continuously monitored and the session was ended for the day if they showed signs of persistent distress. Recordings were made using the same electrodes as were used in the anesthetized experiments. At the conclusion of each session the mice were again anesthetized with isoflurane and the ear tubes were removed. The craniotomy was cleaned and flushed with saline, then covered with a thin layer bacitracin and sealed with UV cure resin. 3-weeks post exposure, animals were anesthetized with Ketamine/ Xylazine and DPOAEs and ABRs were recorded. At the conclusion of these recordings, mice were sacrificed for histology.

IC recording: Custom LabVIEW and MATLAB software controlling National Instruments 24-bit digital input/output boards generated all stimuli. Stimuli were presented using a 200 kHz sampling rate. Raw signals from the electrodes were digitized at 32 bit, 24.4 kHz (RZ5 BioAmp Processor; Tucker-Davis Technologies) and stored in binary format. For awake recordings the point-by-point median of all channels was subtracted from each channel, greatly reducing motion-induced artifacts. Single units were isolated online using a PCA-based sorting method in SpikePac software (Tucker-Davis Technologies). Units were later reprocessed offline using a combination of custom MATLAB software and the Ultra Mega Sort 2000 package (Hill et al., 2011). Raw waveforms were filtered both forward and backward using a fourth-order 300 – 5000 Hz Butterworth filter. Spikes were detected by threshold crossings above 3.5 standard deviations of the waveform in intervals far removed from sound presentation. Threshold crossings occurring less than a 0.6 ms "shadow" period after another spike were removed to prevent the same spike being counted twice due to noise. Single units (SUs) were then sorted by: aligning spike waveforms to the peak, reducing dimensionality using PCA, overclustering using k-means (k>32), and merging clusters based on the interface energy between clusters and violations of the absolute refractory period (Hill et al., 2011). Three example sorts are shown in Figure **S1.1**. Candidate SUs were then checked for good isolation by their separation from other clusters (center-left), estimated number of sub-threshold waveforms (center-right), and interspike interval distributions (right). The majority of channels contained 0 or 1 well-isolated SUs, but some channels contained up to 2 SUs. In some cases, especially for awake recordings, movement of the brain relative to the skull caused SUs to drift from channel to channel, at times back and forth between channels. In these cases spikes were detected and aligned from included channels independently, waveforms were concatenated, and the single-channel procedure was followed beginning with PCA.

Multi-unit and current source density: Multi-unit responses were collected by setting the spike threshold to 3.5 standard deviations of the neural activity (filtered 300 - 5000 Hz) during periods of silence presented during recording of FRAs. Sites that had strong single-unit responses were excluded to avoid biasing the sample.

Current source density was computed by: 1) filtering the raw waveforms using a fourth-order lowpass Butterworth filter with a cutoff of 350 Hz, 2), subtracting the mean of the first 2 ms from each trial, 3) averaging across trials, 4) smoothing using a 2-pass, 3-point moving average, and 5) computing the second spatial derivative across the electrode array. P1 and N1 were calculated from the CSD trace as the peaks and valleys in the trace 4-15 ms and 7-20 ms post-stimulus onset, respectively. Since N1 represents current sinks that are likely dominated by excitatory synaptic potentials, and because it was larger and more stable, it was used in the calculation of most CSD-level functions. CSD-vs.-level functions were also created by the average of the CSD waveform over 5 to 55 ms re stimulus onset.

Stimuli: The search stimulus was a broadband noise burst presented at 60 dB SPL, alternating sides on each presentation.

Frequency Response Areas: Frequency Response Areas (FRAs) were collected by

pseudorandom presentation of tone pips (50 ms on, 200 ms off, 4 ms raised cosine onset/offset ramps) to the ear contralateral to the recording site. Between 2 and 4 trials were collected per tone/level combination. Tone frequencies were a subset of frequencies from 3 kHz to 70 kHz, spaced in 0.1 octave increments. The specific subset was set to cover the response range of the neurons under investigation (generally 2 to 3 octaves wide). In mice recorded under anesthesia, levels were 10 to 80 dB SPL in 5 dB steps, in mice recorded awake, levels were -5 to 80 dB in 5 dB increments. For both groups, a silent condition was added to the list of levels to be randomized. Spontaneous rate (SR) was calculated as rate over the entire 250 ms of this these trials, averaged across trials and 'frequencies.' Thus, the total time used to calculate SR ranged from 10 to 30 seconds. FRAs were calculated over a time window 5 to 55 ms re stimulus onset. The excitatory region of the FRA was determined by setting all FRA pixels below 5 standard deviations of the SR above the SR to zero, grouping non-zero pixels into regions connected by edges, and finding the region with the largest average rate * (number of pixels)^2. This procedure successfully determined the excitatory region for the largest range of FRA shapes, and manual intervention was required only rarely. The CF was defined as the frequency producing the highest response at the lowest responsive level, and the BF as the frequency producing the largest average response across all levels within the excitatory region. The bandwidth 10 dB above threshold (BW_{10}) was calculated as the width of the excitatory region.

Binaural Noise Response Areas: Binaural noise response areas (BNRAs) were collected by pseudorandom presentation of concurrent, dichotic noise bursts (50 ms on, 200 ms off, 4 ms raised cosine onset/offset ramps). Noise was limited from 4 kHz to 80 kHz and shaped to be flat-spectrum by correction for the frequency response of the acoustic system in the frequency domain. Ipsilateral and contralateral levels were randomly varied independently, and 5 trials were collected per level combination. Levels were chosen to encompass the dynamic range of the neurons under investigation, in anesthetized mice this was generally 20 to 70 dB SPL, while in awake mice this was 10 to 70 dB SPL, both in 5 dB steps. As for the FRAs, a silent condition was added to the list of levels to be randomized, so that responses to both contralateral noise alone and ipsilateral noise alone were randomized into this stimulus set. Rate was calculated as an average over a time window 5 to 55 ms re stimulus onset. Single-units were segregated on the basis of responses to BNRAs, see *Results*.

Fits to rate-level functions: Rate-level functions at CF and BF were calculated from FRAs and fit with a four-parameter model (Sachs and Abbas, 1974; Heil et al., 2011). This model specifies firing rate r as a function of sound pressure P (in Pa) by:

$$r(P) = R_D \frac{P^N}{K+P^N} + R_S, \quad \text{and}$$

$$K = 2 * 10^{-5} * 10^{\frac{L_{50}}{20}},$$

where R_D is the driven rate, R_S is the spontaneous rate, N characterizes the steepness of the curve

and L_{50} gives the level at 50% of the driven rate range. Non-monotonic functions were manually selected and fit using the sum of two such models, yielding seven parameters:

.

$$r(P) = R_{D1}\frac{P^{N_1}}{K_1+P^{N_1}} + R_{D2}\frac{P^{N_2}}{K_2+P^{N_2}} + R_S.$$

Curves were fit by *fminsearchbnd*, a bounded version of the built-in MATLAB function *fminsearch* using a least-squares method. Fit was then refined by a robust procedure that iteratively refined weights of each data point before re-fitting.

DPOAEs and ABRs: ABRs and DPOAEs were collected under Ketamine/Xylazine anesthesia. Stimuli were presented unilaterally to one ear at a time, with the mouse on its side, and the acoustic assembly just above the ear canal. After a complete dataset was collected for one ear the procedure was repeated for the other ear.

DPOAEs were recorded in response to two tones f_1 and f_2, each presented to separate speakers to reduce system distortion (frequency ratio f_2/f_1 = 1.2, and level difference $L_1 = L_2 + 10$ dB). DPOAE response was measured at $2f_1$-f_2 by Fourier analysis of the ear-canal sound pressure waveform. Stimulus duration was 1.6 seconds at each level combination (L_2 varied from 20 to 80 dB SPL in 5 dB steps). Threshold was defined as the interpolated f_2 level producing a DPOAE of 5 dB SPL.

ABRs were recorded differentially with subdermal needle electrodes with the common ground at the base of the tail. A dorsal-ventral incision at the intertragal notch of the ipsilateral pinna was made to allow direct visualization of the eardrum. For mice used in anesthetized IC recordings, electrodes were placed vertex (positive electrode) to ipsilateral pinna, with the latter just caudal to the intertragal notch (see Shaheen et al 2015). In mice used for awake IC recordings, the headplate prohibited recording from the vertex. Therefore, responses were measured from both 1) headplate to ipsilateral pinna, and 2) contralateral pinna to ipsilateral pinna. Due to intra-subject variability in the headplate surgery, ABR amplitudes were more variable for the first electrode configuration. Thus, results are reported for the second (interaural) configuration. Pinna electrodes were placed slightly more ventral along the antitragus in order to increase the early ABR waves ($Pinna_V$ in Shaheen et al 2015).

Responses were amplified 10,000X using two Grass P511 amplifiers with a 0.3-3 kHz passband. ABRs were evoked with 5-mesc. tone-pips with 0.5 msec. cos^2 rise–fall presented in alternating polarity at a rate of 40/s. Tone-pip frequencies were 11.3 or 32 kHz. Trials where the response amplitude exceeded 15 μV were rejected; 512 artifact-free trials of each polarity were averaged to compute ABR waveforms. Threshold was defined by visual inspection of the stacked waveforms as the lowest level at which a reproducible peak or trough appears, which usually occurs one level-step below that at which peak-to-peak amplitude begins to grow.

Cochlear Immunostaining and Innervation Analysis: Mice were perfused intracardially with 4% paraformaldehyde. Cochleas were decalcified, dissected into half-turns and incubated in primary antibodies: 1) mouse (IgG1) anti-CtBP2 from BD Biosciences at 1:200 and 2) mouse (IgG2)

anti-GluA2 from Millipore at 1:2000. Primary incubations were followed by 60-min incubations in species-appropriate secondary antibodies. Cochlear lengths were obtained for each case, and a cochlear frequency map computed using a custom ImageJ plugin (http://www.masseyeandear.org/research/otolaryngology/investigators/laboratories/eaton-peabody-laboratories/epl-histology-resources/) that translates cochlear position into frequency according to the published map for the mouse (Müller et al., 2005; Taberner and Liberman, 2005). Confocal z-stacks from each ear were obtained using a glycerol-immersion objective (N.A. =1.4) and 3.17X digital zoom on a Leica TCS SP5 confocal. Synapses in the IHC area were counted using Amira (Visage Imaging) to find the xyz coordinates of all the ribbons (CtBP2-postiive puncta), and custom re-projection software was then used to assess the fraction of ribbons with closely apposed glutamate-receptor patches (i.e. GluA2 puncta).

Statistical Analysis: Statistical testing was performed in MATLAB; functions used are indicated in italics. For spontaneous rates, distributions were normal (assessed with Lilliefors test), so differences were assessed using a 3-way ANOVA (*anovan*). Significant post-hoc differences were assessed using *multcompare* with a Tukey-Kramer correction for multiple comparisons. Rate- and CSD-level functions distributions were normal (assessed with Lilliefors test), so differences were assessed using a using a 3-way repeated measures ANOVA (*rmanova*) with a Tukey-Kramer correction for post-hoc tests. Threshold, maximum driven rates, and slopes were not normally distributed, especially for multi-units and CSDs. Therefore, differences were assessed with paired rank-sum tests. 6 comparisons were made to test effects of exposure, and a Bonferroni-Holm correction was applied. To test effects of anesthesia, populations were pooled across exposure for each frequency bin. Therefore, these tests were corrected for 3 comparisons.

RESULTS

Noise-induced Synaptic Loss after Reversible Noise-Induced Threshold Shift

We exposed 7-wk old mice to an 8-16 kHz, 98 dB SPL noise band for two hours, which our previous work has shown is sufficient to cause substantial cochlear neuropathy with minimal hair cell damage (Shaheen et al., 2015; Valero et al., 2016). As in the previous work, this exposure resulted in a 40 to 50% loss of synapses between inner hair cells (IHCs) and auditory nerve fibers (ANFs) in the basal half of the cochlea (**Fig 2.1A**). No damage to IHCs was observed (data not shown), and loss of OHCs was confined to the extreme basal end of the cochlea (**Fig 2.1D**). We divided the cochlear frequency space into three regions on the basis of the peripheral profile: 'non-neuropathic' (< 16 kHz), where noise exposure caused no effect on thresholds, hair cells, or synaptic counts, 'neuropathic' (16-32 kHz), where exposure caused neuropathy without hair cell damage, and 'threshold-shift' (>32 kHz), where exposure caused neuropathy with some hair cell damage. This same exposure was conducted in two groups of mice, one destined for awake IC recordings, and one for anesthetized IC recordings; in both cases mice were noise-exposed while awake and unrestrained. For efficiency, histology was only conducted in the group used for awake IC recordings, but is presumed to be similar in the unmeasured group, based on extensive

experience with this exact exposure in the Liberman lab (Shaheen et al., 2015; Valero et al., 2016).

Consistent with the morphology, DPOAE and ABR thresholds were not significantly elevated except for at 45 kHz, where DPOAE thresholds were elevated by 5-10 dB (**Fig 2.1B,D**). ABR wave I amplitudes were reduced at 32 kHz, consistent with the synaptic loss in that region (**Fig 2.1C**). DPOAE amplitudes were reduced at 45 kHz, consistent with the DPOAE threshold shift, indicating some OHC damage in that region (**Fig 2.1F**).

Spontaneous rates were unchanged following bilateral neuropathic noise exposure

We examined the central nucleus of the inferior colliculus (IC) of noise-exposed mice for signs of hyperactivity via single unit responses using single-shank, 16-channel silicon electrodes. In the first group of mice, responses were measured under ketamine/xylazine anesthesia, in a single session one to three weeks following noise exposure. Spontaneous rates ranged from 0 to 50 spikes/sec in both control and noise-exposed mice, but were not affected by noise-exposure over any CF region (**Fig 2.2A**).

Anesthesia has a strong effect on IC responses, including spontaneous rates (Torterolo et

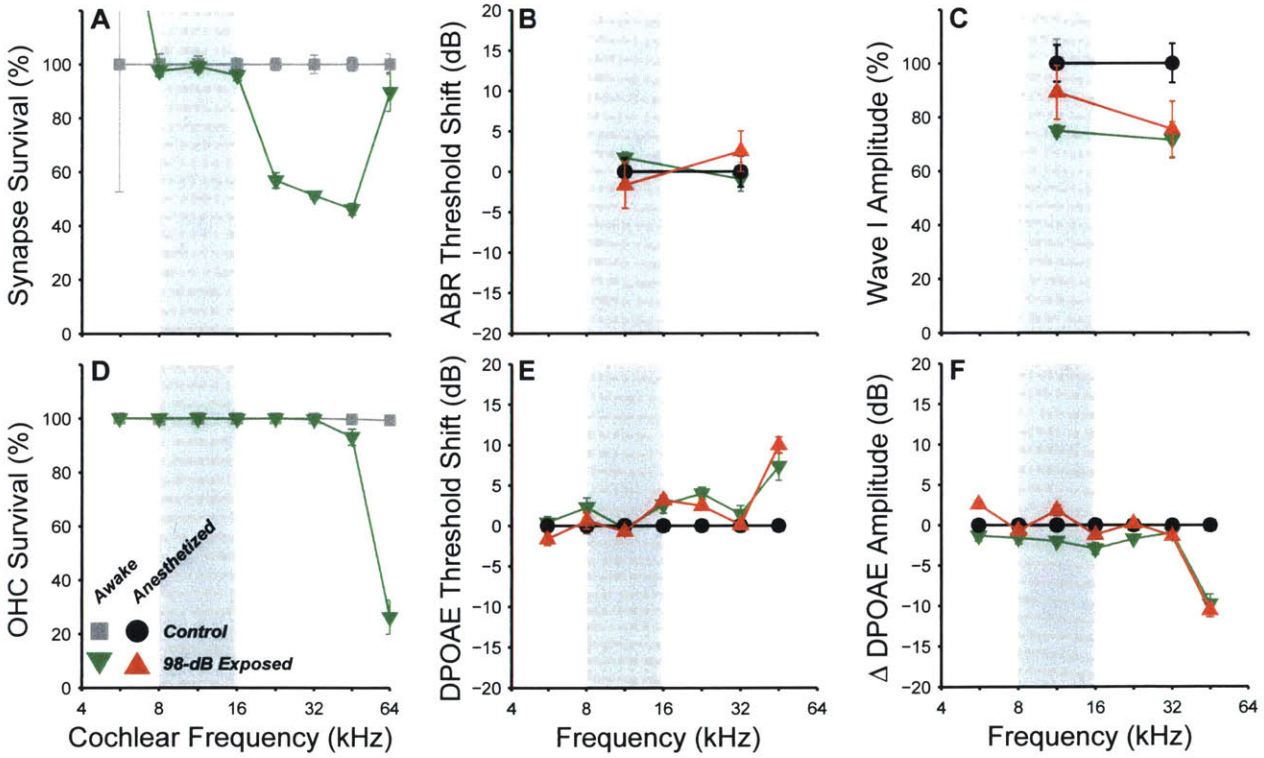

Figure 2.1. Noise-exposure causes permanent synaptic loss with minimal permanent threshold shift. **A,D** Mean IHC synapse and OHC survival following 98-dB exposure in mice used for the awake IC recordings. **B,E,** Mean ABR (**B**) and DPOAE thresholds (**E**) in mice used for both awake (grey, green) and anesthetized (black, red) recordings. **C,F,** Mean change in ABR Wave I (**C**) and DPOAE (**F**) amplitudes, averaged over stimulus levels of 60 to 80 dB SPL. Error bars indicate SEMs. Each group is normalized to its respective control.

al., 2002; Chung et al., 2014). Therefore we recorded responses from a group of awake, head-restrained mice. One to ten (median three) recording sessions were conducted in each mouse, starting from one week post-exposure and ending three weeks post-exposure. Spontaneous rates ranged from 0 to 130 spikes/sec and were significantly elevated relative to anesthetized mice (**Fig 2.2B**). However, there was no effect of noise exposure on spontaneous rates.

SR means were calculated over three CF regions and the significance of effects was evaluated using a three-way ANOVA (**Fig 2.2C**). The main effect of anesthesia was highly significant ($F_{1,436}$ = 110, p<<0.001), but effects of exposure and frequency region were not ($F_{1,436}$ = 0.9, p=0.3; $F_{2,436}$ = 2.6, p=0.08). Post-hoc tests did not reveal significant effects of exposure in any frequency region.

Spontaneous rates were also unaffected by unilateral or more intense exposures

Most studies of noise-induced SR elevation in the inferior colliculus have used more intense noise exposures, causing a greater amount of cochlear pathology (ex. Mulders and Robertson, 2009). Therefore, we raised the noise exposure level to 103 dB SPL while holding all other parameters constant. At this intensity, exposure caused > 40 dB of permanent threshold shift across a wide range of frequencies (**Fig 2.3A,B,** blue diamonds). Surprisingly, spontaneous rate still remained unchanged relative to controls (**Fig 2.4A,B**).

While elevated spontaneous rates have been observed following bilateral exposures, since the majority of studies have used unilateral exposures, we repeated measurements of spontaneous rates in three groups of unilaterally-exposed mice. The exposure band and duration were held constant, but mice were exposed while under ketamine/xylazine anesthesia using a closed-field speaker. Mice exposed to 101 and 103 dB did not exhibit any significant permanent change in DPOAE thresholds (**Fig 2.3A,B,** cyan & magenta), while mice exposed to 104 dB exhibited up

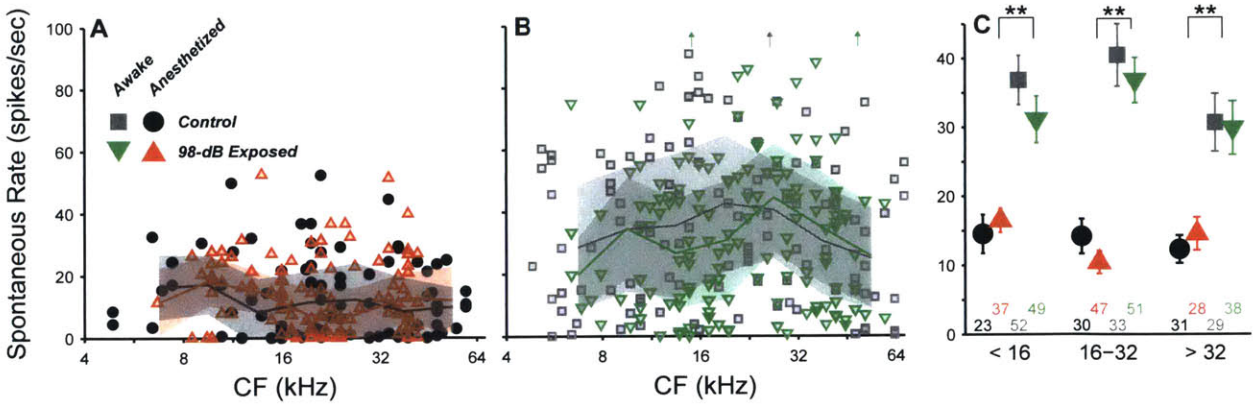

Figure 2.2. Spontaneous rates are unchanged following neuropathic noise exposure. **A,B** Spontaneous rates (SRs) in single-units of control (black, grey) and 98-dB exposed mice (red, green), recorded under anesthesia (**A**), and awake (**B**). While SRs were significantly deceased in anesthetized mice, SR was not affected by exposure in either group. Lines and clouds indicate medians and interquartile ranges, pooled over one-octave bands. **C,** Mean (± SEM) SR binned across cochlear frequencies where noise exposure caused no effect (< 16), neuropathy without hair cell damage (16-32) and neuropathy with some hair cell damage (>32). Black stars indicate significant effects of anesthesia (p<0.001, Tukey-Kramer-corrected post-hoc test following a 3-way ANOVA). Off-axis SRs in **B** were 110, 131, and 104 from left to right.

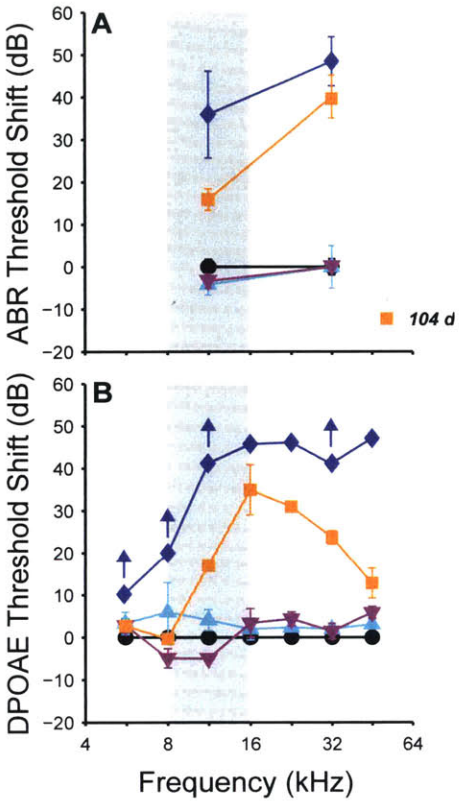

Figure 2.3. Peripheral thresholds in additional noise-exposed groups. **A,B,** Mean ABR (**A**) and DPOAE thresholds (**B**), each normalized to the control group. 103-dB bilateral exposure was conducted while mice were awake and resulted in >40 of threshold shift (blue). Unilateral exposures were conducted while mice were anesthetized. 101- and 103-dB exposures (cyan and magenta) resulted in no threshold shift, while 104-dB exposure (orange) caused shifts of up to 30 dB. Error bars indicate SEMs.

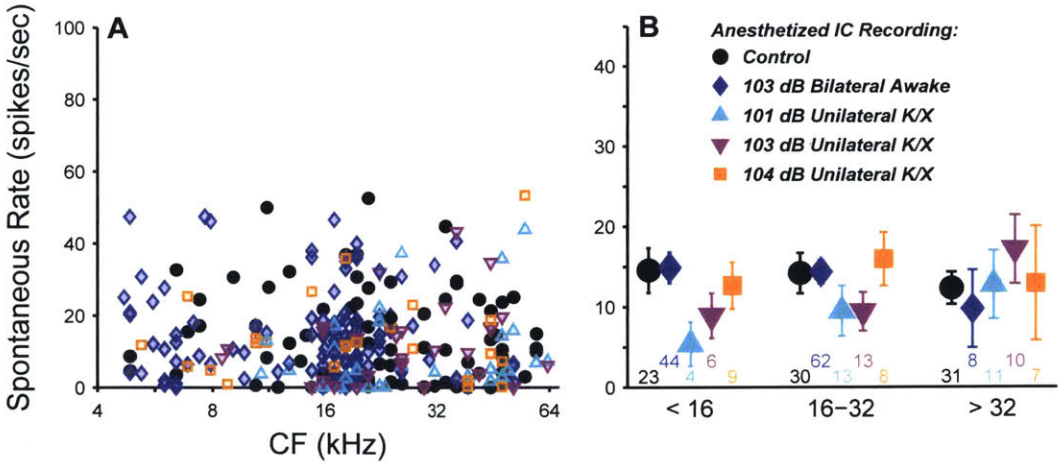

Figure 2.4. Spontaneous rates are not elevated when noise exposure is more intense or unilateral. **A,** SRs in single-units of control (black) and exposed mice. All IC recordings were conducted under K/X. SR was not affected in mice exposed bilaterally to 103 dB while awake (blue diamonds), or to mice exposed unilaterally while under K/X (cyan, magenta, and orange). **B,** Mean (± SEM) SR binned across cochlear frequencies as in **Figure 2.2**.

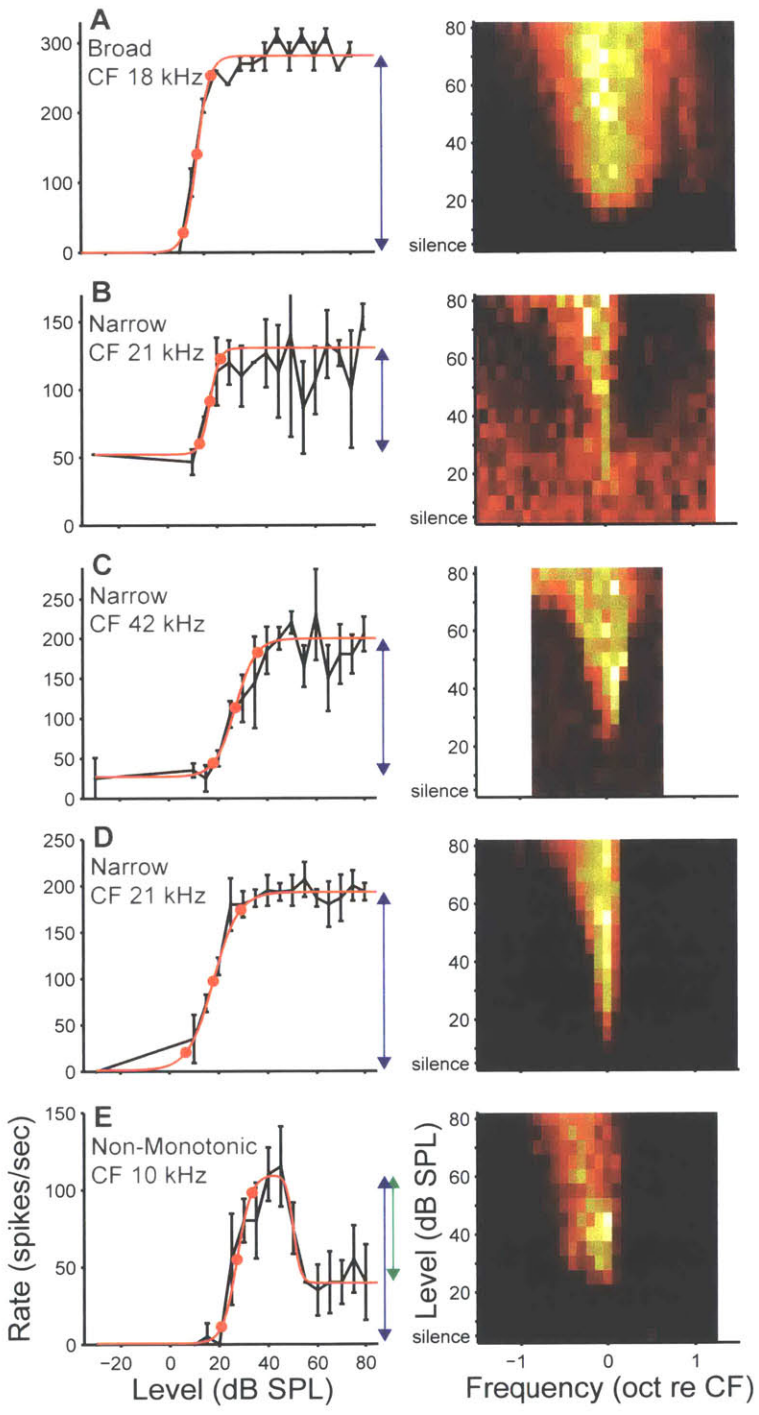

Figure 2.5. Unit types based on frequency response areas. **A-E, Right,** Frequency response areas for five example single-units in control mice. Color scale indicates firing rate, normalized to that unit's maximum rate. **A-E, Left,** Rate responses to a tone at CF. Black points indicate mean rate and standard error. Red indicates fit and the 10, 50, and 90% of the excitatory driven rate range (E_D, blue arrow). Inhibitory driven rate (I_D) is indicated in **E** by green arrow. E/I Balance in this unit: $(E_D - I_D) / (E_D + I_D) = 0.36$.

to 30 dB of permanent threshold shift (orange). Mean spontaneous rate was unchanged relative to controls in all three of these groups (**Fig 2.4**). A two-way ANOVA demonstrated no effect of exposure or frequency region ($F_{4,264} = 0.8$, $p = 0.5$; $F_{2,264} = 0.3$, $p = 0.7$). In sum, in our hands spontaneous rate was not elevated in the mouse IC following an 8-16 kHz, 2 hour noise exposure regardless of anesthesia, intensity or laterality. However, it remains possible that spontaneous rate could be affected by untested combinations of these parameters (for example following a unilateral neuropathic exposure on awake mice, more narrowband exposures, or neuropathic exposures in other species).

Spontaneous rate was unchanged for all tone response types

The central nucleus of the IC (ICc) receives feed-forward axonal projections from nearly-all brainstem auditory nuclei, and it's physiological responses reflect this diversity of input (Ito et al., 2015). The presence and pattern of the inhibition in frequency response areas (FRAs) has been used to divide ICc neurons into response types V, I and O, which were suggested to arise due to dominant inputs from the medial

superior olive (MSO), lateral superior olive (LSO), and dorsal cochlear nucleus (DCN), respectively (Ramachandran et al., 1999).

While there is some anatomical evidence for division of inputs by source into "synaptic domains" at the circuit level (Ito et al., 2015), there also may be significant overlap between inputs from different sources at the regional level (Cant, 2005; Schofield, 2005). Synaptic integration of ICc neurons by a heterogeneous mixture of inputs is further supported by an analysis of a large dataset of FRAs that indicates that that indicates that response types form a continuous distribution rather than falling into discrete classes (Palmer et al., 2013).

With the understanding that that the distribution is continuous, it still may prove informative to divide the population into discrete classes, as such division by has revealed type-specific changes to SR at more damaging exposure levels (Ropp et al., 2014). Therefore, we used FRAs to divide neurons into three discrete classes based on the bandwidth of excitation and the presence of on-CF inhibition (Egorova et al., 2001; Ma et al., 2006). Broad units had a V-shaped excitatory area and a wide bandwidth on both the low *and* high-frequency sides, and a total bandwidth at 10 dB above threshold (BW_{10}) of at least one octave (**Fig 2.5A, Fig S2.1B**). Narrow units had an excitatory area ranging from V- to I-shaped with a particularly narrow bandwidth on the high-frequency side and a BW_{10} of less than one octave (**Fig 2.5B-D**). Non-monotonic units also had a BW_{10} less than one octave and further demonstrated on-CF inhibition at high levels (**Fig 2.5E**).

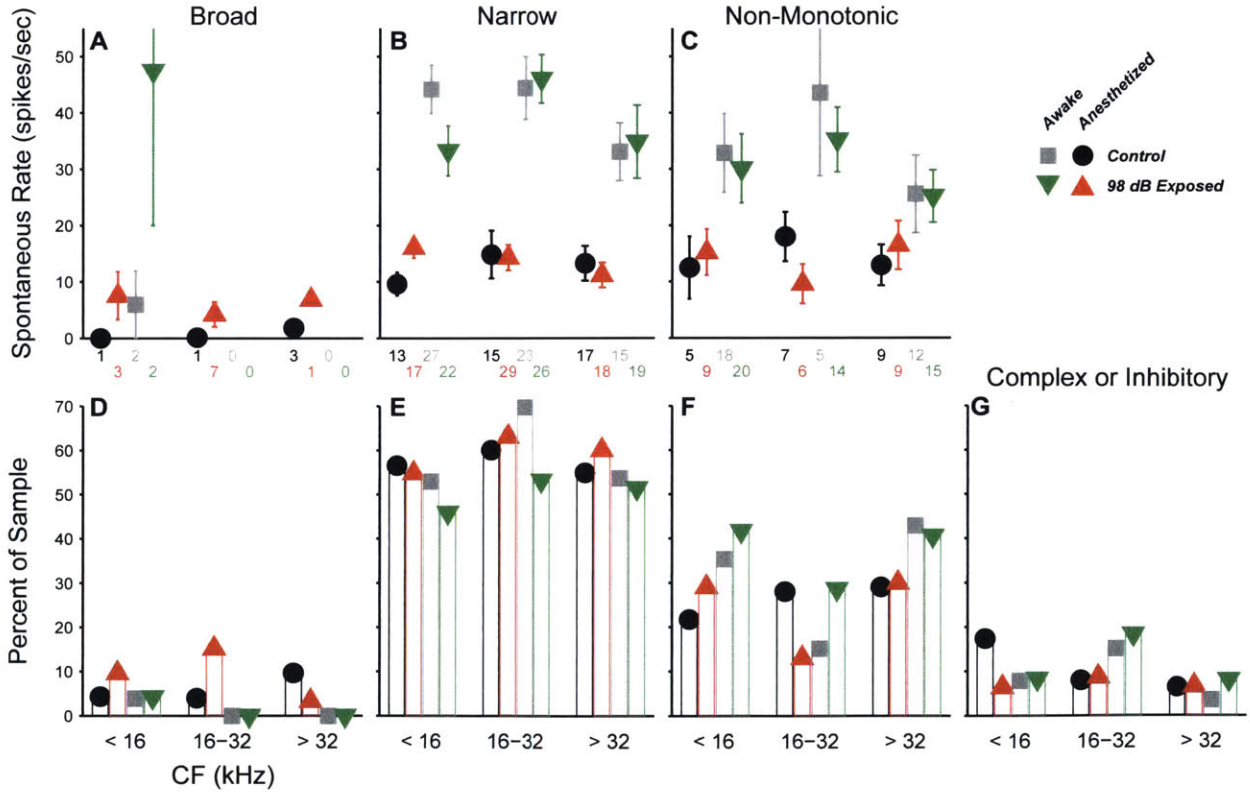

Figure 2.6. Spontaneous rates are unchanged for all tone frequency response types. **A-C** SRs divided into broad (**A**), narrow (**B**), and non-monotonic (**C**) unit types. Groups and colors are the same as in Fig 2. **D-G** Percent of units classified to each type out of the total number found in each frequency bin/animal group. **G,** Percent of neurons that did not fit into one of the three categories, spontaneous rates not shown.

Inhibition most often was moderate (E/I Bal > 0) but in some cases was strong, causing the rate to tones at CF to drop below the spontaneous rate (E/I Bal <0; **Fig S2.2A;** see methods). The frequency extent of this inhibition varied, causing upward-tilting, downward-tilting, and Type O FRA shapes (Palmer et al., 2013). About 10% of units did not fit into these types and were classified at "Other". These included units that were purely inhibitory, had multiple separated excitatory areas, or had CFs that were greater than ½ octave removed from the local multi-unit CF.

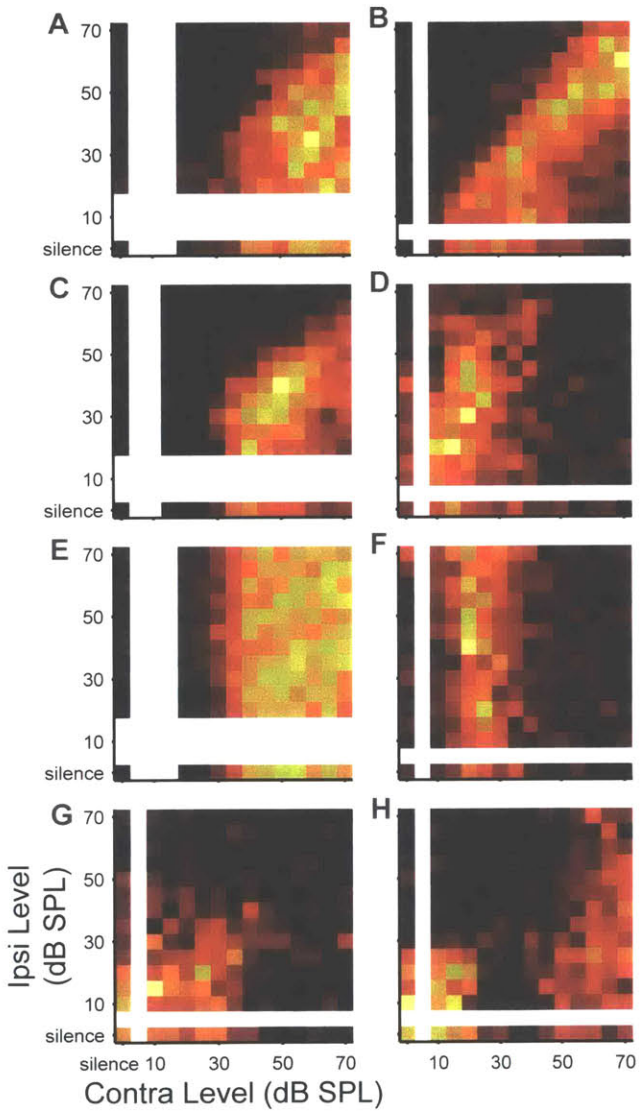

Figure 2.7. Unit types based on binaural noise response areas. **A-D,** Binaural noise response areas for 8 example single-units in control mice. Color scale indicates firing rate, normalized to that unit's maximum rate. **A,** Excitatory/Inhibitory (EI). **B,** Excitatory/ Inhibitory (EI), contra-nonmonotic. **C,D** Excitatory/ Inhibitory with ipsilateral facilitation (EI/f), contra-nonmonotic. **E,** Excitatory/No Response (EO). **F,** Excitatory/No Response (EO), contra-nonmonotonic. **G,** Inhibitory/Inhibitory (II), **H,** Inhibitory/Inhibitory (II), contra-nonmonotonic.

Summed across all groups, the population was 55% narrow, 30% non-monotonic, 5% broad, and 10% other. We calculated the proportions within each anesthesia group and frequency band separately, and compared them across exposure condition (**Fig 2.6D-G**). The differences in proportions were small, and a χ^2 analysis did not reveal any significant differences due to exposure (Anesthetized [<16 kHz: χ^2_3= 2.2, p=0.1, 16-32 kHz: χ^2_3 = 3.8, p=0.05, >32 kHz: χ^2_3= 1.0, p=0.3]; Awake [<16 kHz: χ^2_3= 0.5, p=0.5, 16-32 kHz: χ^2_3= 2.3, p=0.1, >32 kHz: χ^2_3= 0.5, p=0.4]) or anesthesia (Control [<16 kHz: χ^2_3= 2.3, p=0.13, 16-32 kHz: χ^2_3= 3.2, p=0.08, >32 kHz: χ^2_3= 3.7, p=0.05]).

A three-way ANOVA confirmed what is visually obvious: there were no within-type effects of exposure on SRs (**Fig 2.6A-C**). Among narrow units, the effect of anesthesia was highly significant ($F_{1,228}$ = 107, p<<0.001), but effects of exposure and frequency bin were not ($F_{1,228}$ = 0.1, p=0.8; $F_{2,228}$ = 2.7, p=0.07). The same was true for non-monotonic units ($F_{1,117}$ = 18, p<<0.001; $F_{1,117}$ = 0.3, p=0.6; $F_{2,117}$ = 0.8, p=0.5). The number of units in the broad and other categories was too small to make a meaningful comparison of SRs.

Narrow monotonic units are typically subdivided into Type V and Type I units on the basis of the bandwidth of excitatory

tuning and presence of inhibitory sidebands (Ramachandran et al., 1999). In this dataset 75% of narrow units had inhibitory sidebands (ranging from barely-detectable to substantial) and 10% had no detectable sidebands (**Fig 2.5B&C**). The remaining 15% had SRs near zero; assessment of sidebands in these neurons would require a two-tone stimulus paradigm, which was not collected (**Fig 2.5D**). SR was not affected by exposure within any of these subgroups (data not shown).

Spontaneous rate was unchanged for all binaural response types

The binaural response properties of IC neurons can also be used to infer their dominant sub-collicular inputs. Canonically, neurons that are excited by ipsilateral sound receive dominant inputs from the MSO, neurons inhibited by ipsilateral sound (EI) receive dominant inputs from the LSO, and neurons unaffected by ipsilateral sound (EO) receive dominant inputs from the CN (Davis et al., 1999). We constructed binaural noise response areas by playing broadband noise to both ears simultaneously, randomly varying the level in each ear. The majority of neurons (62%) were excited by contralateral noise and inhibited by ipsilateral noise (EI; **Fig 2.7A**). The strength of both ipsilateral and high-level contralateral inhibition varied substantially in this group. Neurons that were inhibited by contralateral sound at low levels, but excited at higher levels were also included in this group (for ex. **Fig 2.7H**). Consistent with the high-frequency hearing and underdeveloped MSO of the mouse, no EE neurons were encountered (Irving and Harrison,

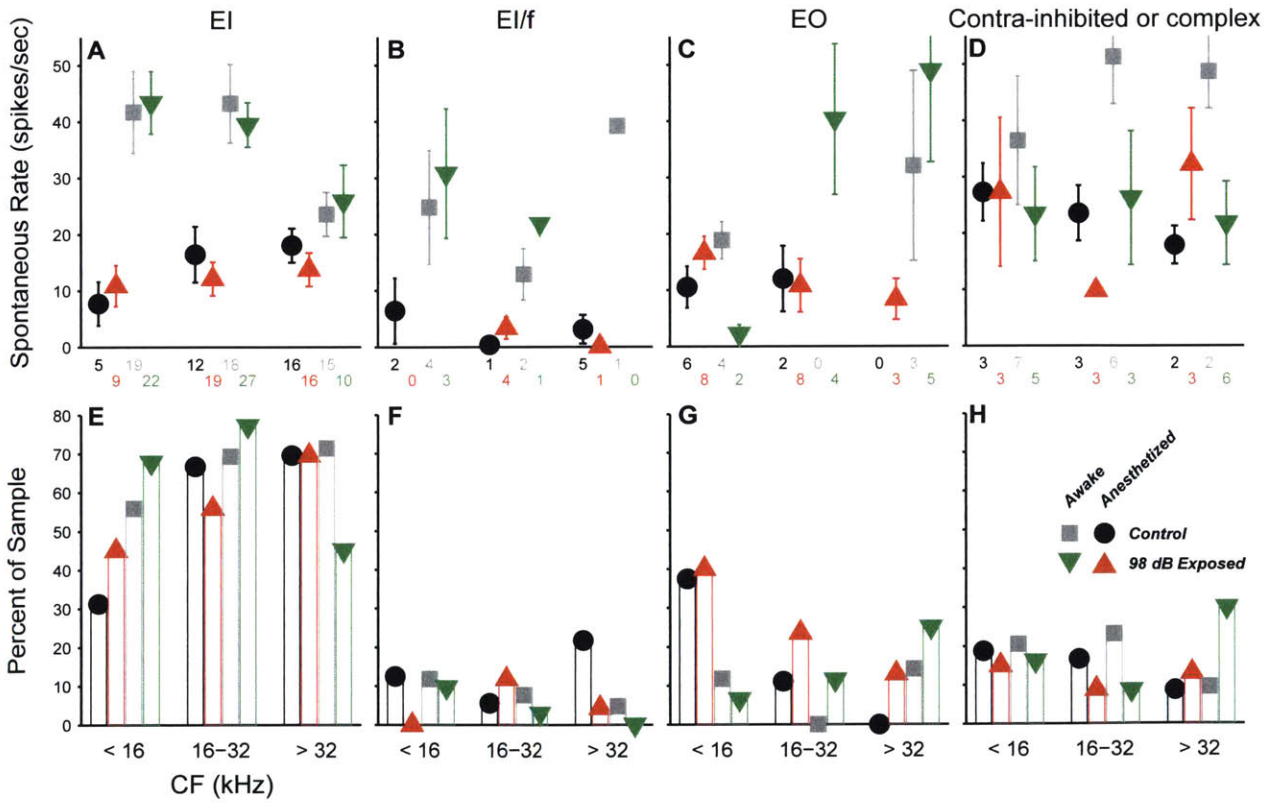

Figure 2.8. Spontaneous rates are unchanged for all binaural noise response types. **A-D** SRs divided into Excitatory/Inhibitory (EI; **A**), Excitatory/Inhibitory with ipsilateral facilitation (EE/f; **B**), Excitatory/No Response (EO; **C**), and Inhibitory/Inhibitory (II), Inhibitory/No Response (IO), or complex (**D**) unit types. **E-H** Percent of units classified to each type out of the total number found in each frequency bin/animal group.

1967; Ollo and Schwartz, 1979). While there were no neurons driven by ipsilateral noise alone, about 8% of neurons were *facilitated* by ipsilateral noise (EI/f; **Fig 2.7C,D**; Park and Pollak, 1993; Davis et al., 1999). 15% of the population was driven by contralateral noise and unaffected by ipsilateral noise (EO; **Fig 2.7E&F**). The remaining neurons (15%) were inhibited by contralateral noise (**Fig 2.7G**), were not driven by noise, or had more complex shapes. We calculated the proportions of neurons in each class within each anesthesia group and frequency band separately, and compared them across exposure condition (**Fig 2.8E-H**). A χ^2 analysis for differences in the population was significant in the >32 kHz anesthetized, 16-32 kHz awake, and >32 kHz awake cases (χ^2_3= 5.8, p=0.015; χ^2_3= 5.9, p=0.015; χ^2_3= 5.0, p=0.026 respectively). However, samples sizes were small, and after applying Yate's correction for small samples no significant differences remained (p=0.09; p=0.09; p=0.13).

There were no within-type effects of exposure on SRs (**Fig 2.8A-D**). Among EI units, the effect of anesthesia was highly significant ($F_{1,174}$= 47, p<<0.001), but effects of exposure and frequency bin were not ($F_{1,174}$ = 0.1, p=0.8; $F_{2,174}$ = 2.4, p=0.09). The number of units in the other categories was too small to make a meaningful comparison of SRs.

Because the number of neurons concentrated in the EI group was so large, neurons were also

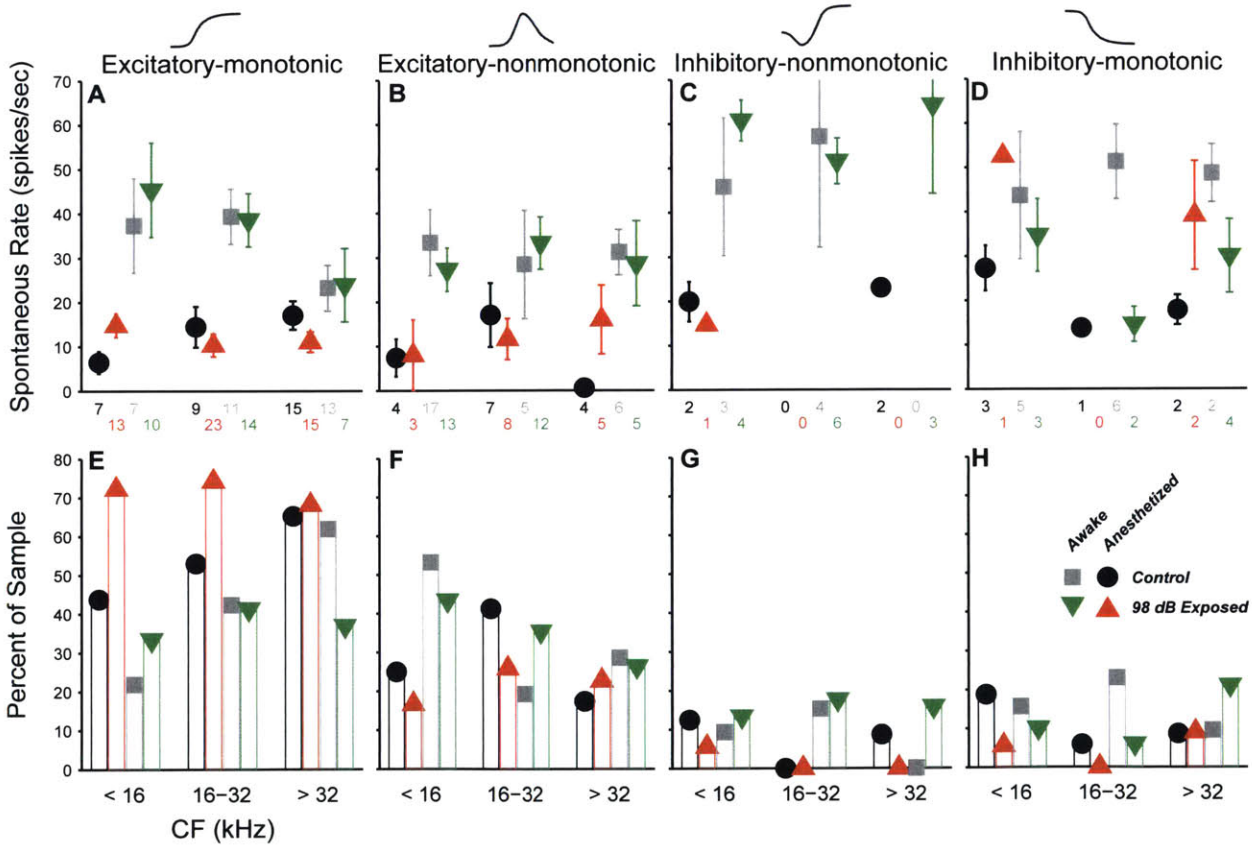

Figure 2.9. Spontaneous rates are unchanged for all contralateral noise response types. **A-D** SRs divided by response to contralateral broadband noise only, in order of increasing presence of inhibition: Excitatory-monotonic (**A**), Excitatory-nonmonotonic (**B**), Inhibitory-nonmonotonic (**C**), and Inhibitory-monotonic (**D**). **E-H** Percent of units classified to each type out of the total number found in each frequency bin/animal group

divided based on the shape of their rate-level responses to contralateral noise alone. Schematized responses are shown at the top of **Fig 2.9,** arranged in order of increasing presence of inhibition: excitatory-monotonic neurons had strictly-increasing functions, excitatory-nonmonotonic neurons had functions that rose and then fell, inhibitory-nonmonotonic neurons had functions that fell and then rose, and inhibitory-nonmonotonic neurons had functions that strictly decreased. No significant differences were found in either the proportion of neurons in each class, or the SR within each class (**Fig 2.9**)

The slope of the response to tones was elevated in neuropathic mice

Noise exposure can cause elevated evoked responses in the ascending auditory pathways, for example: increased local field potential amplitudes and slopes in the IC (Salvi et al., 1990; Auerbach et al., 2014) and elevated maximum rates and slopes in VCN neurons (Cai et al., 2009). Hyperactive evoked EEG and fMRI signals are found humans with an intolerance to high-intensity sound (hyperacusis), even after controlling for audiometric thresholds (Gu et al., 2010, 2012). We therefore searched for elevated evoked responses by quantifying responses to tones at CF measured as a part of the FRA stimuli (**Fig 2.10A-C**). While anesthesia substantially elevated evoked rates, there was no effect of exposure in any frequency bin (3-way repeated-measures ANOVA: <16 kHz: $F_{1,103} = 0.0$, p=0.9; 16-32 kHz: $F_{1,102} = 0.9$, p=0.95; >32 kHz: $F_{1,117} = 1.9$, p=0.2).

Rate-level functions were fit with the four-parameter model of Sachs and Abbas (1974), or a seven-parameter sum of two such models (see Methods); the excitatory portion of this fit was then used to calculate threshold, maximum driven rate, and slope (**Fig 2.11**). In most comparisons there was no effect of exposure. However, in the region of maximal neuropathy (16-32 kHz), slopes were elevated by 65% in awake mice (**Fig 2.11I**, p=0.037, rank-sum test). This elevation is also apparent in the averaged rate-level functions (**Fig 2.10B**). Strikingly, slopes were not elevated under anesthesia within this (or any) frequency range, suggesting that the mechanisms responsible for elevating slopes may be suppressed by anesthesia . Dividing by frequency response type revealed that slope elevations were driven by increased slopes in non-monotonic neurons (**Fig S2.3**).

Anesthesia had a strong effect on all three parameters. Thresholds were significantly elevated by anesthesia in the non-neuropathic and neuropathic regions ($p<<0.001$, $p<<0.001$, rank-sum test). As observed with spontaneous rate, maximum driven rates were reduced in all regions ($p<0.001$, $p<<0.001$, $p<0.001$). Slopes were also significantly reduced across all CFs (p=0.006, p=0.001, $p<<0.001$).

Single-unit (SU) responses are inherently variable. In the IC in particular, response profiles vary continuously over a large range, reducing the power of comparisons across exposure groups. Multi-units (MUs), by contrast, are more stereotyped. Since MU responses are an average of the responses of several SUs, FRA heterogeneity is smoothed, especially at high stimulus levels, where the number of neurons contributing to the MU may increase. MU FRAs are almost always Type V, they have less pronounced inhibitory sidebands, and responses at CF are monotonic. While some of the fine detail is obscured in MU responses, they may still be useful in evaluating

changes due to noise exposure at a more coarse level. We compared MU responses to tones at BF in each group (**Fig 2.10D-F**). BF was used instead of CF because its automated estimation is more stable and the large number of MUs prohibited manual inspection as was done for SUs. While a significant main effect of exposure was not found at any frequency bin, post-hoc tests revealed small effects of exposure at some levels. Rate-level functions were fit with the four-parameter model only (since all units were monotonic). As for the SUs, the most substantial changes were in the slopes of the neuropathic region (**Fig 2.12F**). While elevations were most

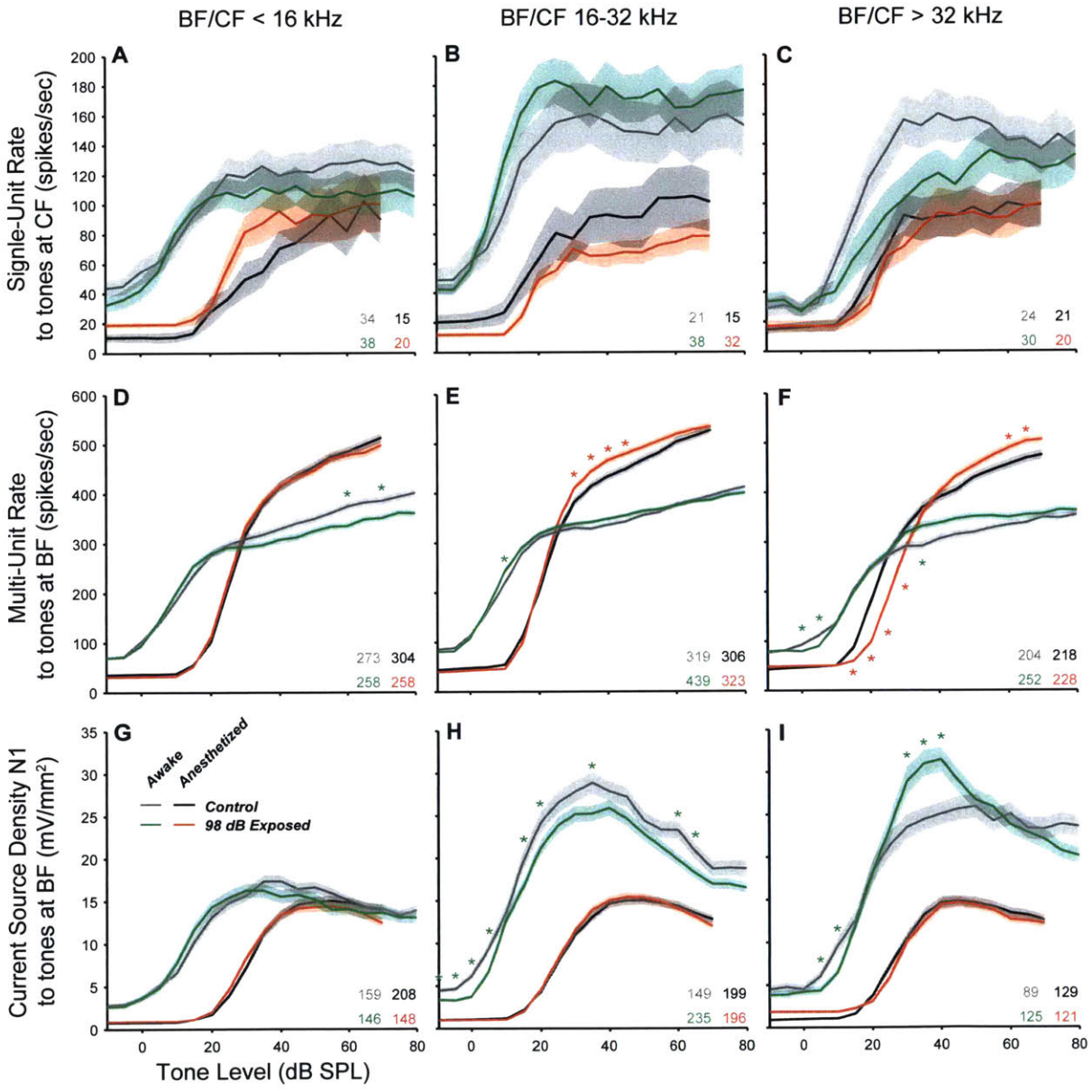

Figure 2.10. Effect of noise exposure on responses to tones. **A-C** Average rate (± SEM) to tones at CF of single-units with CFs <16 kHz (**A**), 16-32 kHz (**B**), and >32 kHz (**C**). **D-F** Average rate to tones at BF of multi-units. **G-I** Average CSD N1 to tones at the local multi-unit BF. The number of units contributing to each average is indicated. Red and green stars indicate significant effects of exposure for the anesthetized and awake groups, respectively ($p<0.05$, Tukey-Kramer-corrected post-hoc test following a 3-way ANOVA).

substantial for anesthetized mice, a significant shift occurred for awake mice, as well in the threshold-shift region. It is not immediately obvious why 16-32 kHz slopes were most strongly elevated in MUs of anesthetized mice while SU slopes were only elevated in awake mice (**Fig 2.11I vs. 2.12F**). Exposure also caused a small amount of threshold elevation, which was larger at high frequencies. Thresholds were elevated by 1.5 dB for 16-32 kHz CFs and by 5 dB for CFs > 32 kHz (**Fig 2.12B,** p=0.02, p<<0.001). Threshold shifts followed the same pattern in awake mice, but did not reach significance. These changes are in agreement with the OHC loss and DPOAE

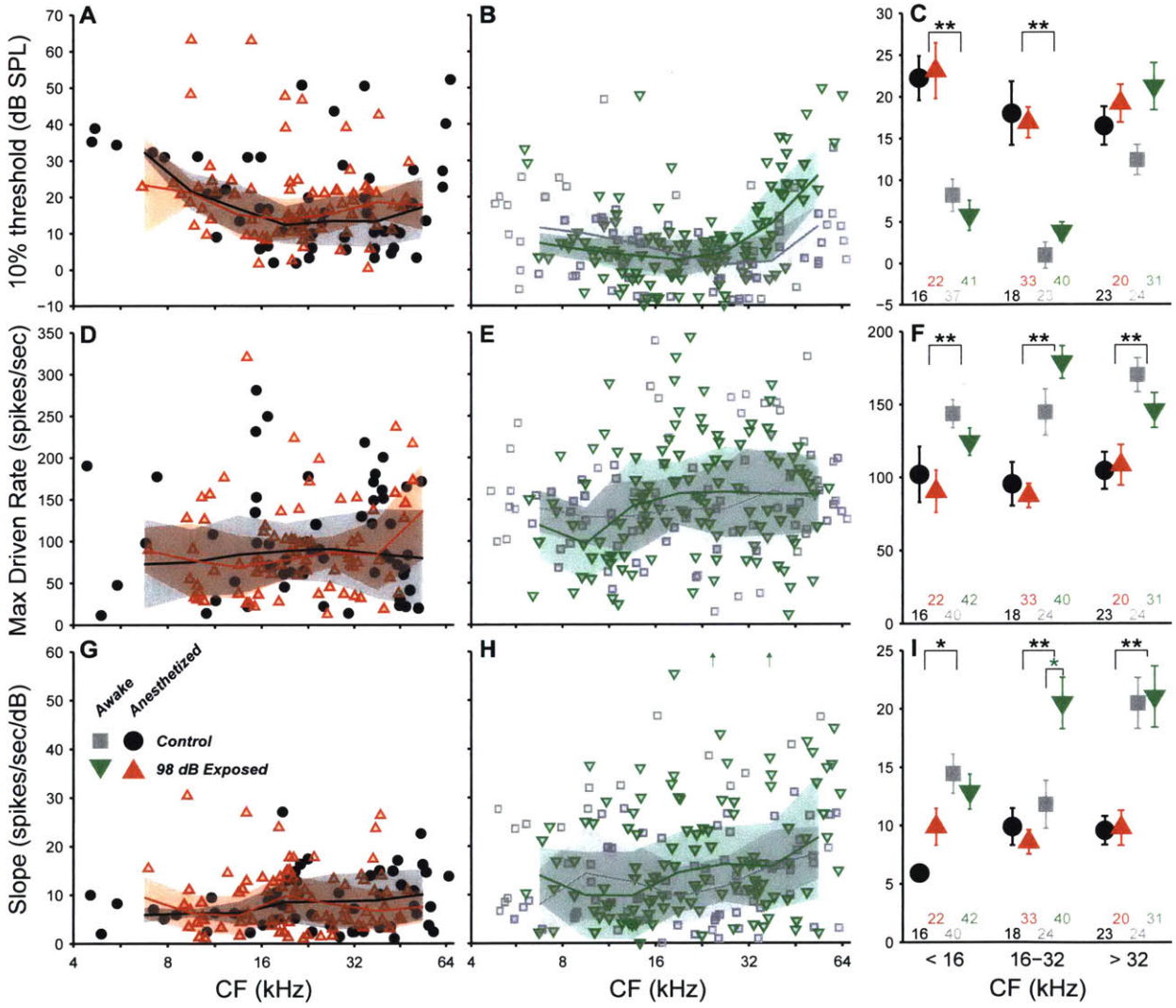

Figure 2.11. Single-unit slope is increased in the neuropathic region. **A-I** Threshold, maximum driven rate, and slope of responses to tones at CF in single-units. **A,D,G** Parameters in mice recorded while under anesthesia. Each point represents the parameter in a SU, and lines and error clouds indicate median and interquartile range, calculated over a 1 octave sliding window. **B,E,H,** Parameters in mice recorded while awake. **C,F,I,** Mean (± SEM) for each parameter, binned across cochlear frequencies where noise exposure caused no effect (< 16), neuropathy without hair cell damage (16-32) and neuropathy with some hair cell damage (>32). Units with inhibitory or complex FRAs are not included. Black stars indicate significant effects of anesthesia (rank-sum test with Bonferroni-Holm correction). Red and green stars indicate significant effects of exposure for the anesthetized and awake groups, respectively. One star: p<0.05. Two stars: p<0.001. Off-axis slopes in **H** were 64.2 and 60.9 from left to right.

shift observed at high frequencies (**Fig 2.1**). Exposure caused small reductions in maximum driven rate in awake mice in both the non-neuropathic and neuropathic regions ($p<0.001$, $p<0.001$).

As for the SUs, anesthesia had a strong effect on all three parameters. Threshold differences were in the same range but more clear in MUs due to the greater uniformity and larger sample size of the groups. In the exact opposite pattern to the SUs, maximum rate was 32% *lower* in the awake group, and slopes were 23% lower. However, the likely culprit for this decrease is not a true hypoactivity, but a difference in the criterion threshold used to detect spikes; median threshold was 70% higher in awake recordings than in anesthetized recordings (**Fig S2.4**). Spike threshold was higher because it was set at 3.5 standard deviations of the spike-filtered activity during silence and spontaneous rates were elevated in awake mice (**Fig 2.2**).

We quantified changes in synaptic activity by calculating current source density (CSD) from the same set of recordings used for spike data. CSD, the second spatial derivative of the local field potential, represents the volume density of the net current entering or leaving the extracellular space (Mulders and Robertson, 2009; Longenecker and Galazyuk, 2011; Manzoor et al., 2012; Ropp et al., 2014). Since synaptic potentials occur over a longer time course than spiking activity, they are thought to have the largest contribution to CSD (Buzsáki et al., 2012). In the present implementation, CSD was calculated in one dimension – along the linear 16-channel electrode oriented dorso-ventrally in the IC. Current flowing orthogonal to this dimension would not be captured by our

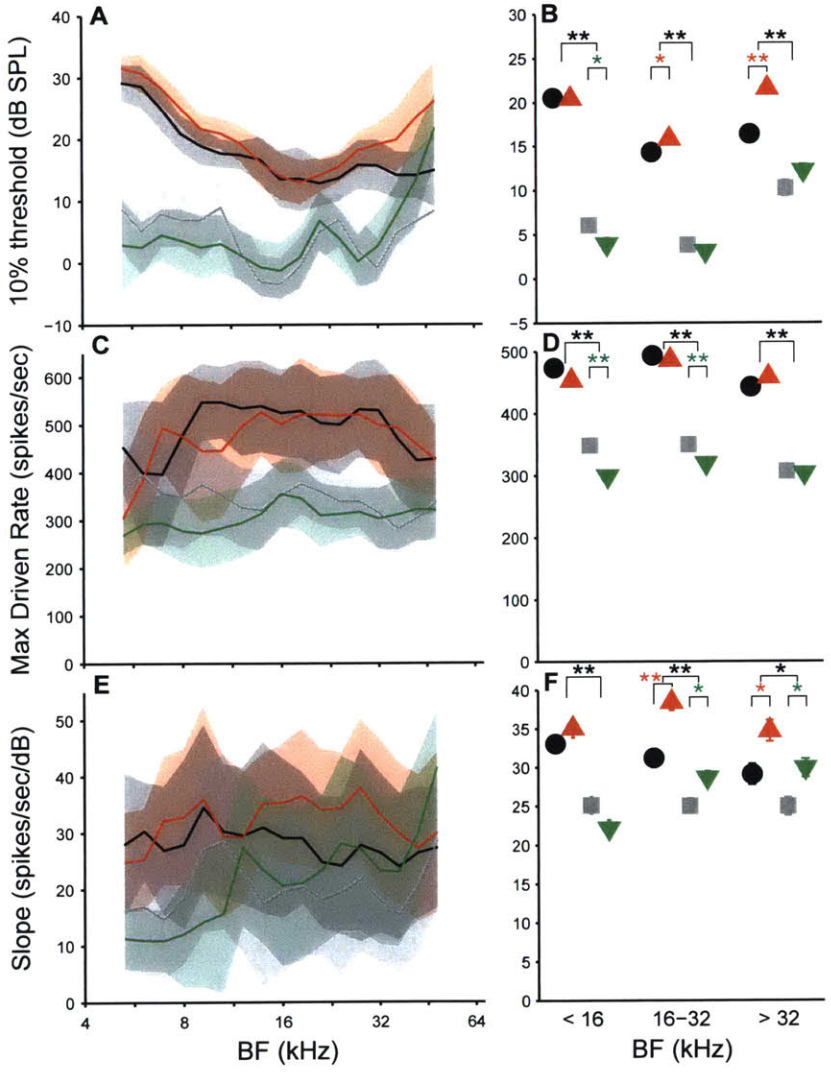

Figure 2.12. Multi-unit slope is increased in the neuropathic region. **A-F** Threshold, maximum driven rate, and slope of responses to tones at BF in MUs. Lines and error clouds indicate median and interquartile range, calculated over a 0.4 octave sliding window. Star conventions as in Figure 2.11

measurment. This unmeasured current is likely to be significant since this orientation is not perfectly orthoginal to the fibro-dendritic laminae of the IC, and since substantial current flow must occur along the neurites comprising the laminae. Thus, our 1-D CSD measurements will not be interpreted as true 3-D CSD, but rather simply as an additional measure of differences arising following cochlear neuropathy. CSD waveforms were quantified by the amplitude of the first valley, and rate-vs.-CSD functions were created in response to tones at the MU BF for each electrode site (**Fig 2.10G-I**; see methods). Negative CSD deflections represent current sinks, which occur when glutamate receptors allow cations to flow into neurons. In awake mice, noise-exposure caused a small reduction in CSD N1 in the neuropathic region for most of the levels tested (3-way repeated-measures ANOVA: $F_{1,775} = 336$, $p<<0.001$). There was no main effect of exposure in the threshold-shift region, but in post-hoc tests indicated a significant increase in exposed mice for levels around 35 dB SPL.

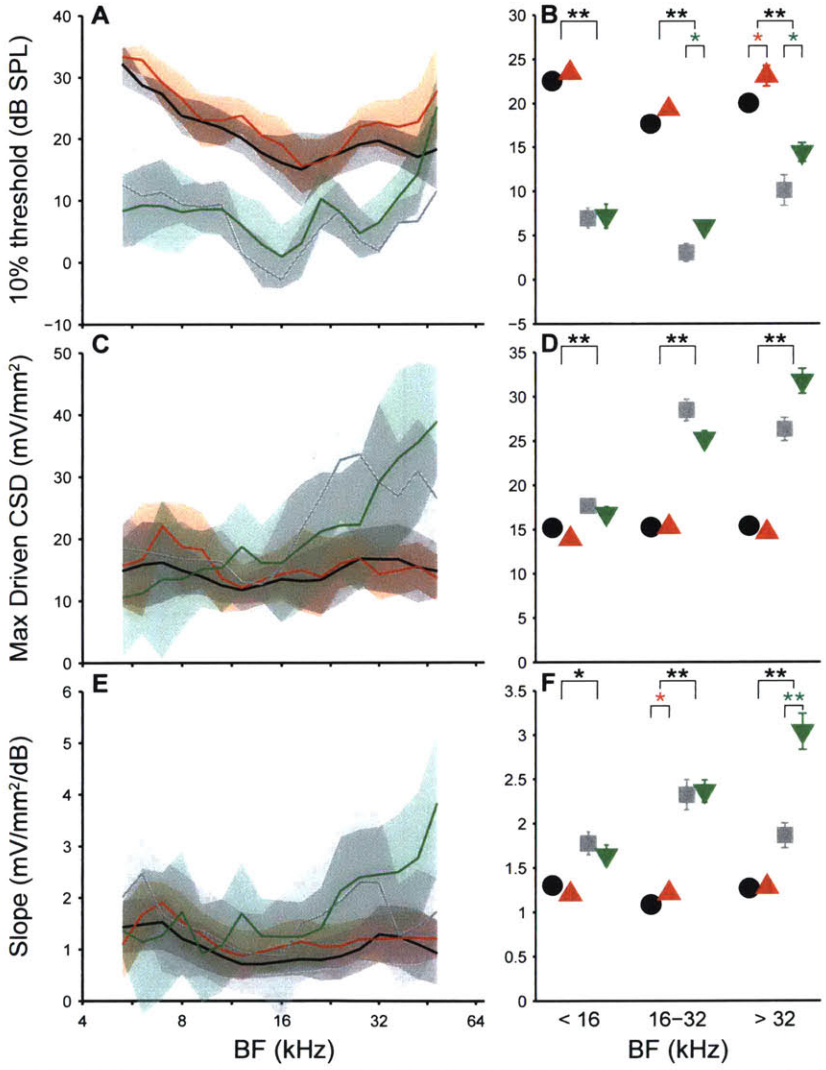

Figure 2.13. Current source density slope is increased in the threshold-shift region. **A-F** Threshold, maximum driven rate, and slope of CSD N1 to tones at the local MU BF. Lines and error clouds indicate median and inerquartile range, calculated over a 0.4 octave sliding window. Star conventions as in Figure 2.11.

Rate-vs.-CSD functions were fit with the seven-parameter model. Slopes were elevated following exposure, but unlike in the SU data, the greatest elevation was in the threshold-shift region of awake mice ($p<0.001$); changes within 16-32 kHz were small and limited to anesthetized mice ($p=0.02$; **Fig 2.13E**). Threshold shifts were small and most prominent above 32 kHz, and there were no significant effects of exposure on maximum driven CSD. Anesthesia caused the same pattern of changes as in the SUs: thresholds were increased, and maximum CSDs and slopes were decreased. Since the calculation of CSD is not effected by background activity, this

provides further evidence that the reductions in driven rate and slope observed in the MU data were a byproduct of spike thresholding.

Inhibitory side bands were reduced in neuropathic mice

Responses to off-CF tones were quantified by plotting driven rate vs. tone frequency for the average of 25-35 dB SPL tones. In the neuropathic region of awake mice, driven rate was elevated at frequencies both above and below CF (**Fig 2.14B,E**). The main effect of exposure was significant for both SUs and MUs (effect of exposure: SU: $F_{1,92} = 5.2$, p=0.025; MU: $F_{1,1383} =$

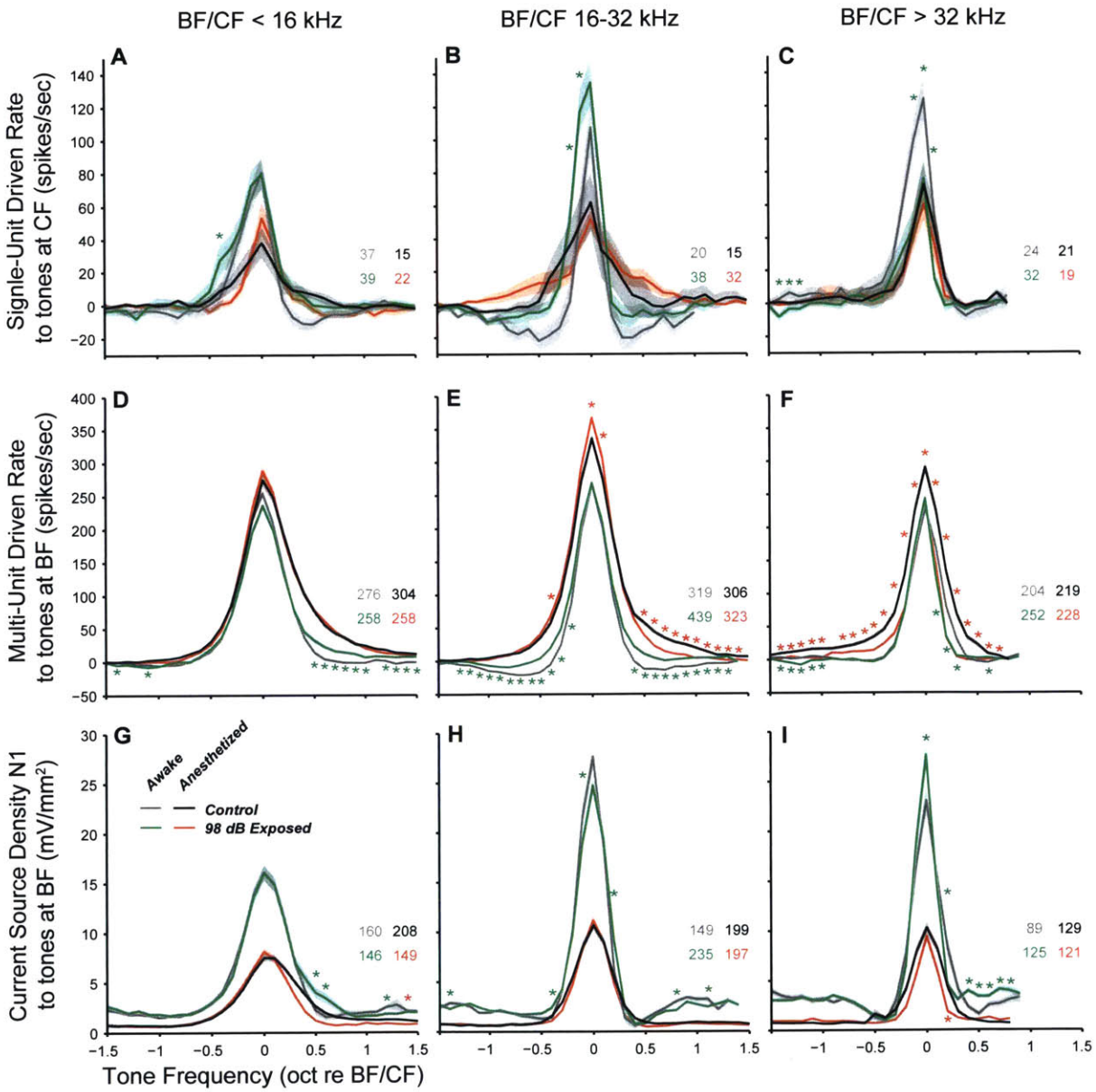

Figure 2.14. Off-CF responses to tones suggest a reduction in inhibition. **A-C** Average rate (± SEM) to 25-35 dB tones at CF of single-units with in SUs with CFs <16 kHz (**A**), 16-32 kHz (**B**), and >32 kHz (**C**). **D-F** Average rate in MUs. **G-I** CSD valley within a window 7-20 ms re tone onset. Functions were inverted (current sink positive) for equal comparison with spike data. The number of units contributing to each average is indicated. Star conventions as in Figure 2.10.

14, p<0.001; anesthesia*exposure interaction: SU: $F_{1,92}$ = 2.5, p=0.12; MU: $F_{1,1383}$ = 16, p<<0.001). Notably, while mean driven rate dropped below 0 in control neurons, indicating inhibition, driven rate remained positive in exposed neurons. This reduction in off-CF inhibition could be related to the elevated rate-level slopes at CF. In the non-neuropathic region, driven rate was higher for tone frequencies 1/2 octave above CF and higher, but unchanged elsewhere; there were no significant main effects of exposure or interactions (**Fig 2.14A,D**). This effect could be caused by changes toinhibition from neurons in the neuropathic region. The most substantial changes in the threshold-shift region were in groups with the most prominent threshold shifts: awake SUs and anesthetized MUs **(Fig 2.14C,F vs. 2.11C & 2.12B**).

Changes to CSD N1 were more minor **(Fig 2.14G-I**). Because CSD N1 represents current sink, and is therefore mostly driven by excitatory currents, this suggests that the dominant cause of elevated driven spike rates is not a change in excitation, and therefore could be a change in inhibition. We further investigated this possibility by extracting additional measures from the CSD waveform that are more strongly influenced by inhibition (**Fig S2.5**). In the neuropathic region of awake mice, there were slight reductions in CSD P1, reflecting peak current source, both above and below BF (**E**). A stronger effect was observed when the effect of excitation and inhibition were combined by computing the mean CSD over the entire tone response period (**B**). This measure should reflect the net current flow, and is computed over the same time period used to compute spike rates. However, since CSD is a linear summation of both excitatory and inhibitory synaptic currents, since CSD can also be influenced by a variety of other current sources in the neuropil (Buzsáki et al., 2012), and since our CSD calculation was limited to one dimention, this conclusion is speculative. More conclusive results would require methods providing a cleaner separation of inhibition and excitation.

Responses to noise were reduced in neuropathic mice

Rate-level functions to contralateral noise were extracted from the bottom row of the binaural noise response maps (**Fig 2.7**). In SUs, there were no significant main effects of exposure, but post-hoc tests revealed significant reductions at some levels for the 16-32 kHz anesthetized and >32 kHz awake groups (**Fig 2.15**). These were clearer in the MU data: exposure caused highly significant reductions in the neuropathic and threshold-shift regions, but not in the non-neuropathic region (<16 kHz: $F_{1,944}$ = 1.4, p=0.2; 16-32 kHz: $F_{1,1201}$ = 33, p<<0.001; >32 kHz: $F_{1,582}$ = 21, p<<0.001). Post-hoc tests demonstrated that these effects are present in both anesthetized and awake mice (**Fig 2.15D-F**). While some of this reduction is caused by threshold shift (**Fig 2.16A,B**), maximum rates were also reduced in exposed MUs (**Fig 2.16D,E**). Though the greatest effects occurred in the neuropathic and threshold-shift regions, a small, significant reduction was observed in the non-neuropathic region of awake mice.

In contrast to the responses to tones at CF, changes to CSD-vs.-level functions to noise did not mirror the changes in MUs. CSD was significantly reduced in exposed mice for sites in the non-neuropathic and neuropathic regions, but not in the threshold-shift region (**Fig 2.15 G-I**; <16 kHz: $F_{1,562}$ = 5, p=0.026; 16-32 kHz: $F_{1,602}$ = 6.7, p=0.001; >32 kHz: $F_{1,325}$ = 0.2, p=0.6). For

neuropathic sites in awake mice, the maximum CSD was reduced by 35% ($p<<0.001$), yet slopes and thresholds were unchanged (**Fig 2.16C,F,I**). Since MU maximum rates were reduced by only 10%, these data indicate a larger decrease in synaptic currents than in spiking responses, indicating that the IC may substantially compensate for a reduced peripheral signal. Furthermore, since the CSD N1 to noise was more strongly affected than the sum of the response to tones across CF (**Fig 2.15H vs. 2.14H**), these data suggest exposure caused substantial non-linear effects to CSD.

DISCUSSION

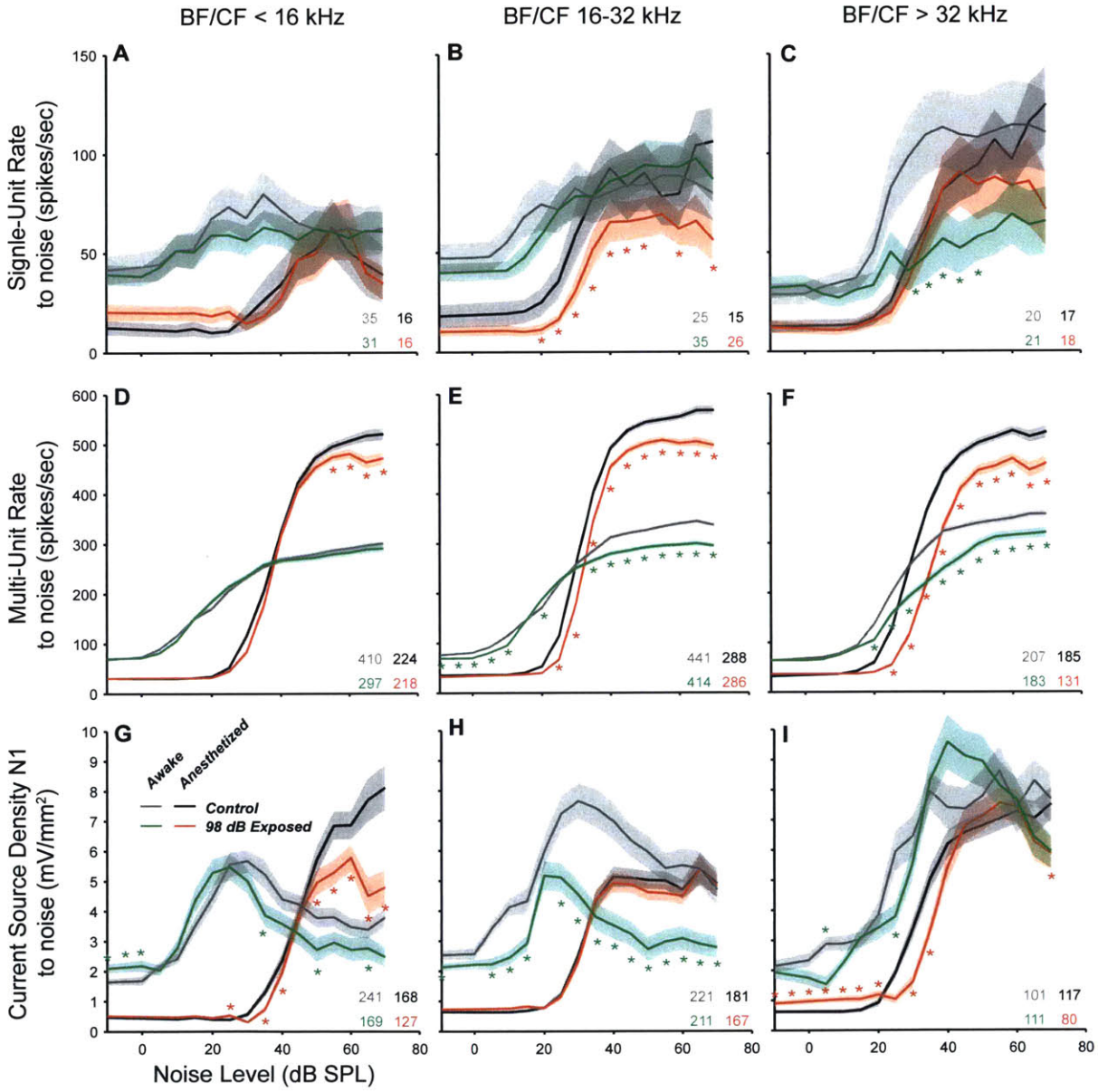

Figure 2.15. Responses to noise are reduced in neuropathic mice. **A-C** Average rate (± SEM) to contralateral broadband noise in SUs with CFs <16 kHz (**A**), 16-32 kHz (**B**), and >32 kHz (**C**). **D-F** Average rate in MUs. **G-I** CSD valley within a window 7-20 ms re tone onset. Functions were inverted (current sink positive) for equal comparison with spike data. The number of units contributing to each average is indicated. Star conventions as in Figure 2.10.

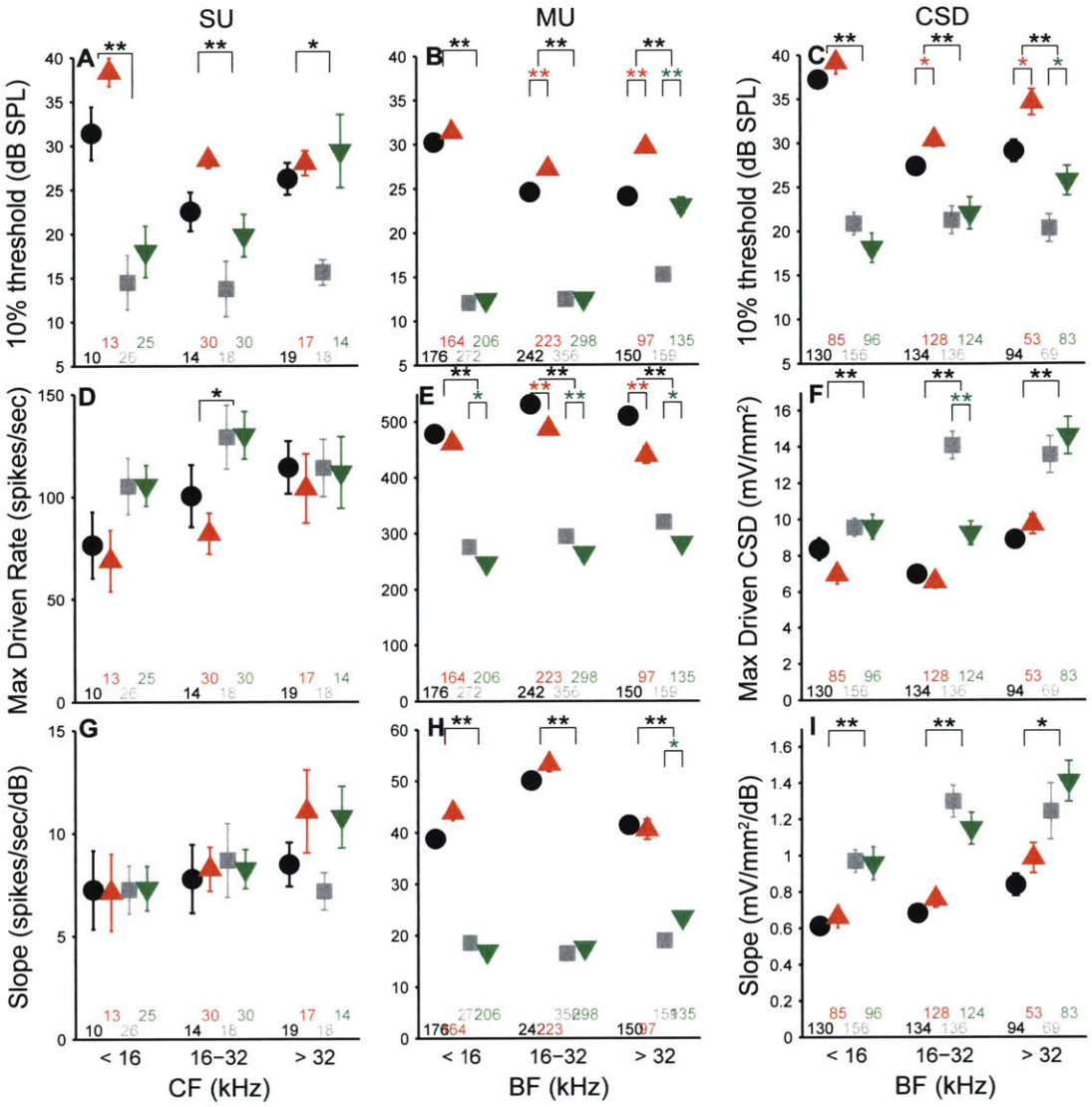

Figure 2.16. Maximum driven rate to noise is reduced in noise-exposed mice. **A-I** Threshold, maximum driven rate, and slope of responses to contralateral broadband noise in SUs (**A,D,G**), MUs (**B,E,F**), and CSD N1 (**C,F,H**). Star conventions as in Figure 2.11.

Effects of noise exposure on spontaneous rate

Spontaneous rate has been reported to be elevated in the IC following acoustic overexposures of many different paradigms: tonal and noise, unilateral and bilateral, and exposure while awake and while anesthetized (Table 1; Mulders and Robertson, 2009; Longenecker and Galazyuk, 2011; Manzoor et al., 2012; Ropp et al., 2014). Reported SR elevations are strikingly large; means are often increased by a factor of 3 to 6 and medians can be increased by a factor of 10 or more (for ex. Mulders and Robertson, 2009). Changes can be observed as soon as 12 hours post-exposure, and persist at 24, 48, and 168 hours (Mulders and Robertson, 2013). The amount of peripheral damage necessary to cause these changes is unclear. Acoustic overexposure can cause a range of peripheral pathologies, generally progressing with increasing exposure intensity and/or duration from IHC/AN fiber synaptic loss, to OHC stereocilia damage, to OHC loss, and finally to IHC loss (Liberman et al., 2010). While the exposures used in most studies elicited > 30 dB of threshold shift, elevated SRs have been measured in the IC following minimal permanent threshold shift (PTS) in both mice (Longenecker and Galazyuk, 2011) and chinchillas (Bauer et al., 2008). However, the degree of synaptic loss was not quantified in these studies. Thus, we set out to carefully quantify the amount of peripheral damage required to cause increased SRs. In the present dataset, exposure to a 98 dB SPL, bilateral, 8-16 kHz noise did not cause a change in SRs, despite substantial permanent synaptic loss (**Figs 2.1&2**). This result was replicated in two separate groups of mice: one recorded while under anesthesia, and one recorded while awake. Dividing the population into physiologically-based response types did not uncover any SR changes that could have been masked in the overall population. Thus, these results strongly suggest that noise-induced synaptic loss is not sufficient to cause increased SRs in the mouse IC.

Surprisingly, SRs were also unchanged after increasing the intensity of the noise exposure to cause > 40 dB of PTS **(Figs 2.3&4,** blue diamonds). While median SR increases of more than 10X have been reported following noise exposure (Mulders and Robertson, 2009; Coomber et al., 2014), Ma et al (2006) measured a modest, 1.7X median SR increase in the mouse IC following a bilateral, ½-octave noise exposure that induced ~ 60 dB of PTS. More substantial increases seem to occur following exposures that are unilateral (Longenecker and Galazyuk, 2011; 10X), tonal (Manzoor et al., 2012; 5X ratio of means) or both (Mulders and Robertson, 2009, 2011; 17-50X). Therefore, we exposed 3 groups of mice unilaterally to 8-16 kHz noise at three different intensities. SRs were not elevated in these groups either, regardless of the amount of PTS.

SRs in unexposed mice were higher in the present study than in other similar studies, both for mice recorded under anesthesia, and those recorded awake. This difference could be related to the absence of exposure-induced SR elevations in the present study. Compared to the SRs in Logenecker and Galazyuk (2011), who also recorded SRs in awake CBA/CaJ mice, mean SR was 6 times higher in unexposed animals. Since the SR distribution was skewed toward low SRs in Logenecker and Galazyuk (2011), but more normally distributed here, median SRs were 14 times higher. The major differences between the two studies are the electrodes used and the restraint of the mice during recording. Logenecker and Galazyuk (2011) used glass micropipettes

which have very fine tips (3 μm) and high impedances (15 MΩ), while we used silicon electrodes having larger contact areas (177 μm^2) and lower impedances (1 MΩ). The smaller surface area of glass micropipettes may allow them to detect signals from smaller neural elements such as axons, so it is possible that the choice of electrode biased our two samples toward different neural populations. In addition, while mice were head-fixed in both experiments, in Logenecker and Galazyuk (2011) their bodies were restrained in small tube, while in the present study they were free to walk on a turntable beneath them. As animals were not under behavioral control in either study, it is possible that differences in SR could be caused by differences in behavioral state. Comparing SRs recorded under ketamine/xylazine, the median SR in unexposed mice was 2.5 times higher in this study than in Ma et al 2006. However, since ketamine/xylazine has a substantial effect on SRs (**Fig 2.2**), it's possible that small differences in the depth of anesthesia maintained in the two studies could cause differences in SRs. Finally, Ma et al used tungsten and platinum-iridium electrodes, which have exposed contact areas and impedances intermediate to glass micropipettes and the Neuronexus electrodes used here, so thus might be expected to have intermediate SU sensitivity. In principle, the atypically high SRs reported in the present study could simply be due to poor SU isolation; SRs would be elevated if sorted SUs clusters contained spikes from multiple neurons. However, since each spike sort was rigorously reviewed, we do not find this explanation likely. **Figure S1.1** illustrates three sorts containing SUs with SRs above the ranges reported by the other studies. Panels **A&B** are from awake control mice, and have SRs of 78 and 61 spikes/sec; panel **C** is from an anesthetized control mouse and has an SR of 52 spikes/sec. Units in **A** and **C** have SU isolation typical of the population. SUs with poorer isolation than these were not accepted. Finally, poor SU isolation would have the largest effect on driven activity, where MU responses are highest. In periods of silence, where SR is measured, the SU isolation was quite good in all units.

We now return to the question of why SRs were not increased in any of the exposure groups tested here. The most comparable study in awake mice is that of Longenecker and Galazyuk (2011) where SRs were increased 10X following a 2.5-octave noise exposure administered unilaterally under ketamine/xylazine. The exposure was shorter (1 hour) and more intense (116 dB SPL) than that used here (1 octave at 103 dB for 2 hours). ABR thresholds were elevated by 20 dB at 8 weeks post-exposure (PE), but fully recovered at 12 weeks. This result is unusual – other studies of noise exposure observe that if thresholds are to recover completely, they do so by 1-2 wks PE (Kujawa and Liberman, 2006, 2009). In all exposure paradigms evaluated thus far in our lab, exposures just under the intensity required to cause PTS have caused substantial cochlear neuropathy (Kujawa and Liberman, 2009; Furman et al., 2013; Jensen et al., 2015). Therefore, while the precise extent of cochlear damage was not quantified by Logenecker and Galazyuk (2011), it is likely that the mice in their study had substantial neuropathy, making the amount of cochlear damage approximately similar the 98-dB bilateral awake and 103-dB unilateral anesthetized exposures used in the present study.

The most significant exposure-related differences are the exposure age and the post-

exposure time. In the present study mice were exposed at 7 weeks of age, while in Logenecker and Galazyuk (2011), mice were exposed at 12 weeks. Vulnerability to noise exposure changes sometime in this period, a noise exposure level that causes 50 dB PTS in 8-week old mice causes no PTS in 16-wk old mice (Kujawa and Liberman, 2006). The cause of this difference is unknown. In humans, detailed behavioral experiments have established that the central auditory system continues developing well into adolescence (reviewed by Sanes and Woolley, 2011). Mice reach sexual maturity at around 7 weeks, thus, it is possible that the adolescent mouse auditory system is capable of adapting in a way that prevents noise-induced SR elevation. While, 50% of tinnitus sufferes report onset to be gradual, in some cases the tinnitus percept begins and persists immediately following noise exposure (Meikle, 1997; Holgers and Pettersson, 2005; Daniel, 2007). In the present study, IC recordings were conducted 1-3 weeks post-exposure to quantify changes remaining as soon as thresholds were recovered. Logenecker and Galazyuk (2011) measured SR changes 5-8 weeks post-exposure . The source of elevated SRs may become more central sometime within this period: in guinea pigs, cochlear ablation up to four weeks post-exposure causes SRs to return to control levels, but ablation eight or more weeks post-exposure does not (Mulders and Robertson, 2009, 2011). However, since 4X elevations in mean SR can be observed as soon as 12 hours post-exposure, and persist at 24, 48, and 168 hours (Mulders and Robertson, 2013), it is not likely that elevated SRs would be found in the present study if post-exposure times were extended.

Finally, there is some evidence that the emergence of exposure-induced SR elevations and tinnitus can depend on pre-exposure state. When given the same noise exposure, gerbils that have low activity in the auditory cortex and brainstem pre-exposure develop "tinnitus" and SR elevations in the cortex, while those that have higher pre-exposure activity do not (Ahlf et al., 2012; Tziridis et al., 2015). The cause of the differences in pre-exposure state between the two groups is unclear. In the present study, mice were handled minimally pre-exposure to reduce variability. Since pre-exposure tests were performed in some (though not all) of the studies reporting exposure-induced SR increases, this could be an important factor.

Effects of noise exposure on evoked rate

Single-and multi-unit rate-level slopes in response to tones at CF were elevated in mice exposed to neuropathic noise (**Figs 2.10-14**). In single-units, the effect was limited to neurons with CFs >16 kHz and most prominent between 16 and 32 kHz, coinciding with the cochlear region where synaptic loss is greatest (**Fig 2.1**). Thus, it appears that the auditory brainstem compensates for a reduced peripheral drive by increasing the gain along the auditory pathway. In SUs, slope was only increased in awake mice, particularly in non-monotonic units (**Figs 2.11I, S2.3C**). In the face of reduced peripheral input, the balance of excitation and inhibition may be shifted toward excitation in order to maintain detectability. Since non-monotonic neurons receive substantial on-BF inhibition, the shape of their rate-level functions may be more sensitive to this balance: an indicator of hyperactivity. Changes to the E/I balance were also observed in response to off-CF tones **(Fig 2.14**). More extensive changes to the E/I balance are observed following

near-complete cochlear neuropathy by administration of ouabain to the round window: while tone responses in awake mice are diminished immediately following neuropathy, an increase in "central gain" causes tone responses to recover in the IC and become hyperactive in the auditory cortex by 30 days post-treatment (Chambers et al., 2016). The present results illustrate that similar, but more modest changes can result from noise-induced neuropathy. However, because slopes were not quantified at multiple time points in the present study, it remains possible that the resported effects are not due to compensatory plasticity, but rather a direct effect of a reduced peripheral drive. For example, elevated slopes could occur due to a specific reduction in input to inhibitory interneurons.

In the chinchilla IC, elevated evoked rates were observed in a larger proportion of non-monotonic neurons than monotonic neurons immediately following exposure to a high-intensity, above-CF tone (Wang et al., 1996). The authors suggest that this difference could be due to a reduction lateral inhibition from the exposed region. Ketamine, an NDMA agonist, reduces excitatory drive, which could mask changes to the excitatory/inhibitory balance, causing slopes to be unaffected by noise exposure in anesthetized mice (**Fig 2.11I**). In MUs, slopes were increased for both anesthetized and awake mice; in fact, the increase was larger in anesthetized mice (**Fig 2.12F**). Since expected on-BF inhibition is not apparent in MUs, perhaps changes to the excitatory/inhibitory balance can be detected even when excitation is reduced by ketamine.

CSD-level slopes were substantially increased in sites where the local multi-unit BF was >32 kHz in awake mice, but not in anesthetized mice or over BFs <32 kHz. 3-D CSD represents the volume density of the net current entering or leaving the extracellular space. Since synaptic potentials occur over a longer time course than spiking activity, they contribute more strongly to the CSD (Buzsáki et al., 2012). However, since CSD was calculated in one-dimension, it does not capture possible changes in orthogonal currents. Thus, changes above 32 kHz may reflext increased synaptic input, or a change in the balance of current flow axial-vs.-lateral relative to the electrode orientation. It is not clear why this effect is confined to BFs above 32 kHz. Hyperactive evoked responses following noise exposure have been described in the CN, IC and auditory cortex (Salvi et al., 1990; Cai et al., 2009; Noreña et al., 2010). In the chinchilla IC, local field potential slopes and amplitudes were increased following a tonal, 5-day long, 105 dB exposure that caused ~ 25 dB PTS (Salvi et al., 1990; Auerbach et al., 2014). In contrast to the pattern observed here, responses were hyperactive only for tone frequencies at and below the exposure frequency. The difference could be due to either differences in the length of the exposure, or amount of PTS. The authors speculate that a reduction in response at areas with PTS could reduce lateral inhibition to CFs below the PTS area, causing them to become hyperactive. In the present study, noise exposure resulted in OHC loss at 64 kHz, so a lateral inhibition mechanism could account for some of the hyperactivity observed in SUs and MUs at 16-32 kHz. However it would not explain the changes to CSD, which is most closely related to the LFP measured by Salvi et al. Furthermore, the DPOAE and neural thresholds were only shifted by 10-15 dB at 45 kHz, so it is doubtful that the entire effect can be accounted for by OHC loss. The dominant

cochlear pathology was a 50% reduction IHC synapses.

Tinnitus, hyperacusis, and central gain

In mice exposed using a very similar noise exposure paradigm, changes to the acoustic startle reflex (ASR) suggested hypersensitivity to moderate level sounds (Hickox and Liberman, 2014). Following exposure, both the ASR and the pre-pulse inhibition (PPI) of the ASR were enhanced when presented in background noise. Since the IC is a dominant contributor to the PPI of startle (Fendt et al., 2001), increased IC rate-level slopes and increased startle responses following cochlear neuropathy may both be driven by the same underlying process. Here, noise exposure did not change SU rate-level slopes in mice recorded under ketamine/xylazine anesthesia. Since sub-anesthetic doses of ketamine cause a decrease in PPI of startle (Mansbach and Geyer, 1991; Bruin et al., 1999), we hypothesize that a changes to rate-level slopes may have been masked by anesthesia.

Introduction of a gap in the background noise as a "pre-pulse" is often used as a test for the presence of a tinnitus percept in animals (Turner et al., 2006). Neuropathic noise exposure resulted in reduced gap PPI only for short gap-startle latencies, suggesting that these mice may not have a "tinnitus" percept filling in the gap, and bringing into question the specificity of this test to "tinnitus" (Hickox and Liberman, 2014). Though the absence of reduced gap PPI at all latencies is consistent with the lack of SR change reported here, assessment of tinnitus percept by an operant paradigm is needed to clarify the presence and extent of tinnitus following this exposure paradigm.

The neural correlate of tinnitus may not be elevated SRs, other possibilities include changes to neural synchrony or increased bursting activity (reviewed by Roberts et al., 2010). Furthermore, it is not clear which neurons along the auditory pathway are responsible for the generation of tinnitus. SRs in the DCN and thalamus are elevated only in animals with reduced PPI (Dehmel et al., 2012; Li et al., 2013; Kalappa et al., 2014), while SRs in the IC and auditory cortex are elevated regardless of PPI (Engineer et al., 2011; Coomber et al., 2014; Ropp et al., 2014). This suggests that the elevated SRs in the IC may not be related to ASR "tinnitus" *per se*. While SRs were unchanged following neuropathic noise exposure in the present study, elevated SRs have been reported in the DCN and IC following likely-neuropathic noise exposures that did not cause PTS (Bauer et al., 2008; Koehler and Shore, 2013). In both of these studies, animals showed behavioral signs of tinnitus using conditioned suppression and ASR, respectively. Together, these results suggest that neuropathy alone is not sufficient to cause elevated SRs in the mouse IC. It remains possible that this exposure causes SR changes in the CN which are not inherited by the IC, but could affect perception via projections from the CN to the thalamus (Malmierca et al., 2002).

However, elevated SU and MU slopes suggest that neuropathic exposures may contribute to hyperacusis. The observed effects are small and in SUs are limited to non-monotonic neurons. Evoked response measurements suggest that many individuals that do not suffer from hyperacusis may have cochlear neuropathy (Bharadwaj et al., 2015). Thus, neuropathy may be a necessary

but not sufficient contributor to hyperacusis.

SUPPLEMENTAL FIGURES

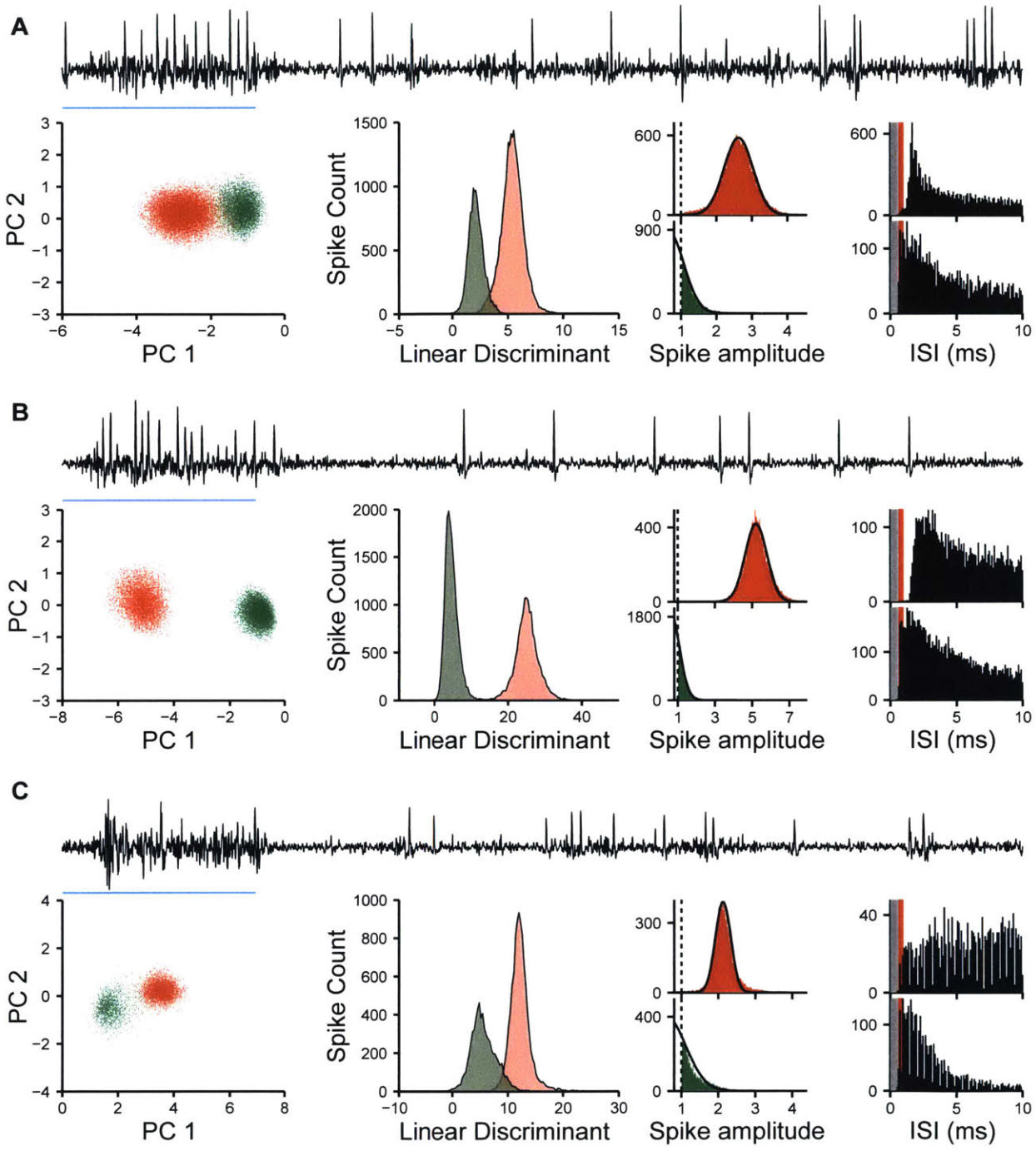

Figure S2.1. Spike sorting examples. **A-C,** each depict an example sort where a SU was separated from the MU background. **A,** Awake Control, CF 14.8 kHz, SR 78 spikes/sec. **B,** Awake Control, CF 12.9 kHz, SR 61 spikes/sec. **C,** Anesthetized Control, CF 20.9 kHz, SR 52 spikes/sec. For each unit: **Top**, Example filtered signal from electrode. **Left,** Scatter plot of first two principal components of all waveforms. Color indicates cluster: red – SU, green – MU. **Center-left,** A histogram of the projection of clusters onto Fischer's linear discriminant, illustrating the separation between MU and SU clusters. **Center-right**, A histogram of the peak amplitude of each spike, normalized by the spike threshold. Black lines: Gaussian fit to histogram used to assess is cluster has missing spikes. **Right**, Interspike interval histogram. Grey indicates shadow period of spike detection, red indicates refractory period.

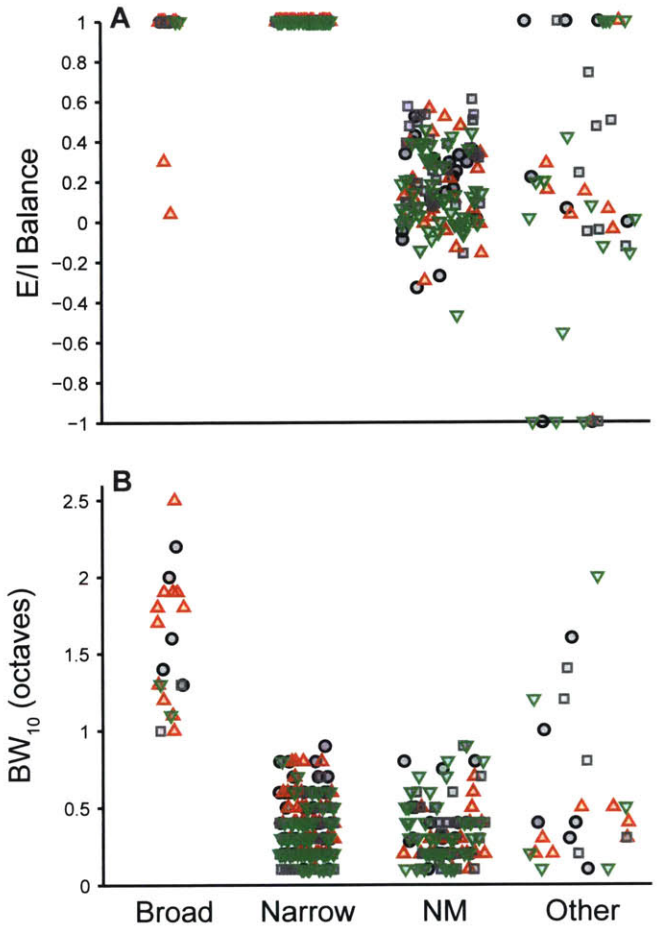

Figure S2.2. Metrics used for unit typing by FRA. **A,** Excitatory/Inhibitory balance, the difference between excitatory and inhibitory drive normalized by their sum. **B,** The bandwidth of the excitatory response at 10 dB above threshold. Colors and symbols are the same as used in Figure 2.6.

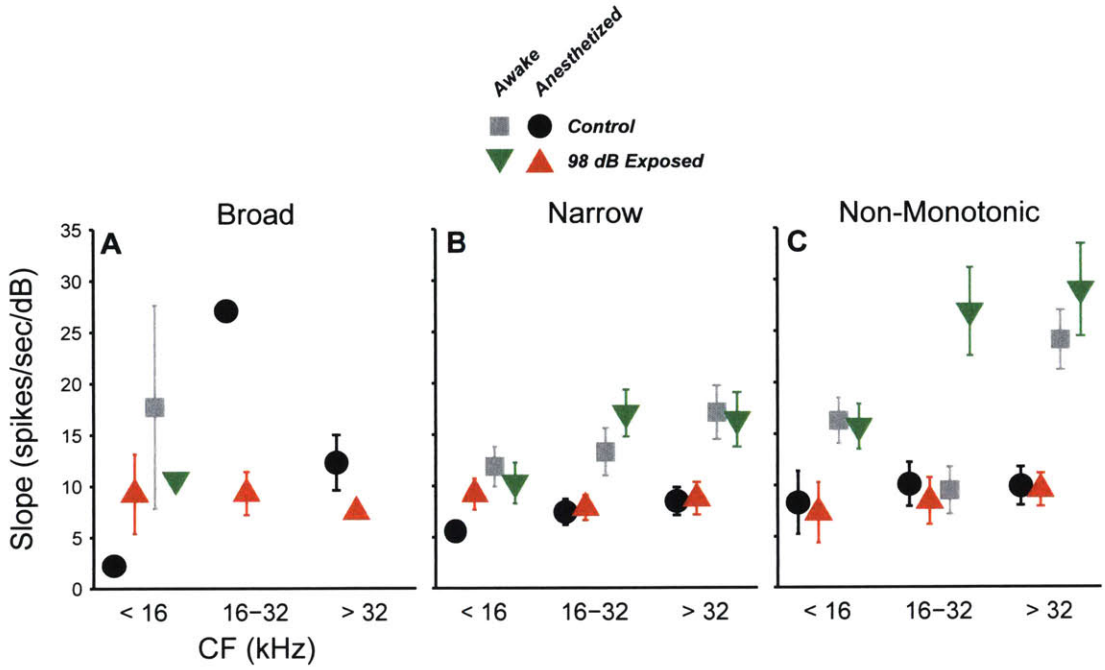

Figure S2.3. Elevations in slope are limited to non-monotonic neurons.

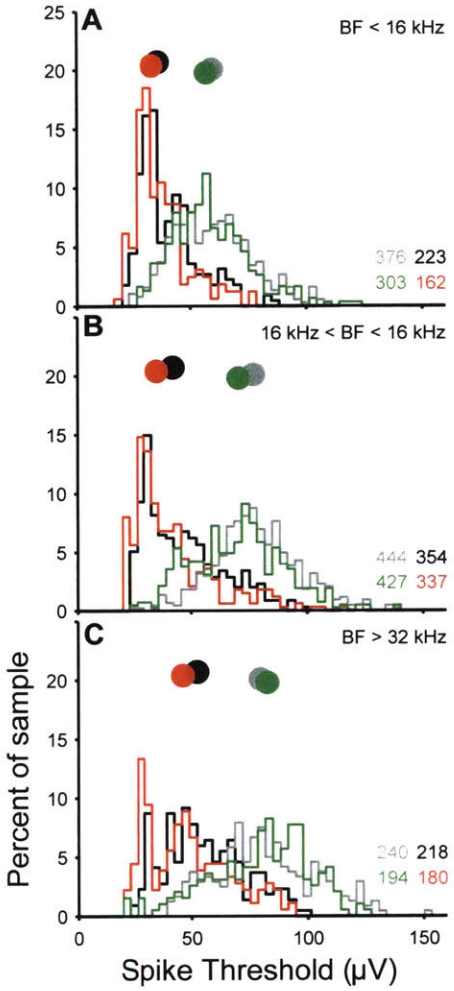

Figure S2.4. Spike threshold is higher in awake mice. **A-B** Spike threshold used for MU data separated into 3 BF ranges. Spike threshold was set at 3.5 standard deviations of the spike-filtered activity during silence. Points above histograms indicate medians for each group. Colors are the same as used in Figure 2.6.

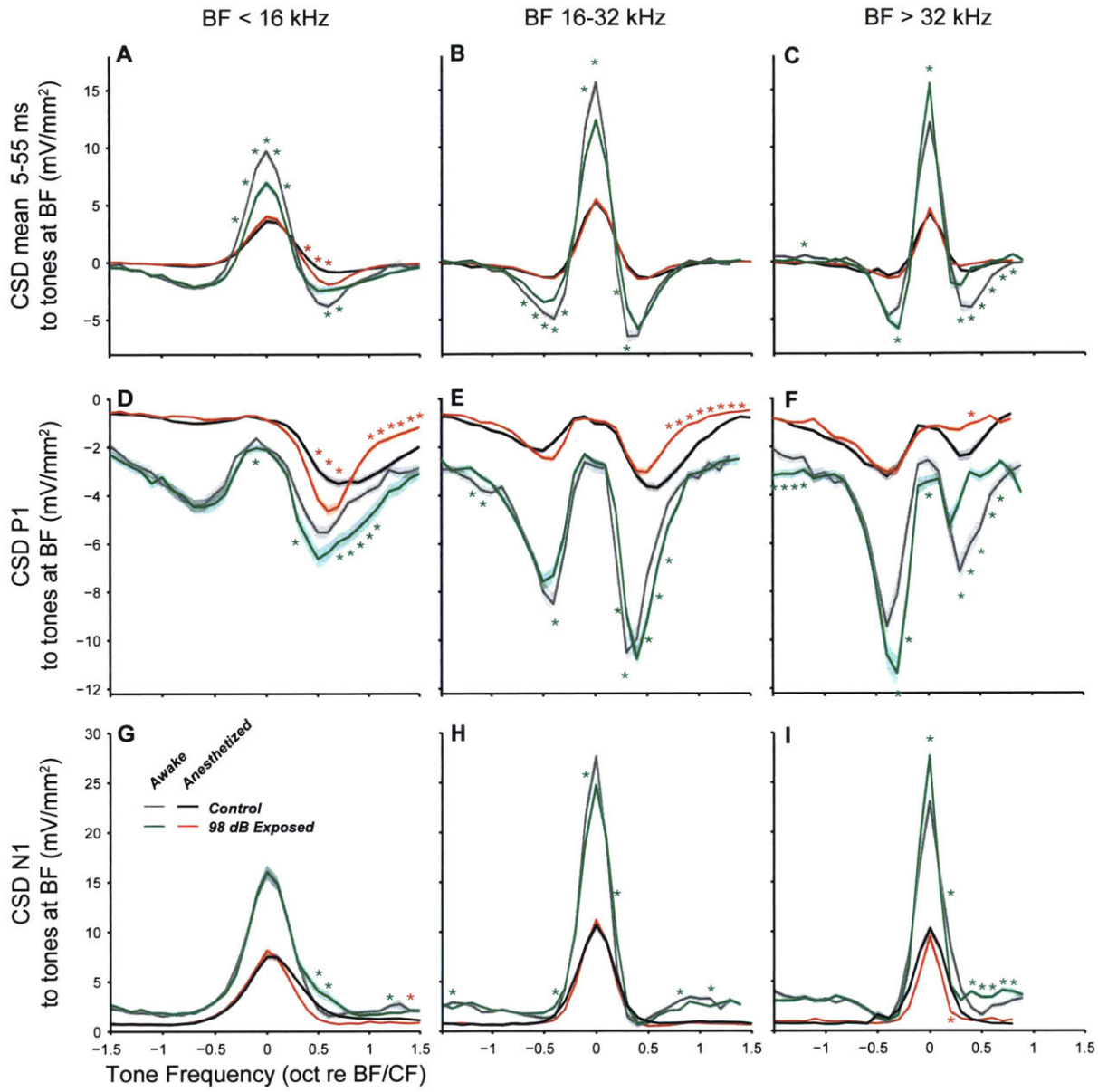

Figure S2.5. CSD tuning functions. **A-I** Average CSD to 25-35 dB tones at local MU BF for BFs <16 kHz (**A,D,G**), 16-32 kHz (**B,E,H**), and >32 kHz (**C,F,I**). **A-D** Mean CSD over the stimulus on time (5 to 55 ms re tone onset). **D-F** CSD peak within a window 4-15 ms re tone onset. **G-I** CSD valley within a window 7-20 ms re tone onset. For all three measures, functions were inverted (current sink positive) for equal comparison with spike data. Star conventions as in Figure 2.10.

Table 2.1. Summary of studies measuring SRs in the IC following noise exposure.

Reference	Species	Exposure						Peripheral Condition			IC Physiology											Tinnitus Behavior		Condition
		Exposure Laterality	Type	Freq (kHz)	Level	Time (hrs)	Exposure W/A	Exposure age	TTS (dB)	Post-Exp Time (wks)	PTS (dB)	Post-Exp Time (wks)	Freq Region (kHz)	Control SR Contra (sp/sec)		Exposed SR Contra (sp/sec)		SR Ratio Contra		SR Ratio Ipsi		Recording W/A	Electrode	Test	% with 'tinnitus'	
														mean	med	mean	med	mean	med	mean	med					
Manzoor et al 2012	GH	B	Tone	10	115	4	Awake	10-17 wk	NM	2-4	40	2-4	ALL	2.0		10.0		**5.0**	**NR**	NM		K/X	M Glass (.5 MΩ)	NM		
												2-4	ALL	2.0		2.0		1.0	NR	NM		K/X	M Glass (.5 MΩ)	NM		DCN Ablated
Manzoor et al 2013	GH	B	Tone	10	115	4	Awake	10-17	NM	9	40	9	ALL	2.0		10.0		**5.0**	**NR**	NM		K/X		NM		
												19		2.0		16.0		**8.0**	**NR**	NM						
												39		2.0		32.0		**16.0**	**NR**	NM						
Ma et al 2006	M	B	.5 OBN	16	103	1	K/X	9-17 wks	NM	4	60-70	4	10-30		4.7		7.8	NR	1.7	NM		K/X	S P-I or Tung	NM		
Shaheen & Liberman 2050	M	B	1 OBN	11	98	2	Awake	7 wk		1-3 wks	10@ 45k	1-3 wks	16-32	15.5	13.8	10.9	6.6	0.7	0.5	NM		K/X	S Silic 16-Ch	NM		
Shaheen & Liberman 2050	M	B	1 OBN	11	98	2	Awake	7 wk		1-3 wks	10@ 45k	1-3 wks	16-32	41.7	40.5	37.5	38.5	0.9	0.9	NM		Awake HF On Wheel	S Silic 16-Ch	NM		
Shaheen & Liberman 2050	M	B	1 OBN	11	103	2	Awake	7 wk		1-3 wks	>50	1-3 wks	> 16	15.5	13.8	14.3	12.1	0.9	0.9	NM		K/X	S Silic 16-Ch			
Ma et al 2006	M	U	.5 OBN	16	103	1	K/X	9-17 wks	NM	4	60-70	4	10-30					NM	NM	NR	2.0	K/X	S P-I or Tung	NM		
Mulders & Robertson 2009	GP	U	Tone	10	124	1	At/Diaz/Hyp	adult	70 @ 0 hr	0	70	0	ALL	1.2	0.0	1.4	0.0	1.1	1.0	NM		At/Nmb/Hyp	S Tung	NM		
										1	15	1	ALL	1.2	0.0	4.5	0.7	**3.7**	**17.5**	NM						
												2	ALL	1.2	0.0	8.1	2.0	**6.7**	**50.0**	NM						
												4	ALL	1.2	0.0	7.5	2.2	**6.2**	**55.0**	NM						
												1-4	ALL	1.2	0.0	1.4	0.2	1.2	**5.0**	NM						Cochlea Ablated
Dong et al 2010	GP	U	Tone	10	124	1	At/Diaz/Hyp	adult	>60 @ 0 hr	0	>60	0	ALL	0.9		1.2		1.3	NR	NM		At/Nmb/Hyp	S Tung	NM		
										2	0-20	2	ALL	0.9		6.1		**6.6**	**NR**	**3.8**	**NR**					
										4	0-10	4	ALL	0.9		5.4		**5.9**	**NR**	NM						
Mulders & Robertson 2011	GP	U	Tone	10	124	1	Diaz/Hyp	adult	70 @ 0 hr	8-12 wk	15	8-12 wk	ALL	2.3	0.0	6.0	0.7	**2.6**	**17.5**	NM		Nemb/Hyp	S Tung	NM		
												8-12	ALL	2.3	0.0	2.8	0.5	1.2	**12.5**	NM						Cochlea Ablated
Mulders & Robertson 2013	GP	U	Tone	10	124	2	At/Diaz/Hyp	adult	70 @ 0 hr	0-4 hr	70	0-4 hr	ALL	1.4		1.5		1.1	NR	NM		Nemb/Hyp	S Tung	NM		
										12 hr	15	12 hr		1.4		5.0		**3.6**	**NR**	NM						
Vogler et al 2014	GP	U	Tone	10	124	1	At/Diaz/Hyp	adult	70 @ 0 hr	2 wk	30	2 wk	ALL	1.5		6.1		**4.1**	**NR**	NM		Nemb/Hyp	S Tung	NM	NM	affected: Tonic* and onset Mon* and non-mon* v-shaped* and non-* EE, EI, EO*
Ropp et al 2014	R	U	Tone	16	116	2	Awake				20-40				10.4		14.1		1.4	NM		K/Ace	S Tung	Gap ASR	0.44	All Units
													All		1.7		7.7	**NR**	**4.5**							Type V
															8.0		10.5	**NR**	**1.3**							Type I
															28.4		19.5		0.7							Type O
Bauer et al 2008	Ch	U	Tone	4	85	1	K/X	1.5-2y	10 @ 0 hr	34-38	10	34-38	ALL	6.0		21.0		**3.5**	**NR**	0.5	NR	K/X	S Silic 16-Ch	Cond Supp	All?	
Coomber et al 2014	GP	U	1/7 OBN	10	120	1 .5s on .2	K/X	adult 300 - 500g	40	8	30	8	All	2.4	0.0	4.0	0.3	**1.7**	**30.0**	**NR**	**45**	Ureth/K/X	S Tung 2 MΩ 2x1x2	Gap ASR Pryer	0.75	Tinnitus
													All	2.4	0.0	3.4	0.5	**1.4**	**50.0**	**NR**	**70**				0.25	No tinnitus
Kalappa et al 2014	R	U	OBN	16	116	1	K/X	1-2y	40	2-3 ms?	0	2-3 ms?	All	5.6		11.7		**2.1**	**NR**	NM		Awake free-moving	Tetrode 4x4	Gap ASR	1	**In Thalamus Leminical (ventral)**
													All	3.5		6.1		**1.7**	**NR**	NM			1 MΩ		1	**Non-leminical**
Shaheen & Liberman 2050	M	U	1 OBN	11	101	2	K/X	7 wk		1 wk	0	1 wk	> 16	15.5	13.8	9.5	4.8	0.6	0.3	NM		K/X	S Silic 16-Ch			
Shaheen & Liberman 2050	M	U	1 OBN	11	103	2	K/X	7 wk		1 wk	0	1 wk	> 16	15.5	13.8	9.4	8.2	0.6	0.6	NM		K/X	S Silic 16-Ch			
Shaheen & Liberman 2050	M	U	1 OBN	11	104	2	K/X	7 wk		1 wk	20-30	1 wk	> 16	15.5	13.8	15.9	12.1	1.0	0.9	NM		K/X	S Silic 16-Ch			
Longenecker & Galazyuk 2011	M	U	2.5 OBN	16	116	1	K/X	12 wks	50 @ 1 day	5	0 @ 12 wk	5	ALL	5.9	2.5	25.9	25.0	**4.4**	**10.0**	NM		Awake Head-Fixed	S Glass 20 MΩ	Gap ASR		

GH -golden hamster, M - mouse, GP - guinea pig, R - rat, Ch - chinchilla, B - bilateral, U - unilateral, OBN - octave-band noise, K/X - ketamine/xylazine, At - Atropine, Diaz - Diazep
NM - not measured, NR - not reported, S - single-unit, M - multi-unit, P-I platinum-iridium, ASR - acoustic startle reflex, Cond Supp - conditioned suppression

Chapter 3

Effects of neuropathy on coding of tones in noise and synchronization to envelopes in the inferior colliculus

Luke A. Shaheen and M. Charles Liberman

ABSTRACT

Moderate noise exposure can cause a loss of auditory nerve (AN) fibers without causing hair cell damage or permanent threshold shift. This type of neuropathy may be the root cause of a number of deficits that can occur in listeners with normal audiograms, such as impaired speech discrimination in noise and ability to use envelope cues. Both abilities may crucially depend on high-threshold AN fibers, which are most vulnerable to noise-induced neuropathy. We searched for neural correlates of these deficits in the mouse auditory midbrain following a neuropathic noise-exposure. As hypothesized, neural detectability and discrimination of tones at low signal-to-noise ratios were impaired in the presence of high-level broadband masking noise. However, impairment was only present when noise level was changed every 600 milliseconds. When noise level changed every minute, responses were similar to those of unexposed mice, implicating changes to adaptation. Consistent with a high-threshold specific loss, synchronization to envelopes of amplitude-modulated tones and to click trains was impaired at moderate-to-high stimulus levels. However, synchronization was improved at near-threshold levels. In sum, we found compensatory effects on coding in the midbrain beyond the simple direct effects expected by peripheral neuropathy.

INTRODUCTION

Nearly all information about the acoustic environment is conveyed to the brain by type I auditory nerve (AN) fibers. While essential for hearing, these fibers may also be the most vulnerable link in the auditory pathway: moderate noise exposure can cause 50% loss of synapses between cochlear hair cells and AN fibers, followed by a slow degeneration of AN cell bodies and central axons without causing hair cell damage or permanent threshold shift (Kujawa and Liberman, 2009). This neuropathy is undetectable by standard clinical examination, but post-mortem evidence suggests that it is widespread in humans (Makary et al., 2011; Viana et al., 2015). Since loss of up to 80% of the AN fiber population can remain hidden behind normal thresholds (Schuknecht and Woellner, 1955; Lobarinas et al., 2013), the impact of such primary neural degeneration on suprathreshold hearing ability is likely profound, but is not well understood.

Redundancy in the auditory system may help to counteract this pathology: each inner hair cell (IHC) synapses with 10-30 AN fibers (Liberman et al., 1990; Maison et al., 2013). These fibers are not homogeneous, but distributed into functional subgroups based on spontaneous discharge rate (SR), sensitivity to sound, and post-synaptic targets in the cochlear nucleus (Liberman, 1978, 1991). Single-fiber recordings in guinea pigs suggest that noise-induced neuropathy is selective for high-threshold, low-SR fibers, and that the remaining low-threshold, high-SR fibers exhibit normal responses (Furman et al., 2013).

Low-SR AN fibers have higher thresholds and greater dynamic ranges (Liberman, 1978), and thus are more resistant to continuous masking noise (Costalupes et al., 1984; Young and Barta, 1986) and likely important for hearing in noisy environments. Synchronized far-field responses to amplitude-modulated stimuli, termed envelope following responses (EFRs), may be particularly sensitive to low-SR neuropathy; their amplitude is decreased in mice with neuropathy (Bharadwaj et al., 2014; Shaheen et al., 2015). The number of significantly-synchronized far-field electrical responses to tones simultaneously-modulated in both amplitude and frequency is correlated with word recognition in masking noise in young and older listeners with normal (to 4 kHz) thresholds (Dimitrijevic et al., 2004). Since this measure includes EFRs, the impairments observed by Dimitrijevic et al. (2004) may be caused by AN fiber loss. Fiber loss could be the missing cause of "obscure dysfunction," an enigmatic disease in which patients have impaired understanding of speech in noise despite normal thresholds (Saunders and Haggard, 1992; Strelcyk and Dau, 2009). Selective low-SR fiber loss may also reduce the strength of the medial olivocochlear (MOC) and middle ear (MEM) reflexes, which can counteract the effects of masking noise (Kawase et al., 1993). Inputs to MOC neurons arise from two cochlear nucleus (CN) cell types: small cell cap neurons (Ye et al., 2000) and planar multipolar neurons (Darrow et al., 2012), both of which may be predominantly driven by low- and medium-SR AN fibers (Liberman, 1991, 1993). The MEM reflex may also be driven by low-SR AN fibers (Rouiller et al., 1986; Kobler et al., 1992), and is substantially reduced following noise-induced cochlear neuropathy (Valero et al., 2016). Since these studies all suggest that low-SR neuropathy may cause an impairment of coding in noise, we compared the response to tones in a continuous background noise in the inferior colliculus (IC) of

neuropathic and control animals.

Temporal envelopes are critical for speech perception – vocoded speech can still be understood in quiet with a strikingly small number of spectral channels as long as envelope information is preserved (Shannon et al., 1995). Since phase-locking to temporal envelopes is particularly good in low-SR fibers (Joris and Yin, 1992), and EFRs to sinusoidally amplitude-modulated (SAM) tones are impaired by neuropathy (Shaheen et al., 2015), temporal coding of envelopes is also likely to be impaired by neuropathy. In normal hearing listeners, correlations have been found between measures of temporal perception and electrophysiological tests designed to quantify cochlear neuropathy (Bharadwaj et al., 2015; Mehraei et al., 2016). Loss of 90 - 95% of AN fibers without hair cell damage causes severe disruption of temporal envelope coding in the IC (Chambers et al., 2016). Do similar deficits occur with a more moderate, and low-SR specific, neuropathy? To answer this question we compared responses to SAM tones and click trains in the IC of neuropathic and control animals.

METHODS

Animals and groups: Seven week-old male CBA/CaJ mice were exposed awake and unrestrained to octave-band noise (8-16 kHz) for 2 hrs, within a cage suspended directly below the horn of the loudspeaker in a small, reverberant chamber. Noise calibration to target SPL was performed immediately before each exposure session. Control mice were of the same age, gender, and strain, but were not exposed to the noise. Two groups of mice were used to measure IC responses while awake: 1) control (8 mice) and 2) exposed at 98 dB SPL (6 mice). The responses reported in this chapter were recorded from the same mice as used in **Chapter 2**.

All procedures were approved by the Institutional Animal Care and Use Committee of the Massachusetts Eye and Ear Infirmary.

Preparation for IC recordings: Recording methods were the same as used in **Chapter 2.** After neurons were characterized by the FRA and BNRAs described in **Chapter 2**, selected neurons were tested for coding of tones-in-noise and temporal envelopes. Neurons were selected for strong spike quality, so that the introduction of background noise did not contaminate single-unit isolation.

Stimuli:

Frequency Response Areas: Frequency Response Areas (FRAs) were collected and CF and threshold were defined as detailed in **Chapter 2**.

Tone-in-Noise: Tone-in-noise responses were collected separately in two different paradigms (**Fig 1**). For the blocked noise paradigm, each trial was 250 ms, and tones were 50 ms (4 ms raised cosine onset/offset ramps; **Fig 1C**). Tone levels were chosen to encompass the dynamic range of the neurons under investigation, and were generally -10 to 80 dB SPL in 5 dB steps. Continuous noise was presented concurrently. Noise level remained constant while complete set of tone responses was collected by pseudorandom presentation (15 trials per level). Noise level was

then increased by 5 dB and the process was repeated until all noise levels were tested (**Fig 1A**). Thus the duration of the noise blocks used for each neuron varied from 60 to 75 sec, depending on the number of tone levels used. Noise levels were chosen to encompass the dynamic range of the neuron under investigation, and were generally 0 to 80 dB SPL in 5 dB steps. Noise was unfrozen, limited from 4 kHz to 80 kHz and shaped to be flat-spectrum by correction for the frequency response of the acoustic system in the frequency domain. For the interleaved noise paradigm, both tone and noise level were varied pseuodrandomly from trial to trial. To ensure responses to the tone were not affected by sudden jumps in noise level at the start of each trial, trials were lengthened to 600 ms, and tone onset was moved to 500 ms re trial/noise onset (**Fig 1D**). Tones were 100 ms (4 ms raised cosine onset/offset ramps). Both stimuli were presented to the ear contralateral to the recording site for both paradigms. To avoid distortion, two separate speakers were used to present tone and noise stimuli (see **Chapter 2** for details of the acoustic system). For both paradigms, average rate was calculated over +5 to +55 ms re tone onset to allow for comparison between paradigms.

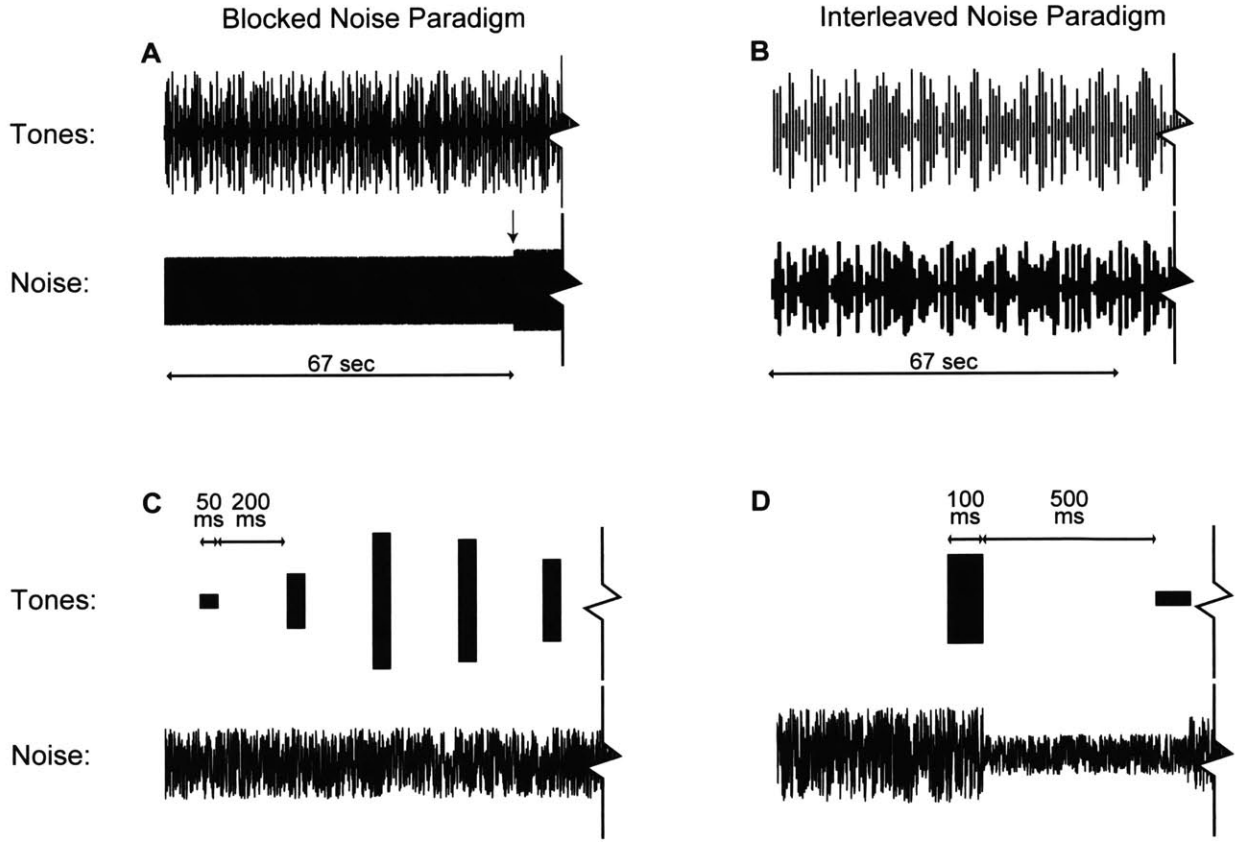

Figure 3.1. Tone-in-noise stimuli. **A,C,** blocked noise paradigm. **B,D,** interleaved noise paradigm. **A,B**, tone (top) and noise (bottom) stimuli at a coarse level, duration shown ~80 sec. For the blocked paradigm the length of each "block" over which noise level was constant depended on the number of tone levels presented, ranging from 60 to 75 sec. Noise level is sequentially increased in each block, change in level is indicated by arrow. **C,D,** tone and noise stimuli at a fine level, duration shown 1.2 sec. See Methods for stimulus details.

Tones were presented at CF. Since online spike-sorting was less rigorous than offline spike sorting, CF estimated online was sometimes different that CF estimated online. For all results presented here, tone frequency was within 0.1 octaves of the offline CF. Responses to the interleaved paradigm were collected in 51 control and 54 exposed neurons. Responses to the blocked paradigm were collected second, so some single-units were lost before data could be collected; data were collected for 35 control and 43 exposed neurons.

SAM tones: SAM tones were presented at CF (400 ms on, 600 ms off) to the contralateral ear. Responses were collected for modulation frequencies from 8 to 1024 Hz in 1/3 octave steps, and levels of 15 dB re pure tone threshold, 30, 50, and 70 dB SPL. These 22*4=88 stimuli were presented pseuodrandomly; 6 trials were recorded per condition. In cases where pure tone threshold was 15 dB below 30, 50, or 70, only 3 levels were presented.

Click trains: Broadband click trains were presented to the contralateral ear (400 ms on, 600 ms off). Clicks were monophasic (condensation, 100 μs duration), and presented at rates from 8 to 1024 Hz in 1/3 octave steps and levels of 30, 50 and 70 dB peak SPL. These 22*3=66 stimuli were presented pseuodrandomly; 6 trials were recorded per condition. 30 dB peak SPL clicks evoked little response in the majority of the population, so only responses to 50 and 70 dB are described.

Fits to rate-level functions: Rate-level functions to tones were fit with a four-parameter model (Sachs and Abbas, 1974; Heil et al., 2011). This model specifies firing rate r as a function of sound pressure P (in Pa) by:

$$r(P) = R_D \frac{P^N}{K+P^N} + R_S, \text{ and}$$
$$K = 2 * 10^{-5} * 10^{\frac{L_{50}}{20}},$$

where R_D is the driven rate, R_S is the spontaneous rate, N characterizes the steepness of the curve and L_{50} gives the level at 50% of the driven rate range. Non-monotonic functions were identified algorithmically and fit using the sum of two such models, yielding seven parameters:

$$r(P) = R_{D1} \frac{P^{N_1}}{K_1+P^{N_1}} + R_{D2} \frac{P^{N_2}}{K_2+P^{N_2}} + R_S.$$

Curves were fit by *fminsearchbnd*, a bounded version of the built-in MATLAB function *fminsearch* using a least-squares method. The fit was then refined by a robust procedure that iteratively refined weights of each data point before re-fitting. Threshold and saturation level were calculated as the levels eliciting 10 and 90% of the tone driven-rate range in the rising excitatory portion of the function.

D prime at low SNRs: Tone level was transformed to SNR by the simple ratio between broadband signal and noise level. d' was computed for a given noise and SNR condition between the spike count distribution in that condition and the distribution at the lowest tone level presented. d' was calculated using Hedge's g, the difference in means divided by the pooled standard deviation (Hentschke and Stüttgen, 2011).

Mutual Information: Mutual information (MI) between spike count and SNR was calculated at each noise level over -20 to 0 dB SNR as described by Day & Delgutte (2105). Briefly, MI between SNR X and spike count Y was calculated as:

$$I(X;Y) = \sum_x \sum_y p(x)p(y|x)log_2\left(\frac{p(y|x)}{p(y)}\right)$$

in units of bits. The stimulus distribution was assumed to be uniform over $M=5$ SNRs, $p(x) = 1/M$. The maximum possible MI was $log_2 M = 2.32$. The conditional spike count distribution, $p(y|x)$, was parameterized by a gamma distribution, and fit using the MATLAB function *gamfit*. The marginal spike count distribution, $p(y)$, was computed as the joint distribution summed over x.

Synchrony: Synchrony measures were computed over the steady-state portion of the response (100 to 400 re onset). Response window was slightly reduced by a variable amount for each modulation frequency/pulse rate such that the window encompassed an integer number of stimulus periods. Synchrony was computed as vector average of spike phases (Johnson, 1980):

$$VS = \frac{1}{N}\sqrt{\left(\sum_{i=1}^{N}\cos\theta_i\right)^2 + \left(\sum_{i=1}^{N}\cos\theta_i\right)^2}$$

where N is the total number of spikes and θ_i is the phase of each spike in radians.

Smoothing and Averages: Individual data was smoothed using a 3-point triangular-weighted moving average before averaging across neurons.

Statistical Analysis: Statistical testing was performed in MATLAB; functions used are indicated in italics. In order to facilitate testing of main effects and interactions, differences were assessed using a 2-way repeated measures ANOVA (*rmanova*). Significant post-hoc differences were assessed using *multcompare* with a Tukey-Kramer correction for multiple comparisons. Normality could not be assessed due to the low number of neurons (<15) in some conditions. Significance levels were similar when using paired rank-sum tests with Bonferroni-Holm correction for multiple comparisons, but results are described using ANOVA in order to report main effects and interactions.

RESULTS

Noise-induced synaptic loss after reversible noise-induced threshold shift

The neural responses reported in this chapter were recorded from a subset of the population described in Chapter 2. We exposed 7-wk old mice to an 8-16 kHz, 98 dB SPL noise band for two hours, causing a 40 to 50% loss of synapses between inner hair cells (IHCs) and auditory nerve (AN) fibers in the basal half of the cochlea, with loss of OHCs confined to the extreme basal end of the cochlea (**Fig 2.1**). Consistent with the morphology, DPOAE and ABR thresholds were not significantly elevated except for at 45 kHz. As in **Chapter 2**, we divided the cochlear frequency

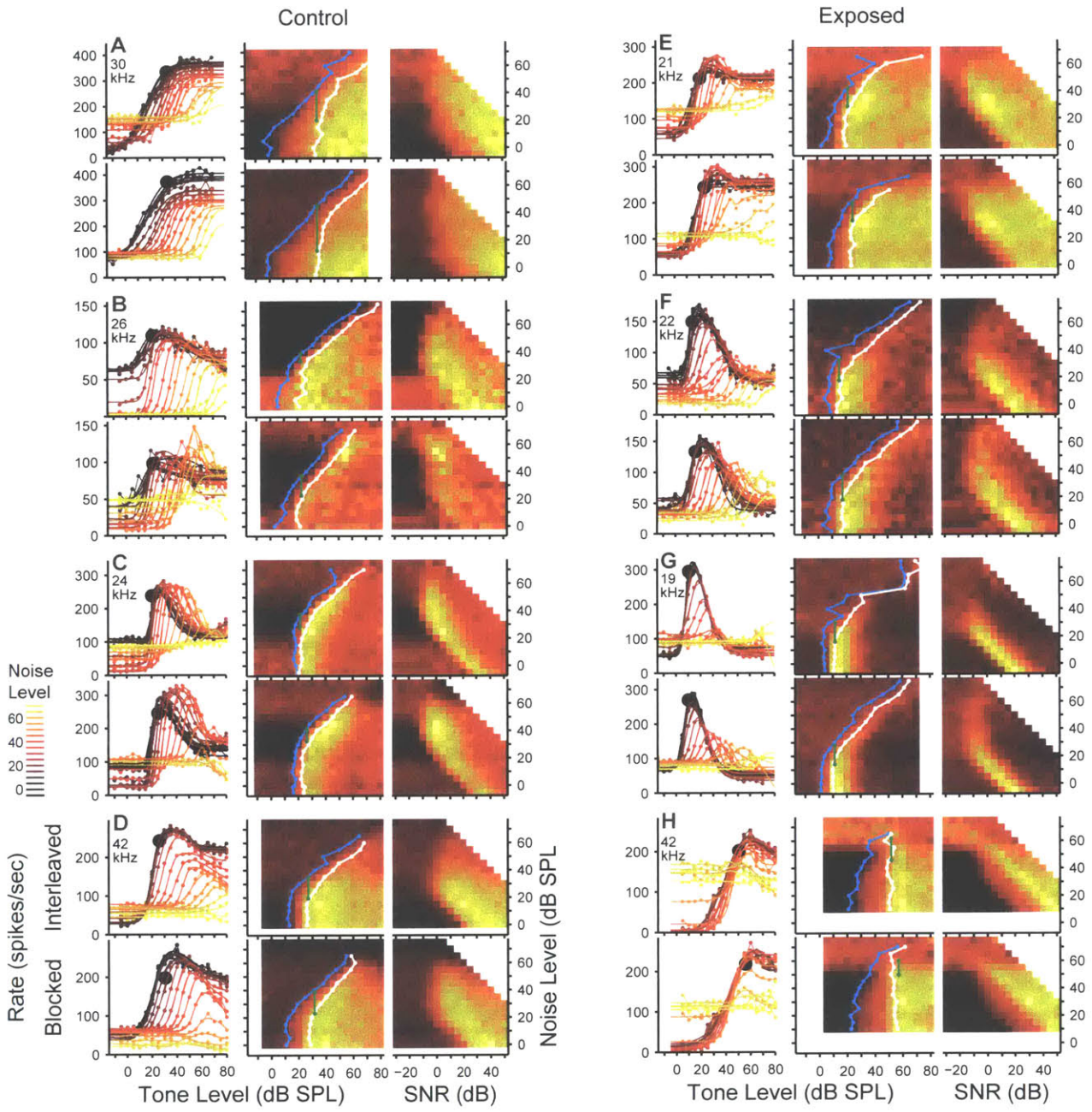

Figure 3.2. Example responses to tones in noise. Left three columns show responses in four control neurons, right columns show responses in four exposed neurons. For each neuron, responses are shown for both the interleaved (top) and blocked (bottom) paradigms. The CF of each neuron is shown in the upper left. **Left**, Thin lines and points indicate average rate during presentation of the tone, thick lines indicate fits. Color indicates noise level. Large black circle indicates saturation level of the tone response in quiet, L_{Q90} (90% of the excitatory portion of the fit function). **Center**, Average rates on a tone X noise level grid. Blue and white lines indicate tone threshold and saturation (10 and 90% of the excitatory portion of the fit function). Green line indicates the dynamic range of the response to a tone at L_{Q90} (10-90%). **Right**, Average rates on a SNR*noise level grid. Signal-to-noise ratio (SNR) is expressed as the broadband tone:noise level difference. Un-measured rates to low-SNR values are filled with the lowest SNR measured for visualization purposes only. For all grids, color scale is normalized to the maximum rate of each grid.

axis into three regions on the basis of the peripheral profile: 'non-neuropathic' (< 16 kHz), where noise exposure caused no effect, 'neuropathic' (16-32 kHz), where exposure caused neuropathy without hair cell damage, and 'threshold-shift' (>32 kHz), where exposure caused neuropathy with some hair cell damage.

Rate responses to tones in noise following neuropathy

Single-unit responses were collected in the inferior colliculus (IC) of awake, head-fixed mice using single-shank, 16-channel silicon electrodes. Frequency response areas (FRAs) were collected and used to estimate characteristic frequency (CF) and threshold. For each neuron, responses to tones at CF embedded in continuous noise were collected in two paradigms. In the interleaved noise paradigm, both noise and tone level varied randomly from trial to trial; in the blocked noise paradigm, noise level was sequentially increased in ~1 minute blocks, and tone level was varied randomly within in each block (**Fig 3.1**). The blocked noise paradigm was designed to test coding in conditions of static noise. The interleaved noise paradigm was designed to test coding in more dynamic conditions. Because noise level varied on every trial, trials were lengthened to 600 ms in the interleaved noise paradigm to ensure that the onset response to the noise had fully decayed before the tone was presented (**Fig 3.1D**).

Responses to tones in noise were quantified by the mean firing rate during the tone presentation. Example responses are shown in **Figure 3.2**. The first column depicts rate-vs.-tone level functions, with noise level indicated by color. In the second column the same data is visualized on a tone X noise level grid, with firing rate indicated by color. Responses exhibited remarkable diversity, ranging from purely excitatory responses reminiscent of AN fibers (**A**), to inhibition at high noise levels (**B**) or high tone levels (**C**). Similar diversity was observed in the exposed population (**E-G**). Neurons **A-C** and **E-G** had CFs in the neuropathic region, neurons **D** and **H** had CFs in the threshold-shift region.

Noise reduced sensitivity to the tone in two distinct ways: 1) by shifting the dynamic range to higher tone levels, and 2) by compressing the range of tone-driven rates. To quantify these changes, rate-level functions at each noise level were fit by a seven-parameter model adapted from Sachs and Abbas (1974) to capture non-monotonicity (thick lines, left columns). Threshold and saturation levels were calculated from the rising portion of the fit (blue and while lines, middle columns). In quiet, neural thresholds were unchanged below 32 kHz, but increased above 32 kHz in noise-exposed mice (**Fig 3.3**). Shifts were surprisingly higher than DPOAE threshold shift (**Fig 2.1E**), ranging from 20-40 dB. Once the noise level reached threshold, it caused tone thresholds to increase at ~1 dB/dB (**Fig 3.4**), consistent with reported shifts in the decerebrate cat IC (Ramachandran et al., 2000). Thresholds in noise were unchanged in noise-exposed mice for CFs < 32 kHz (two-way repeated-measures ANOVA; Interleaved: < 16 kHz: $F_{1,32} = 1.0$, $p = 0.3$; 16-32 kHz: $F_{1,30} = 0.1$, $p = 0.8$; Blocked: < 16 kHz: $F_{1,21} = 0.8$, $p = 0.4$; 16-32 kHz: $F_{1,23} = 0.01$, $p = 0.9$). For CFs >32 kHz, thresholds were elevated in quiet but returned to control levels when noise level was above 50 dB SPL (main effect: Interleaved: $F_{1,33} = 10$, $p = 0.003$; Blocked: $F_{1,27} = 15$, $p < 0.001$; exposure*noise level interaction: $F_{1,33} = 12$, $p = 0.002$; Blocked: $F_{1,27} = 13$, $p = 0.001$).

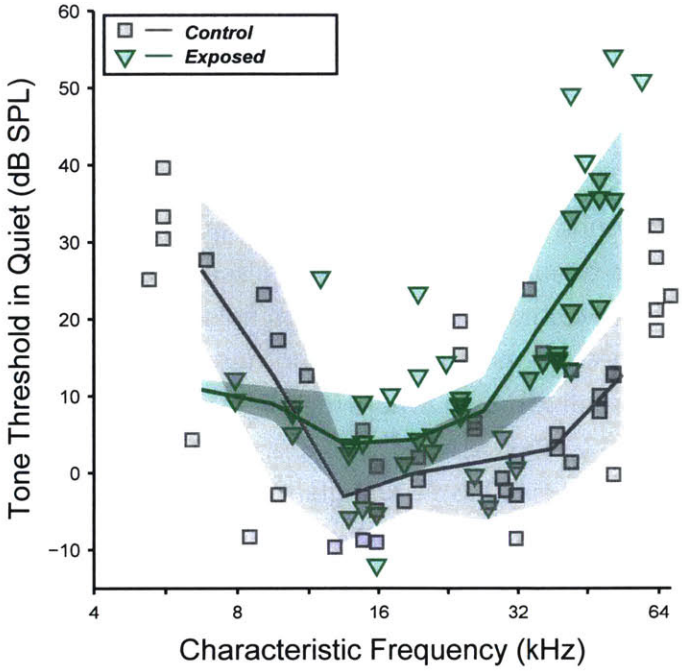

Figure 3.3 Tone thresholds in quiet. Threshold to a tone at CF in "quiet" was calculated as the level at 10% of the rate range over the excitatory portion of the fit to the tone rate-level function at the lowest noise level presented.

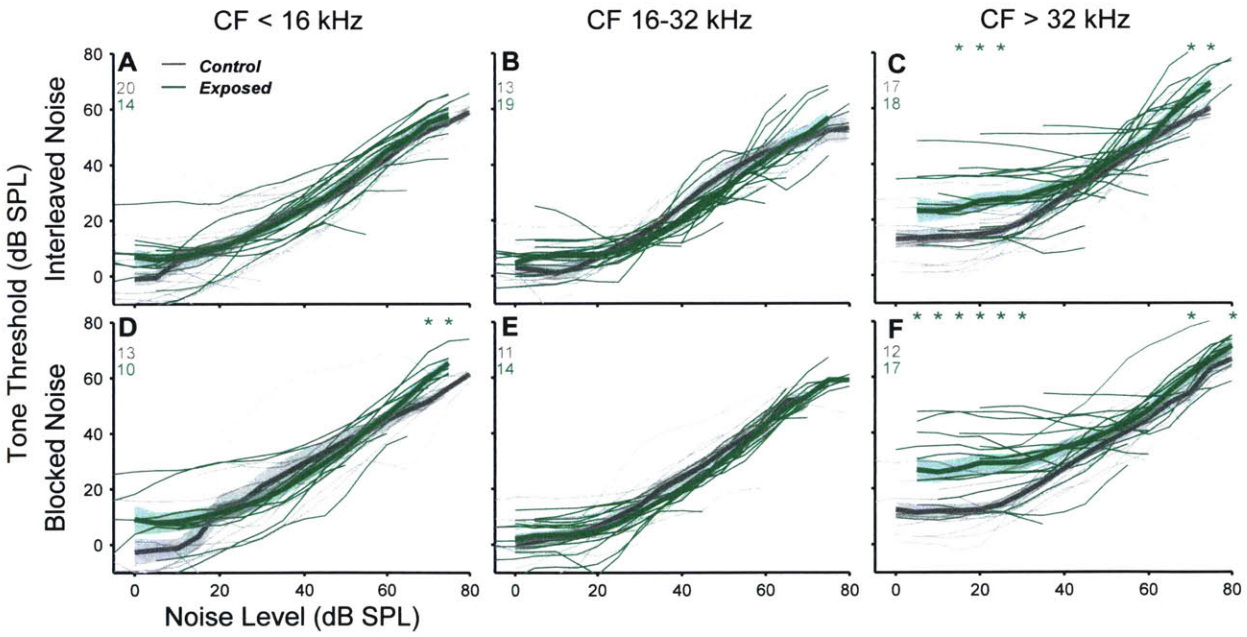

Figure 3.4. Tone thresholds in noise. **A-C**, Interleaved noise paradigm. **D-F**, Blocked noise paradigm. For each panel, tone threshold was calculated for each noise level as the level at 10% of the rate range over the excitatory portion of the rate-level fit. Thin lines indicate individual neurons, smoothed using a 3-point triangular-weighted moving average. Thick lines and clouds indicate means ± SEs. Thresholds were excluded from analysis at noise levels where tone-driven rate was less than 5% of the tone-driven rate in quiet, avoiding contamination by rate-levels too nosy to accurately fit. Numbers in the upper left indicate the number of control (grey) and exposed (green) units in each category. Stars indicate significant effects of exposure ($p<0.01$, Tukey-Kramer-corrected post-hoc test following a 2-way ANOVA).

Effects on suprathreshold responses were quantified by the tone-driven rate range (TDRR), the range of firing rates elicited across all tone levels for a given noise level. While noise generally decreased TDRR (**Fig 3.2A,E**), in conditions where noise was suppressive, TDRR could increase due to a decrease in response at subthreshold tone levels (**Fig 3.2B,F**), or an increased response at high tone levels (**Fig 3.2C**). Changes to TDRR by the introduction of background noise were quantified by the ratio between TDRR in background noise and the TDRR in quiet. This metric has been used in both the AN and IC, where it has been referred to simply as 'scale' (Costalupes, 1985; Ramachandran et al., 2000). For the interleaved noise paradigm, high noise levels caused a greater reduction in TDRR for neurons in both the non-neuropathic and neuropathic regions (**Fig 3.5A,B).** Reduction was stronger in the neuropathic region, where the effect of exposure was significant (main-effect: <16 kHz: $F_{1,35} = 1.9$, $p = 0.17$; 16-32 kHz: $F_{1,30} = 4.8$, $p = 0.036$; interaction: <16 kHz: $F_{1,35} = 4.5$, $p = 0.04$; 16-32 kHz: $F_{1,30} = 8.7$, $p = 0.006$). A first-glance, it is surprising that relative TDRR is *higher* for CFs > 32 kHz of exposed mice (**Fig 3.5C**; main-effect: $F_{1,34} = 11$, $p = 0.002$; interaction: $F_{1,34} = 10$, $p = 0.003$). However, this effect is likely driven by the threshold shift in that region. Two example neurons from this region are shown in **Fig 3.2D&H**. Due to threshold shift, noise did not affect the tone response in the exposed neuron (**H**) below 40 dB SPL. Once noise was supra-threshold, relative TDRR decreased rapidly, returning to control-levels by 60 dB SPL (**Fig 3.5C**).

Curiously, relative TDRR was not affected by exposure in either the non-neuropathic or

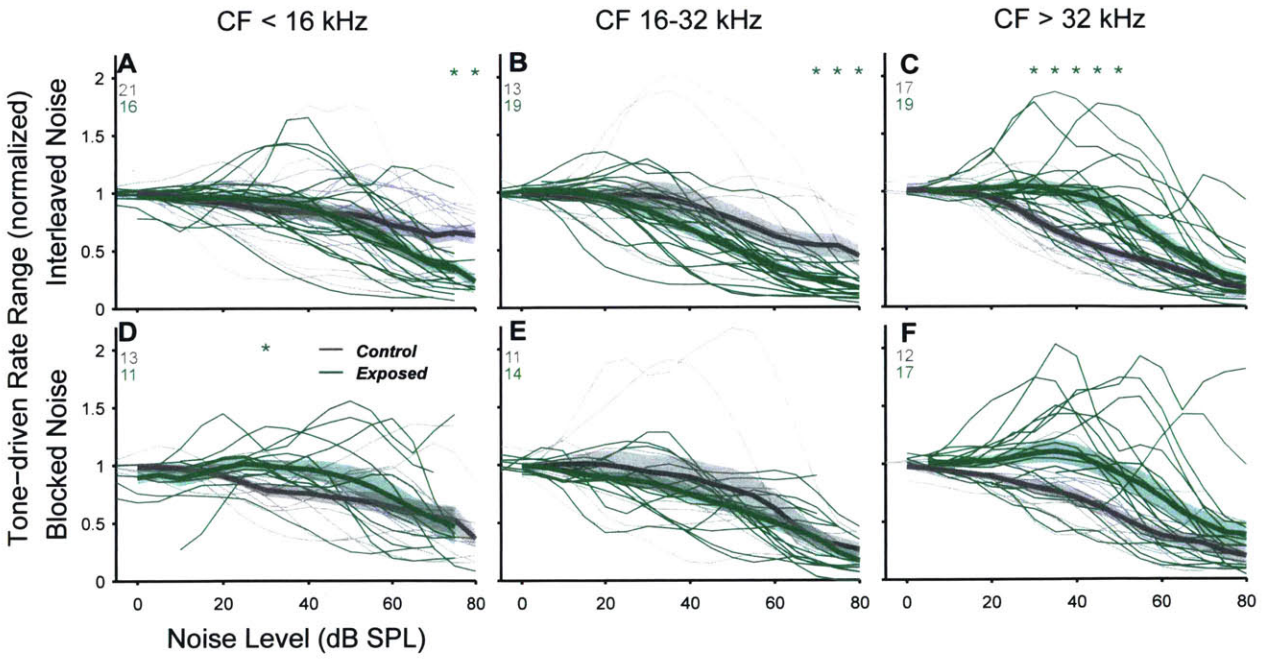

Figure 3.5. Effect of noise on tone-driven rate range. **A-C**, interleaved paradigm. **D-F**, blocked paradigm. For each panel, tone-driven rate range was calculated for each noise level as the range of rates over 10 to 90% of the excitatory portion of the rate-level fit, and normalized to the tone-driven rate range at the lowest noise level tested, effectively in quiet. Line and star conventions are as in Figure 3.4.

neuropathic regions when the effect was quantified in the same neurons using the blocked noise paradigm (**Fig 3.5D,E**). Since the noise level switches every 600 ms in the interleaved paradigm, but remains constant for ~70 seconds in the blocked paradigm, this suggests that neuropathy may cause an impairment of short-term adaptation that is only apparent under dynamic signal conditions.

Long-term adaptation caused clear changes to the response to noise in the blocked paradigm relative to the interleaved paradigm. In neurons with monotonically-increasing noise rate-level functions, adaptation caused a reduced response to high noise levels in the blocked paradigm (**Fig 3.2A,E,H,** top vs. bottom rows). In such neurons this mechanism increases the fidelity of the tone response by expanding the TDRR. In neurons with monotonically-decreasing functions, however, adaptation increased the response to noise at high levels, counteracting the noise-driven increase in TDRR observed in the interleaved paradigm (**Fig 3.2B,F**). In neurons with non-monotonic noise responses the behavior was complex, improving tone-driven responses at some noise levels while decreasing them at others (**Fig 3.2 C,G**). Since changes in firing rate between

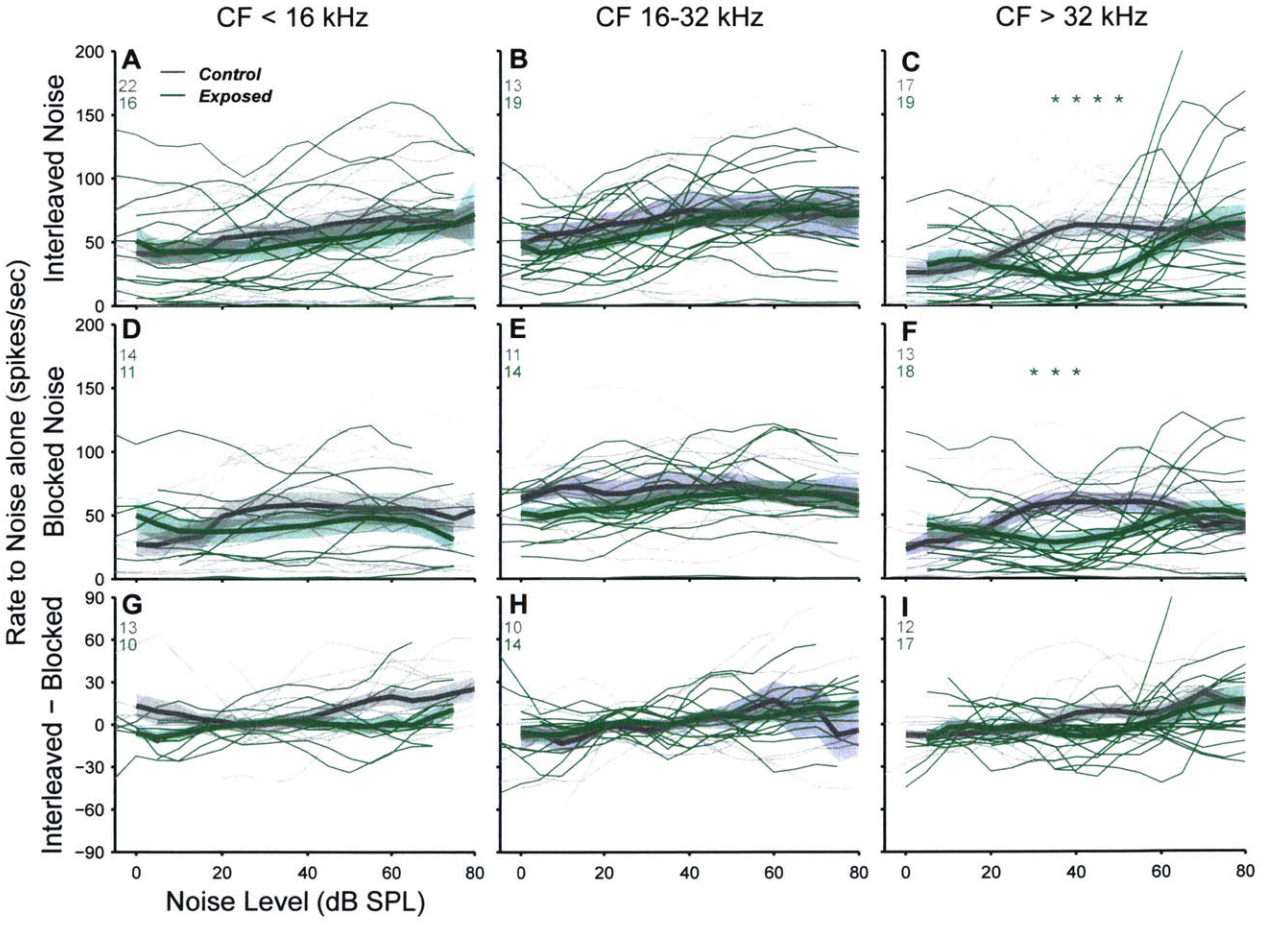

Figure 3.6. Response to noise alone is not affected by neuropathy. **A-C**, interleaved paradigm. **D-F**, blocked paradigm. **G-I**, difference between the interleaved and blocked conditions. For each panel, rate to noise alone was calculated for each noise level as rates at the lowest tone level tested. Line and star conventions are as in **Figure 3.4**.

the interleaved and blocked paradigms were roughly equivalent to changes that would occur by decreasing the noise level, these results suggest adaptation that occurs below the level of the IC, either in the brainstem nuclei or in the cochlea.

On average, there were no effects of exposure on the response to noise alone for both the interleaved and blocked paradigms in neurons outside the threshold shift region (**Fig 3.6A,B,D,E**). For CFs >32 kHz, threshold shift caused reduced noise responses at noise levels of 30-45 dB SPL for both conditions, but no significant main effect or interactions were detected (**Fig 3.6C,F**, main effect: Interleaved: $F_{1,34} = 2.1$, $p = 0.16$; Blocked: $F_{1,29} = 0.9$, $p = 0.35$; exposure*noise level interaction: Interleaved: $F_{1,34} = 1.7$, $p = 0.2$; Blocked: $F_{1,29} = 1.3$, $p = 0.26$). For each, neuron, we calculated the difference in noise response between the two paradigms (**Fig 3.6G-H**). As observed in the examples, noise response was sometimes elevated under the blocked paradigm, sometimes reduced. There were no significant effects of exposure. Thus, long-term adaptation

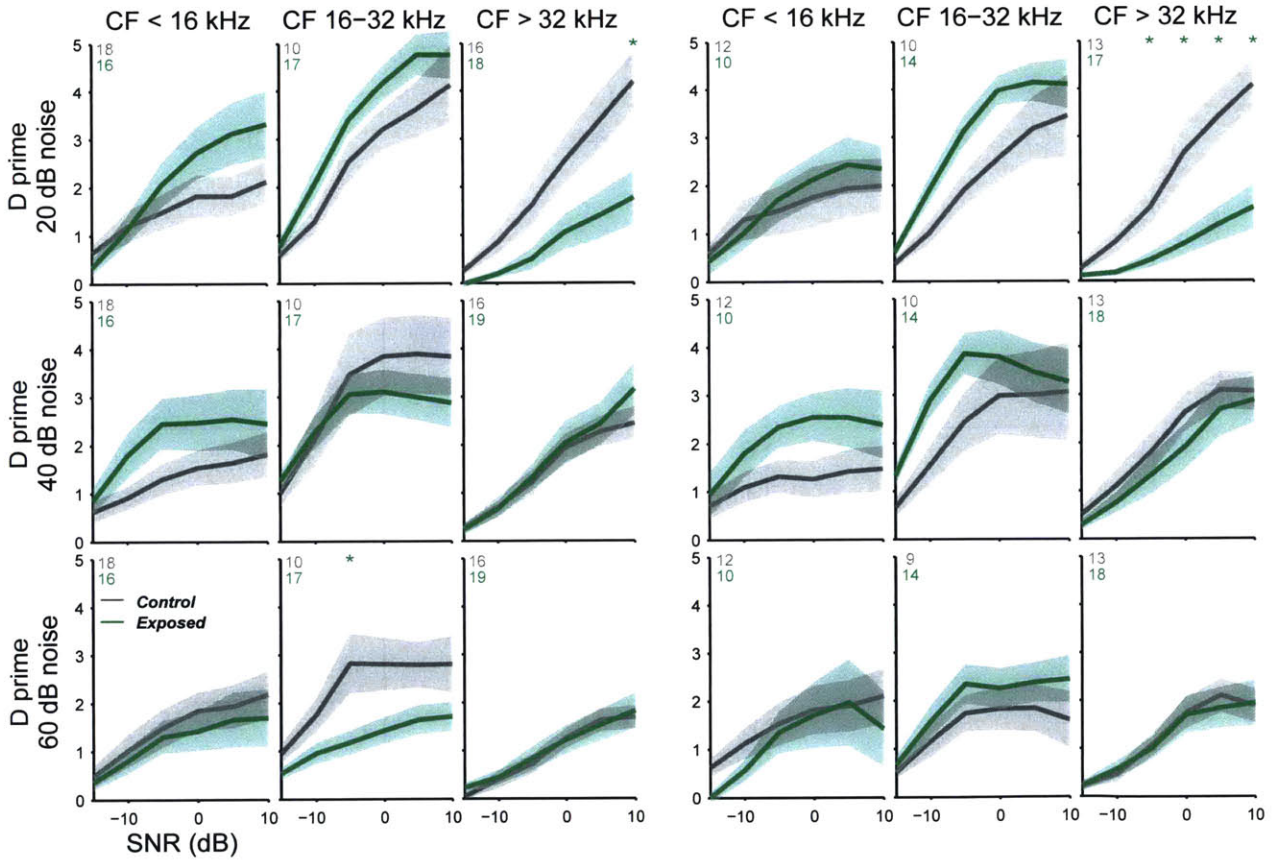

Figure 3.7. Neural detection of low-SNR tones is impaired at moderate noise levels in exposed mice. Detection is not impaired when noise is continuous. **Left columns**, interleaved paradigm. **Right columns**, blocked paradigm. For each panel the D prime between the spike count distribution at the indicated tone:noise SNR and the lowest tone level presented is plotted. D prime was computed using Hedge's g, the difference in means divided by the pooled standard deviation. For each noise level (20, 40, 60, top-to-bottom), D prime was averaged for each neuron over noise levels ranging from -5 to +5 re the level indicated. Thick lines and clouds indicate means ± SEs, stars indicate significant effects of exposure ($p<0.01$, Tukey-Kramer-corrected post-hoc test following a 2-way ANOVA).

could both help and hinder coding of tones, but the effect overall did not seem to contribute to the difference in coding of tones at high noise levels between the two paradigms (**Fig 3.5B vs. 3.5E**).

Neural detection of low-SNR tones

High-threshold AN fibers are likely to take a leading role in difficult auditory environments, such as when signal-to-noise (SNR) ratio is low. Thus, the greatest effect of noise-induced neuropathy, which is specific to these fibers, should be observed at low SNRs. We examined evidence for this hypothesis by replotting rate responses on a SNR*noise level grid (**Fig 3.2,** right sub-columns). Whereas the tone levels encoded by an individual neuron shifted as noise level increased, the SNRs encoded remained constant once the tone level was sufficient to elicit a response (**A**). Responses to 0 dB SNR tones at high noise levels appear to be diminished in neurons of exposed mice (ex. **A vs. E, B vs. F, C vs. G**). We quantified the detectability of tones at low SNRs by computing the d prime (d') between the spike count distributions at a given SNR and at the lowest tone level presented. Average d' was reduced by a factor of 1.6 to 2.4 in exposed neurons in the neuropathic (16-32 kHz) region at moderate (60 dB) noise levels for the interleaved paradigm (**Fig 3.7**, bottom row; exposure effect: $F_{1,25} = 6.7$, $p = 0.02$; exposure*SNR interaction $F_{1,25} = 6.0$, $p = 0.02$). The effect was greatest at -5 dB SNR ($p = 0.009$). In parallel with the exposure effects on TDRR (**Fig 3.5**), d' was unchanged in exposed neurons at high noise levels for the blocked paradigm ($F_{1,21} = 0.9$, $p = 0.3$).

Consistent with the effect of threshold shift, d' was reduced at 20 dB noise levels for both the interleaved and blocked paradigms for neurons with CFs > 32 kHz (**Fig 3.7,** $F_{1,32} = 8.1$, $p = 0.008$; $F_{1,28} = 13$, $p = 0.001$; respectively); at 20 dB SPL the tone level is barely above threshold in exposed neurons (**Fig 3.2D vs. H**). Surprisingly, d' was slightly *elevated* in exposed neurons in the neuropathic (16-32 kHz) region at low (20 dB) noise levels for both the interleaved and blocked paradigms, though main effects were only marginally significant ($F_{1,25} = 3.0$, $p = 0.09$; $F_{1,22} = 4.7$, $p = 0.04$, respectively). The source of this exposure-induced improvement is unclear, but could be related to the increased rate-level slopes to tones and decreased maximum rates to noise observed in these neurons (**Chapter 2**).

In order to evaluate the ability of neurons to discriminate tone level at low-SNRs without making assumptions on the shape of the SNR-vs.-noise level function, we calculated the mutual information (MI) between firing rate distributions and SNR for each noise level. MI was reduced in the neuropathic (16-32 kHz) region of exposed mice at noise levels above 50 dB, but remained more stable in control mice (**Fig 3.8B**). Exposure effect and interactions did not reach significance, but post-hoc tests indicated significant effects from 70 to 75 dB ($p < 0.01$). This effect was not observed in the blocked noise paradigm (**Fig 3.8E**). In keeping with the d' results, MI was *higher* in the exposed group for noise levels around 20 dB SPL for both paradigms, though the differences did not reach significance. A clear and substantial exposure effect was revealed in the difference between MI of the two paradigms: MI was on average 0.2 bits worse in the interleaved paradigm for exposed neurons, while MI was on average 0.1 bits better in control neurons (**Fig 3.8H**, exposure effect: $F_{1,18} = 8$, $p = 0.01$; interaction: $F_{1,18} = 15$, $p = 0.001$).

Surprisingly, MI was *elevated* at moderate levels in the non-neuropathic region (**Fig 3.8A,D**). While the main effect of exposure was not significant and interaction was marginally-significant, post-hoc tests indicated significant effects for noise levels between 35 and 50 dB SPL in the blocked paradigm (exposure effect: interleaved: $F_{1,32} = 0.8$, $p = 0.4$; blocked: $F_{1,20} = 4$, $p = 0.1$ interaction: interleaved: $F_{1,32} = 0.3$, $p = 0.6$; blocked $F_{1,20} = 4.8$, $p = 0.04$). Hints of this effect, though not significant, were also seen in elevated d' values at 40 dB SPL noise in the non-neuropathic

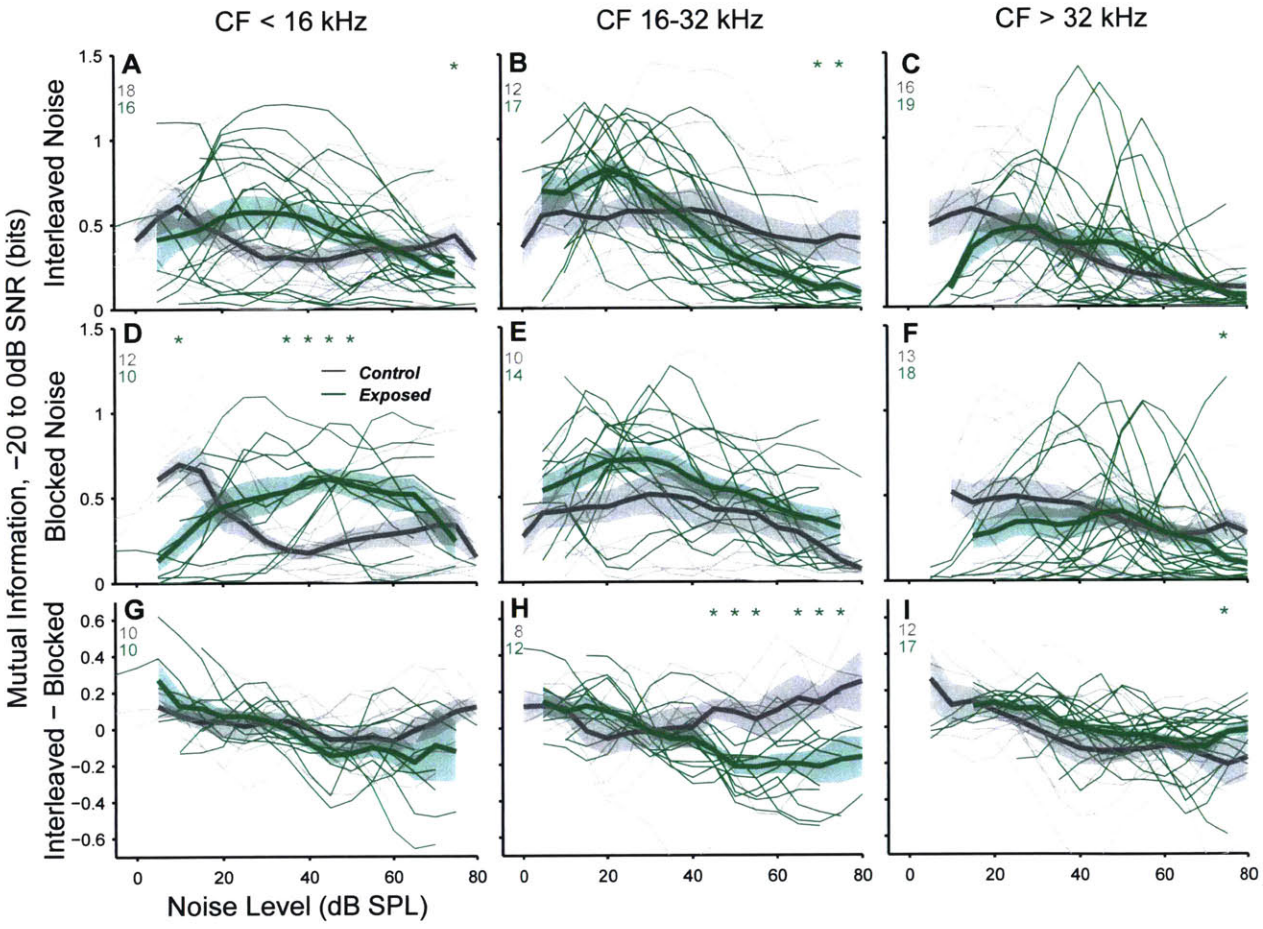

Figure 3.8. Mutual information is reduced in the neuropathic region for the interleaved, but not blocked noise paradigm. **A-C**, interleaved noise paradigm. **D-F**, blocked noise paradigm. **G-I**, difference between the interleaved and blocked paradigms. For each panel, mutual information (MI) was calculated for each noise level for tone levels between -20 and 0 dB SNR. Line and star conventions are as in **Figure 3.4**.

region **(Fig 3.7)**. We speculate that this improvement could arise from a reduction in sideband inhibition (see Discussion).

Dynamic range of tone-driven rate was not affected by neuropathy

Convergence of low- and high-threshold AN fibers may improve the dynamic range of central auditory neurons. We further assessed changes in dynamic range by evaluating how the coding of a specific tone level changed with the introduction of noise. The tone level evaluated was equalized across neurons by comparing responses to tones at the saturation level in quiet, L_{Q90}. This level is indicated in example neurons by a large black circle (**Fig 3.2**, left sub-columns). The effect of noise on relative tone-driven rate at L_{Q90} was remarkably constant across neurons, with the exception of neurons in the threshold shift region (**Fig 3.9A-C,E-G**). To remove the effect of differing noise thresholds we calculated the dynamic range over which response rates ranged

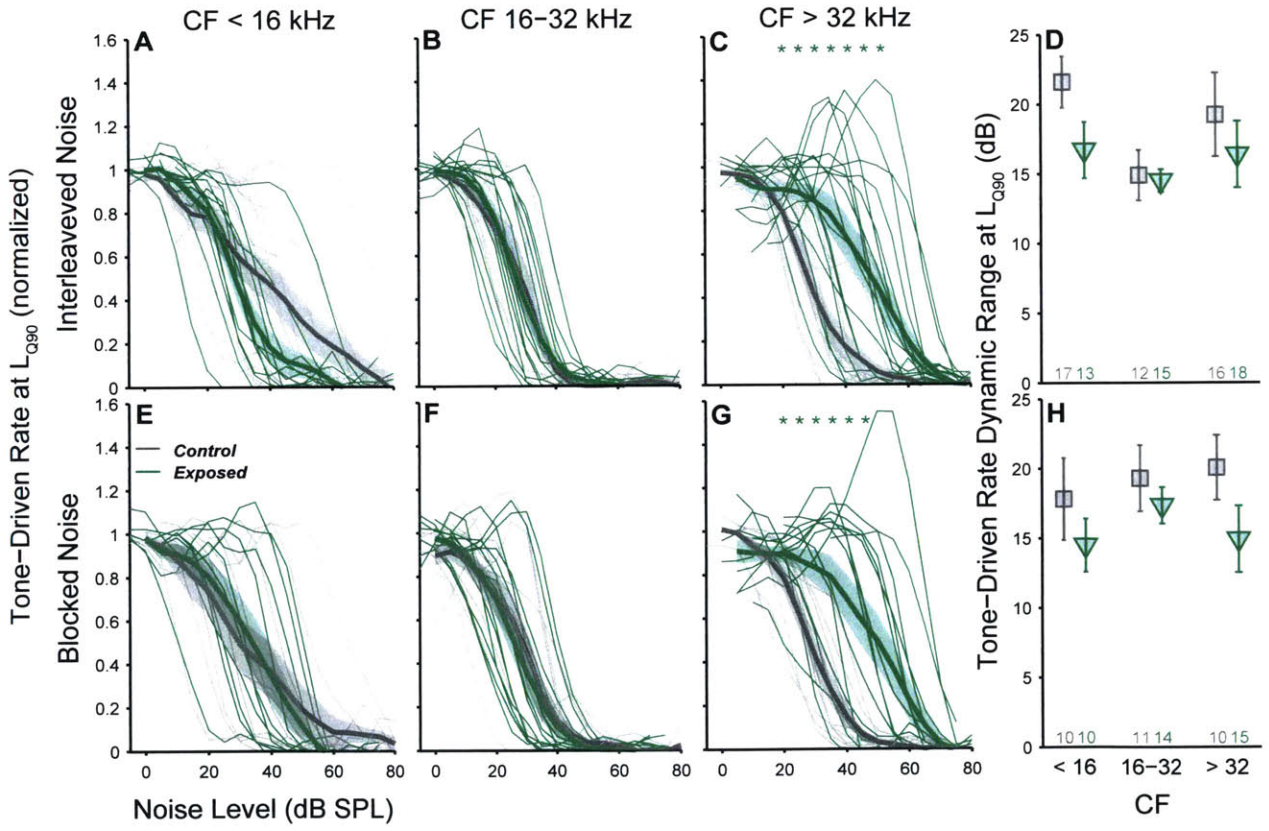

Figure 3.9. Tone-driven rate dynamic range at L_{Q90} is unchanged in exposed mice. **A-D**, interleaved paradigm. **E-H**, blocked paradigm. **A-C,E-G,** For each panel, tone-driven rate was calculated for each noise level as the range of rates from the lowest tone level tested to the L_{Q90}, and normalized by the response at the lowest noise level tested. Line conventions as in figure 4.3. **D,H**, The dynamic range was calculated for each neuron as the range of levels encompassing 10% to 90% of the tone-driven rate-vs.-noise level function. Point and bars are mean ± SEs. Post-hoc tests did not reveal any significant effects of exposure.

from 90% to 10% by a four-parameter fit to each function. Dynamic range was not affected by exposure for any frequency region for both the interleaved and blocked noise paradigms (two-way ANOVA, $F_{1,85} = 2.3$, $p = 0.13$; $F_{1,64} = 3.5$, $p = 0.065$).

Tone slopes were elevated at low and moderate noise levels in the non-neuropathic region

Tone rate-level slopes in quiet were elevated in the neuropathic region when estimated from FRAs in a larger set of neurons (**Fig 2.11I**). The neurons described here are a subset of those neurons. Tone slopes were estimated in noise using the same method: the slope over the excitatory portion of the rate-level fit. Consistent with the slopes in quiet, slope was elevated in the neuropathic region at sub-threshold noise levels (**Fig 3.10B,E**). In the interleaved noise paradigm, noise caused tone slopes to rapidly decrease in exposed neurons, becoming shallower than control neurons at moderate noise levels. In the blocked noise paradigm, tone slopes decreased to control levels at moderate noise levels, but were not depressed *re* controls. Two-way ANOVAs failed to detect any significant effects of exposure or interactions, but post-hoc tests revealed a significant difference in the interleaved noise paradigm around 60 dB SPL.

Surprisingly, there was a strong effect of exposure in the non-neuropathic region. Slopes were unchanged by exposure in quiet (see also **Fig 2.11I**), but decreased more slowly in exposed neurons than in controls (**Fig 3.10A,B**). For the blocked paradigm, exposed slopes did not decrease at all, and in two neurons became steeper at high noise levels. Effect of exposure and interaction were significant under both paradigms (exposure effect: interleaved: $F_{1,30} = 10$, $p =$

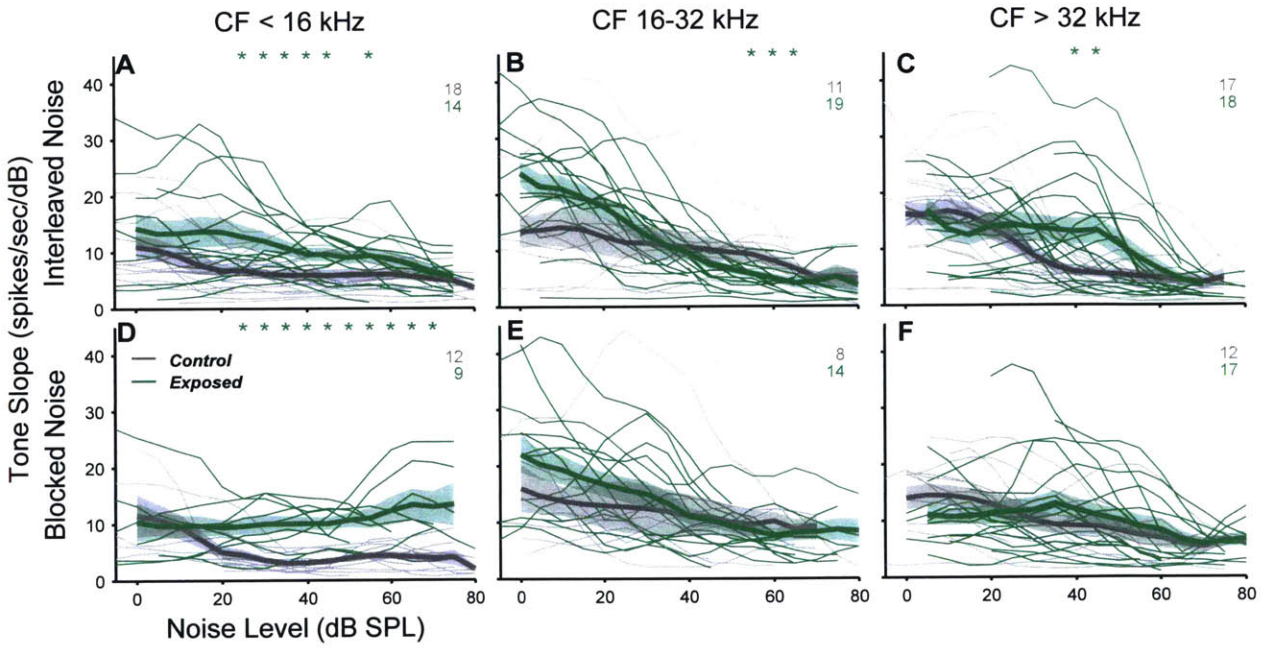

Figure 3.10. Tone slope is elevated in noise in the non-neuropathic region of exposed mice. **A-C**, tone slopes under the interleaved paradigm. **D-F**, slopes under the blocked paradigm. For each panel, tone slope was calculated for each noise level as the slope over the excitatory portion of the rate-level fit. Slopes were excluded from analysis at noise levels where tone-driven rate was less than 5% of the tone-driven rate in quiet, avoiding contamination by rate-levels too nosy to accurately fit. Line and star conventions are as in **Figure 3.4**.

0.003; blocked: $F_{1,19} = 24$, $p << 0.001$; exposure*noise level interaction: interleaved: $F_{1,30} = 11$, $p = 0.002$; blocked: $F_{1,19} = 34$, $p << 0.001$). Elevated slopes are likely responsible for improved MI in these neurons, and may be driven by changes to sideband inhibition (see Discussion).

Tone in noise in multi-units

Tone in noise responses were also collected for multi-unit data, as well as for multi-units recorded in anesthetized mice. The results were surprisingly different from the single-unit results; see **Chapter 3 Supplement** for complete details. Briefly, while there were no effects of exposure on tone thresholds and tone-driven dynamic range at L_{Q90} as observed for single-units, unlike single-units, relative TDRR was unchanged and d' at low SNRs was increased in awake multi-units. Under anesthesia, multi-units in the neuropathic region exhibited deficits in both tone-driven rate and d' at low SNRs for the blocked noise paradigm (**Fig S3.5, S3.7**). While no data

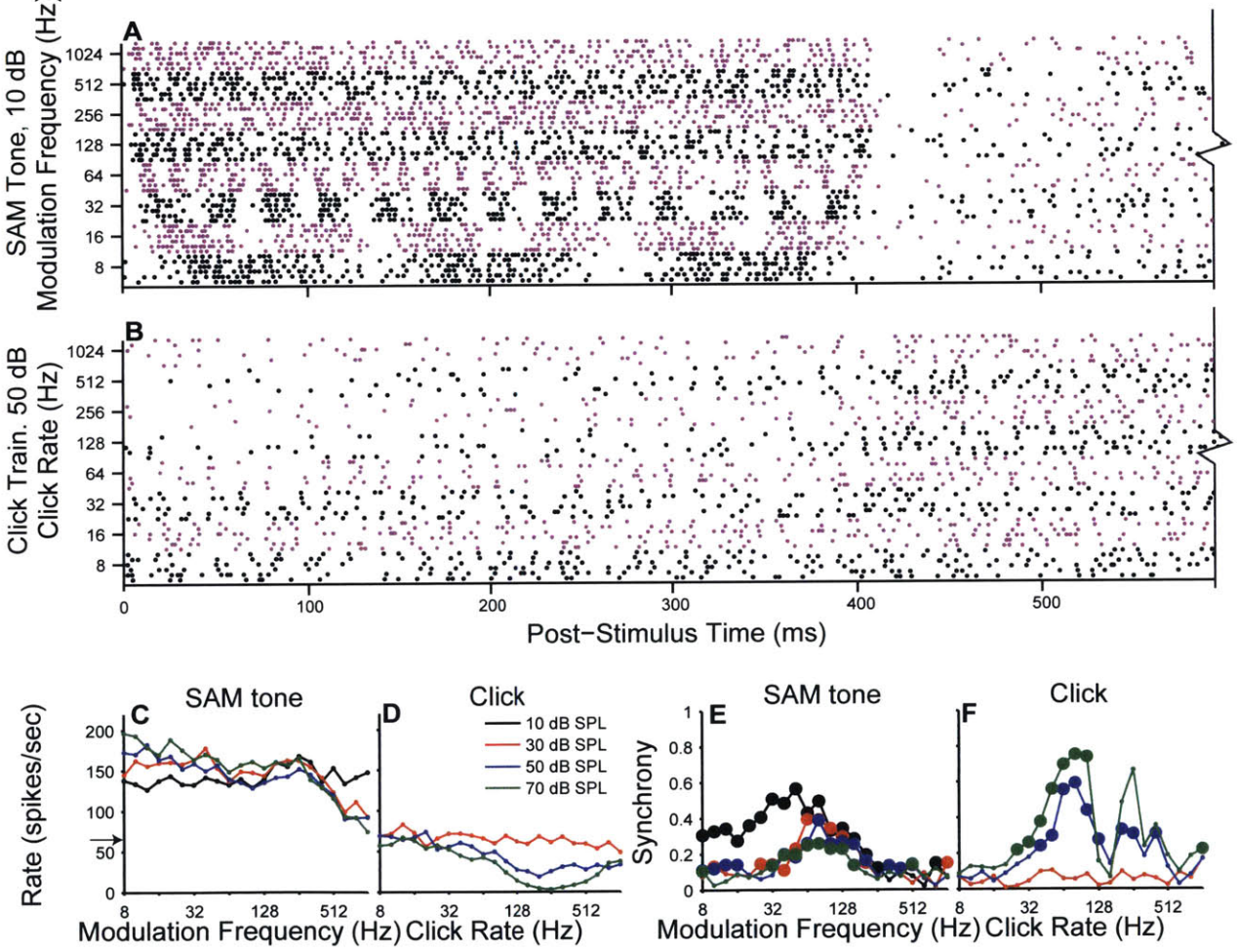

Figure 3.11. Example response to temporal envelope stimuli. **A,B,** Spike raster plots for responses to 10 dB SAM tone at CF **(A)** and 50 dB click train **(B)** in a control neuron, CF= 24 kHz. For each panel each dot indicates a single spike, each row is the response to a different trial, and alternating colors indicate stimuli of different modulation rates. Stimuli were 400 ms on, 600 ms off, most of the inter-stimulus period is cut off to improve clarity. **C,D** Average Rate, **E,F**, Synchrony (vector strength). Significant synchrony is marked by large points. Arrow in **C** indicated the spontaneous rate

was collected for the interleaved noise paradigm in anesthetized mice, these results suggest substantial interaction between the effects of exposure and anesthesia.

Temporal coding was impaired by neuropathy

We probed for changes in the coding of temporal envelopes by measuring the timing of responses to sinusoidally amplitude modulated (SAM) tones and click trains. Since the effect of low-SR neuropathy was expected to affect responses only at higher intensities, responses were collected at three levels: 30, 50, and 70 dB SPL. Since temporal precision is highly dependent on stimulus level, we also collected SAM-tone responses at 15 dB *re* pure tone thresholds, which is near the level that elicits maximum synchrony for most IC neurons (Krishna and Semple, 2000).

A typical response to SAM tones is shown in **Fig 3.11A**. As for this example neuron, rate modulation transfer functions (rMTFs) to SAM tones were most often all-pass over the range tested (**Fig 3.11C**). Temporal precision was quantified by synchrony, or vector strength, which evaluates the degree to which spike responses are clustered on one phase of the stimulus envelope. Temporal modulation transfer functions (tMTFs), were predominantly low-pass near threshold, becoming band-pass as level was increased (**Fig 3.11E**). A response to clicks is shown for the same neuron in **Fig 3.11B**. This response was again typical of the population: an all-pass or slightly band-reject rMTF, and a band-pass tMTF (**D,F**). 30 dB SPL clicks elicited a response in very few neurons, so results are not shown at the population level.

Responses were pooled across neurons in the non-neuropathic, neuropathic, and threshold-shift regions. In the neuropathic region, synchrony was reduced for moderate-level stimuli (50

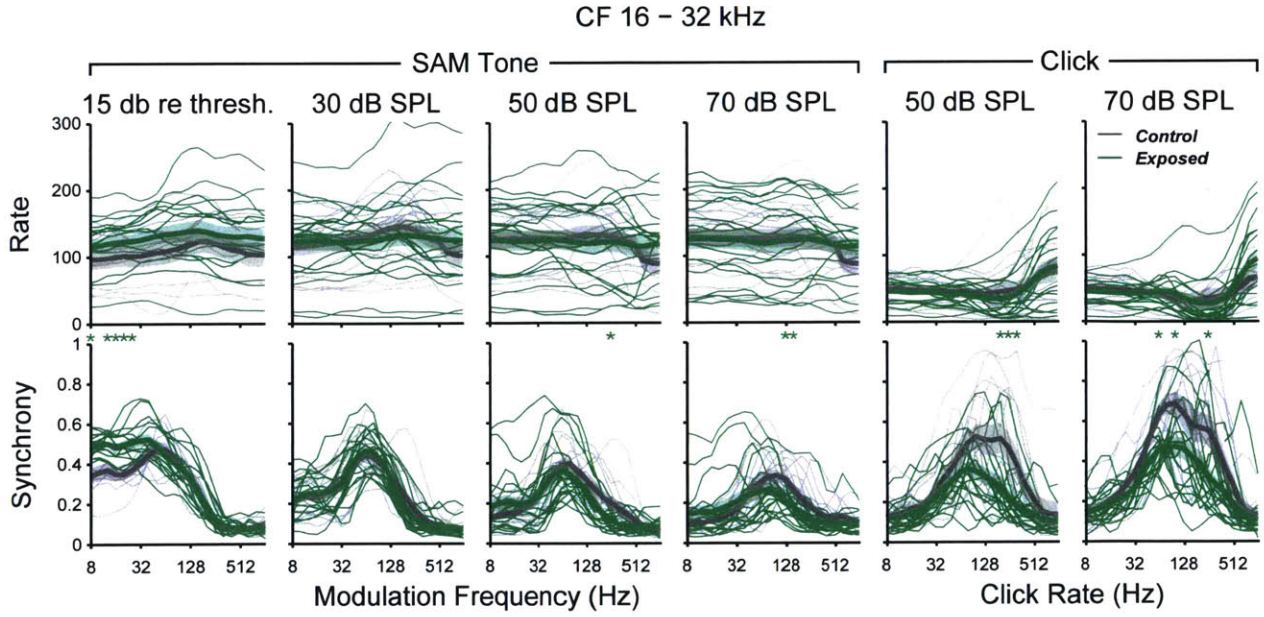

Figure 3.12. Synchronization to temporal envelopes at moderate levels is impaired in the neuropathic region. Responses are pooled from neurons with CFs 16-32 kHz (neuropathic region). **Left,** Responses to SAM tones at CF. First column was presented at 15 dB re pure tone threshold. **Right,** Responses to a click trains. Mean rate (**Row 1**), synchrony (**Row 2**), and synchronized rate (**Row 3**) were all computed over the steady-state portion of the stimulus. Line and star conventions are as in **Figure 3.4**.

& 70 dB SPL) with intermediate modulation frequencies (64-128 Hz), but unchanged at 30 dB SPL (**Fig 3.12**). Since noise-induced neuropathy is selective for medium- and high-threshold AN fibers, the absence of an effect at 30 dB might be simply due to the relative dominance of low-threshold neurons at this level. Surprisingly, for SAM tones 15 dB re threshold, synchrony was *elevated* at low modulation frequencies. While tMTFs are entirely low-pass in the AN, the prevalence of other shapes, most commonly band-pass shapes, increases in the CN and IC (Joris et al., 2004). Furthermore within the IC and CN, tMTFs tend to transition from low-pass to band-pass with increasing level (Rees and Møller, 1987; Krishna and Semple, 2000). Since thresholds were not elevated by exposure in this region **(Fig 3.3, 2.11C**), the effect is unlikely to be due to a simple shift in input level. The effect could be driven by an elevation in pure tone slopes in these neurons (**Fig 2.11I**). However, within neuropathic neurons there was no correlation between pure tone slope and synchrony to 15 dB re threshold, below 32 Hz SAM tones (not shown).

Synchronization to SAM tones was not affected by exposure for neurons in the non-neuropathic region (**Fig 3.13**). While there was a trend for average rate to be depressed in response to SAM

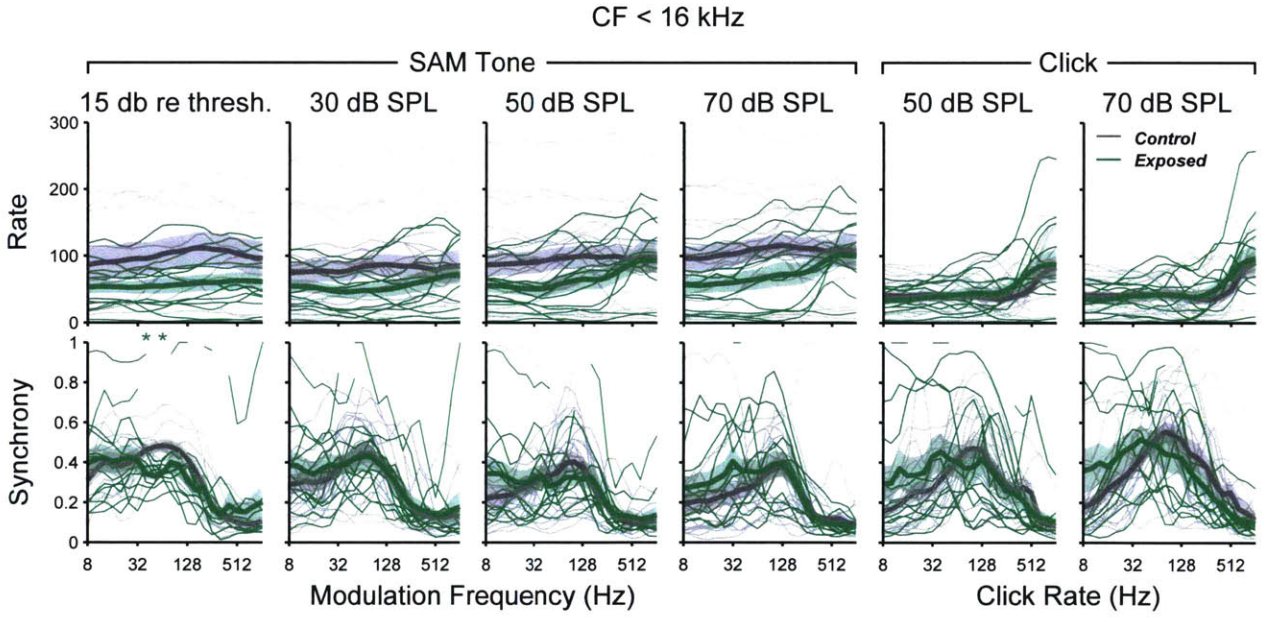

Figure 3.13. Exposure effects on synchrony were minimal in the non-neuropathic region. Responses are pooled from neurons with CFs less than 16 kHz (non-neuropathic region). **Left,** Responses to SAM tones at CF. First column was presented at 15 dB re pure tone threshold. **Right,** Responses to a click trains. Mean rate (**Row 1**), synchrony (**Row 2**), and synchronized rate (**Row 3**) were all computed over the steady-state portion of the stimulus. Line and star conventions are as in **Figure 3.4**.

tones, effect of exposure was not significant for any panel. For stimuli 15 dB re pure tone threshold, post-hoc tests indicated small reductions in synchrony at 40 and 51 Hz.

Neurons in the threshold shift region exhibited changes to their SAM-tone responses that were consistent with a loss of sensitivity (**Fig 3.14**). At 30 dB, rate was depressed; At 50 dB, synchrony was enhanced for low modulation frequencies. Since tMTFs transition from low-pass to band-pass with increasing level (Rees and Møller, 1987; Krishna and Semple, 2000), and because 50 dB is 10-30 dB above threshold for exposed neurons, but 30-50 dB above threshold for control neurons, this change is likely driven by the simple effect of threshold shift. When stimuli were presented at 15 dB re pure tone threshold, there were no differences in SAM tone response (**Fig 3.14, left**).

Mirroring the SAM-tone changes, synchronization to click trains was also reduced in the neuropathic region (**Fig 3.12, right**). As for 50 and 70 dB SAM tones, changes were limited to frequencies around 64-128 Hz. Synchronization to clicks was unaffected in both the non-CF < 16 kHz

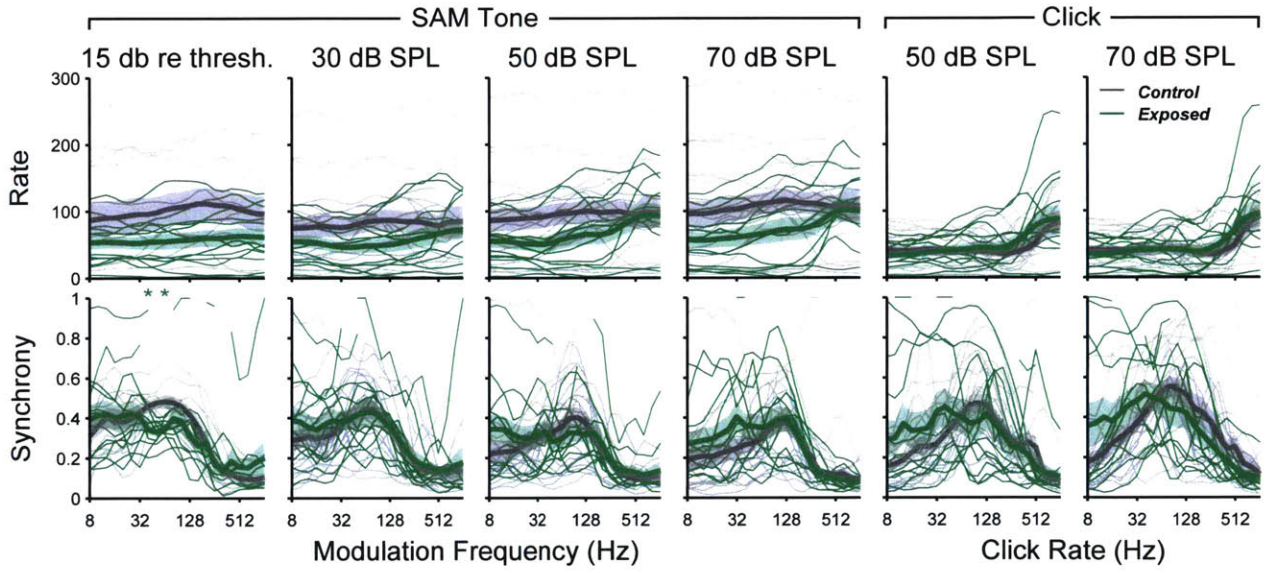

Figure 3.14. Synchronization changes in the threshold-shift region are consistent with a loss of sensitivity. Responses are pooled from neurons with CFs >32 kHz (threshold shift region). **Left,** Responses to SAM tones at CF. First column was presented at 15 dB re pure tone threshold. **Right,** Responses to a click trains. Mean rate (**Row 1**), synchrony (**Row 2**), and synchronized rate (**Row 3**) were all computed over the steady-state portion of the stimulus. Line and star conventions are as in Figure 4.4.

neuropathic and threshold shift regions (**Figs 3.13, 3.14**).

DISCUSSION

Encoding of signals in noise across the auditory system

Separating signal from noise is a general problem faced by any communications system. While behavioral tests indicate that the auditory system is remarkably good at this task, the mechanisms that underlie this ability remain incompletely understood. From the peripheral view, the central auditory system faces a daunting task: individual AN fibers, the gateway to the auditory system, encode stimuli over a limited dynamic range, ranging from 10 to 40 dB (Sachs and Abbas, 1974). Thus, moderate level noise can drive these neurons into saturation, disrupting their ability to encode transient signals. Fortunately, the human auditory nerve is not made up of one neuron, but some 36,000 (Jahn and Santos-Sacchi, 2001). Each inner hair cell is contacted by 10-30 AN fibers (Liberman et al., 1990), which can be divided based on sensitivity to sound. Relative to behavioral detection thresholds, low-threshold fibers encode levels of 0 to 15 dB, medium-threshold fibers encode 10 to 30 dB, and high-threshold fibers encode 30 to 60 dB (Liberman, 1978). In a moderate level background noise, tone-driven rate range (TDRR) is less affected in high-threshold fibers than in low-threshold fibers (Costalupes, 1985). Moderate acoustic overexposures such as those used in this study cause a preferential neuropathy of medium- and high-threshold fibers (Furman et al., 2013). Thus, in isolation, the decrease in relative TDRR and mutual information between spike count and SNR observed in the neuropathic region at high noise levels observed using the interleaved paradigm could be a direct result of neuropathy (**Fig 3.5B**).

However, the results as a whole are inconsistent with a simple, direct effect of high-threshold AN fiber neuropathy. Relative TDRR was also decreased at high levels for neurons in the non-neuropathic region, and was only changed for both regions when measured using the interleaved noise paradigm, not when using the blocked noise paradigm **(Fig 3.5**). Furthermore, mutual information and d' analysis indicate that coding of low-SNR tones was improved for 40 dB noise levels when measured in the blocked paradigm.

The effect of a continuous background noise on the coding of tones in the inferior colliculus has been examined in both anesthetized guinea pigs and in decerebrate cats (Rees and Palmer, 1988; Ramachandran et al., 2000). Both studies used a paradigm similar to the blocked noise paradigm used here. Noise-induced shifts in tone thresholds were similar to those observed here – about 1 dB/dB once noise threshold was reached. Both studies divided the population into distinct response types based on the shape of frequency/level tuning. Because the cochlear frequency region where exposure caused neuropathy without threshold shift was an octave-wide (**Fig 2.1**), the number of neurons with CFs in this region was limited. Therefore, further division by unit type would have resulted in too few neurons in each category for a meaningful comparison. Furthermore, analysis of a large dataset indicates that frequency response types form a continuous distribution rather than falling into discrete classes (Palmer et al., 2013), and a clear correspondence between morphological and physiological cell type has proven elusive. Within narrowly tuned, monotonic (type I) units, Ramachandran et al (2000) report a noise-induced

decrease in TDRR (or "scale") of -1.5%/dB. Since we pooled all unit types together, we did not evaluate the rate of decrease for each individual neuron, but the slope of the average relative TDRRs-vs.-noise level function was approximately the same, about -1.4%/dB.

The differences between the interleaved and blocked noise paradigms suggest that adaptation to the recent stimulus history may be altered by neuropathy. Like auditory nerve fibers, the dynamic range of most inferior colliculus neurons is limited, ranging from 20 to 40 dB. However, when tested using continuous stimuli, the most sensitive range of the rate-level function shifts toward the most frequently occurring level (Dean et al., 2005). This dynamic range adaptation has also been observed in the primary auditory cortex (Watkins and Barbour, 2008), and to a lesser extent, in the auditory nerve (Wen et al., 2009). Adaptation to mean stimulus levels also improves the coding of dynamic signals in the face of a static noise background (Rabinowitz et al., 2013). Dynamic range adaptation occurs with time constants of 100 to 400 ms (Dean et al., 2008; Wen et al., 2012). Therefore, the deficits in tone responses observed in neuropathic neurons under the interleaved noise paradigm could be caused by changes to dynamic range adaptation. However, deficits in dynamic range adaptation should also manifest as deficits in tone responses under the blocked noise paradigm. Tone responses were not affected by exposure under the blocked paradigm. Therefore, it seems neuropathy may alter medium-term adaptation, while preserving long-term adaption.

Another form of adaptation is found in the medial olivocochlear (MOC) and middle ear muscle (MEM) reflexes, which can decrease the effective input to inner hair cells, improving signal detection in noise (Kawase et al., 1993; Pang and Guinan, 1997). Since dynamic range adaptation can occur under anesthesia, which almost completely inhibits the MOC reflex (Chambers et al., 2012), and since it can occur at lower stimulus levels than the MEM reflex (Dean et al., 2005; Wen et al., 2009), it is likely that these are three distinct forms of adaptation. Anatomical studies suggest that both MOC and MEM reflexes may be preferentially-driven by high-threshold AN fibers (Rouiller et al., 1986; Liberman, 1991; Kobler et al., 1992; Darrow et al., 2012). In anesthetized mice, the MEM reflex is substantially reduced by cochlear neuropathy; the MOC reflex is substantially attenuated by anesthesia, so assessment of the effects of neuropathy await testing in awake animals (Chambers et al., 2012; Valero et al., 2016). In both the AN and the IC, activation of the MOC reflex counteracts the effect of masking noise by restoring TDRR (Winslow and Sachs, 1988; Kawase et al., 1993; Seluakumaran et al., 2008). MOC neurons produce anti-masking effects on both fast (on the order of 100 ms) and slow (10s of seconds) timescales (reviewed by Guinan, 2011). The MEM reflex has a rapid (<100 ms) onset (Pang and Guinan, 1997; Valero et al., 2016). Thus, while MEM and MOC fast effects could be expected to affect coding for both the interleaved and blocked noise paradigms, MOC slow effects may only affect coding for the blocked noise paradigm. Differential changes to these effects by neuropathy could explain differences between tone coding in the interleaved and blocked noise paradigms.

Changes to tone-in-noise encoding in the non-neuropathic region

Despite the lack of any effect of noise exposure on cochlear function below 16 kHz, neurons

with CFs in this region exhibited substantial changes in their responses to tones in noise. Most notably, the MI between spike counts and -20 to 0 dB SNR tones was enhanced for noise levels between 15 and 60 dB SPL, indicating that neural discrimination of tone level *exceeds* control levels. Detection of low-SNR tones was also improved in this same range (**Fig 3.7**). Both of these effects are likely due to steeper tone rate-level slopes in moderate noise. At the single neuron input-output level, slope is elevated by a reduction in inhibitory synaptic strength but unaffected changes to excitatory synaptic strength (Carvalho and Buonomano, 2009). In the IC, pharmacological blockade of GABA-ergic inhibition causes elevated rate-level slopes (Yang et al., 1992). While responses to on-CF tones where unaffected by noise exposure, inhibition by above-CF tones was reduced in non-neuropathic neurons (**Fig 2.14**). Since the bandwidth of inhibitory tuning to contralateral tones is over 2 octaves in the IC (Xie et al., 2007; Xiong et al., 2013), changes to slope could be caused by reduced sideband inhibition from neurons in the neuropathic region. Furthermore, since in this explanation inhibition is driven by the masking noise, it is consistent with the observed pattern of slope increases only at moderate and high noise levels.

Encoding of temporal envelopes in neuropathy

Phase-locking to both SAM tones and click trains was impaired in the neuropathic region for high stimulus levels, but enhanced for near-threshold SAM tones. In mice exposed using the same exposure paradigm used here, envelope following responses (EFRs) are reduced in response to SAM tones with 32 kHz carrier frequencies but not in response to SAM tones with 11 kHz carrier frequencies (Shaheen et al., 2015). Furthermore, no EFR reduction is observed for near-threshold SAM tones; reduction is greatest at 50 dB SPL. Both EFR and single-unit changes are consistent with high-threshold specific neuropathy. However, EFRs were not measured at modulation frequencies below 400 Hz, prohibiting direct comparison. At low modulation frequencies, EFRs are increasingly dominated by responses from multiple auditory nuclei (especially in animals with small heads), so measurements at these frequencies would be difficult to interpret. Encoding of amplitude modulation is also impaired in the IC of aged rats: both the maximum synchrony and the maximum modulation frequency eliciting a synchronized response are reduced (Rabang et al., 2012). Temporal processing may be impaired in aging due to a reduction in inhibition: presynaptic markers of Gaba-ergic axons are reduced in both the IC and auditory cortex (Burianova et al., 2009; Rabang et al., 2012; reviewed in Caspary et al., 2008). Rabang et al use a model to demonstrate how loss of tuned inhibition can cause changes to the shape of both rate and temporal modulation transfer functions. In the present study, temporal modulation transfer functions in the neuropathic region were more lowpass in response to near-threshold SAM tones, causing synchrony to be *enhanced* relative to controls. The slope of the rate-level function to pure tones is also enhanced in these neurons. Both changes could be the result of exposure-induced changes to the excitatory/inhibitory balance.

More extensive changes to this balance are observed following near-complete cochlear neuropathy by administration of ouabain to the round window: while tone responses are diminished

immediately following neuropathy, an increase in "central gain" causes tone responses to recover in the IC and become hyperactive in the auditory cortex (Chambers et al., 2016). Despite full recovery of tone responses, encoding requiring precise timing - synchronization to envelopes and encoding of speech sounds – is drastically impaired. Similar compensatory mechanisms may occur on a smaller scale following the more limited neuropathy described here.

Consequences to perception

Cochlear neuropathy is likely widespread in humans, manifest as a progressive loss of AN fibers with age due to a lifetime of moderate noise exposures (Viana et al., 2015). Neuropathy may be the root cause of a number of deficits identified in listeners with normal audiograms, such as speech discrimination in noise and ability to use temporal cues (Frisina and Frisina, 1997; Strelcyk and Dau, 2009; Ruggles et al., 2011; Bramhall et al., 2015). In normal hearing listeners, correlations have been found between measures of temporal perception and electrophysiological tests designed to quantify cochlear neuropathy: ABR wave V latency shift in noise is correlated with envelope ITD thresholds (Mehraei et al., 2016), and envelope following response slope is correlated with both modulation depth detection thresholds and envelope ITD thresholds (Bharadwaj et al., 2015). Here, we found that both that coding of tones in noise and precision of temporal coding were impaired in neuropathic mice. However, the results were not straightforward: coding of tones in noise was only impaired when noise level varied every 600 ms, and was actually better for some conditions when noise level was held constant for ~70 seconds. Coding of temporal envelopes was decreased for high-level stimuli, but improved at near-threshold levels. Furthermore, the changes to coding were subtle. Together, these results suggest that either the effects of peripheral fiber loss are partially compensated by compensatory plasticity, or that the midbrain auditory circuit is configured in such a way that a low-SR specific loss has little effect on the responses tested.

SUPPLEMENTAL METHODS

Multi-unit data: The multi-unit responses described here were recorded in a subset of the multi-units described in **Chapter 2**.

SUPPLEMENTAL RESULTS

Rate responses to tones in noise following neuropathy

Tone-in-noise data was collected in both awake and anesthetized groups. In the anesthetized group, results were only collected using the blocked noise paradigm. Continuous noise had a greater effect on single-unit quality in anesthetized mice, resulting in a paucity of anesthetized, single-unit data. Here, we describe multi-unit responses for both awake and anesthetized groups. Multi-unit responses to prolonged stimuli such as these should be interpreted with caution, because drift in the location of the recording electrode could cause a change in the population of neurons comprising the response over time. Drift was detected and controlled for in single-unit data (see **Chapter 2 – Methods**), but is difficult to detect in multi-unit data.

Exposure-related differences in tone thresholds followed a similar pattern in multi-units as they did in single-units. Thresholds in quiet were unaffected below 32 kHz, and shifted by 10-30 dB above 32 kHz (**Fig S3.3)**. Thresholds in noise were generally unaffected by exposure, but were elevated 5 - 10 dB in the neuropathic region at some moderate noise levels for both awake and anesthetized groups (**Fig S3.4**). Main effects were not significant, and interaction was only significant for the interleaved paradigm (2- and 3-way ANOVAs, exposure effect: Interleaved: $F_{1,59}$ = 1.8, p = 0.2; Blocked: $F_{1,77}$ = 0.0, p = 0.9; exposure*noise level interaction: $F_{1,59}$ = 5.2, p = 0.025; Blocked: $F_{1,77}$ = 0.1, p = 0.7).

As in the single-unit results, threshold shift caused an apparent improvement in relative tone-driven rate range (TDRR) due to exposure above 32 kHz (**Fig S3.5C,F**). Contrary to the single-unit results, relative TDRR was unaffected by exposure in the neuropathic region (**Fig 3.5B vs. S3.5B**). However, TDRR decreased more rapidly in exposed mice recorded while under anesthesia for the blocked paradigm (**Fig S3.5E**). A three-way ANOVA found no significant main effects or two-way interactions, but a marginally-significant exposure*anesthesia*noise level interaction due to significant effects of exposure at high noise levels ($F_{1,79}$ = 4.3, p = 0.04; p < 0.005 for post-hoc tests). These results suggest that the mechanisms driving changes to TDRR are affected by ketamine/xylazine anesthesia.

We found further evidence of a significant anesthesia difference in the responses to noise alone. In the non-neuropathic region, responses to noise under anesthesia were elevated compared to controls for the blocked paradigm (**Fig S3.6D**). While the three-way interaction was significant ($F_{1,61}$ = 7.0, p = 0.01), results should be interpreted with caution as the number of multi-units in the comparison was small (for anesthetized: 5 control, 14 exposed). In the neuropathic region, exposure caused a reduction in noise response at high noise levels (**Fig S3.6E**). A decrement in noise-driven rate was also observed in the single- and multi-unit responses recorded as part of

the binaural noise response areas (**Fig 2.15B,E**).

Neural detection of low-SNR tones

Returning to the awake dataset, d' at low SNRs was unexpectedly elevated in multi-unit responses to the interleaved paradigm at 40 and 60 dB in both the neuropathic and threshold-shift regions (**Fig S3.7**), where it was decreased or unchanged in single-units (**Fig 3.7**). While the improvement above 32 kHz could be due to a reduction in the strength of the noise signal passed to these neurons due to threshold shift, the mechanism behind the elevations below 32 kHz are unclear. As in the single-units, effects of exposure were largely limited to the threshold-shift region for the blocked paradigm.

Exposure caused a decrease in d' in the neuropathic region for anesthetized multi-units recorded under the blocked paradigm (**Fig S3.7, left**). Mutual information (MI) about low-SNR tones was also reduced for neuropathic, anesthetized multi-units (**Fig S3.8E**). Both findings provide further evidence that exposure-related changes to adaptation were affected by anesthesia.

Mirroring the single-unit results, MI was slightly elevated at low noise levels for multi-units in the neuropathic region recorded for both noise paradigms (**Fig S3.8B**). However, contrary to single-unit results, MI did not fall below control levels for neurons in the neuropathic region at high noise levels. Like the single-unit results, MI was slightly elevated for multi-units in the non-neuropathic region, though only under the blocked paradigm (**Fig S3.8D**).

Dynamic range of tone-driven rate was unchanged

As in single-units, dynamic range of masking for tones at L_{Q90} was unchanged by exposure (**Fig S3.9**).

As in the single-units, tone slopes in the neuropathic region were elevated in quiet but returned to control levels when noise was introduced (**Fig S3.10**). However, contrary to the single-units, tone slopes were not elevated in noise in the non-neuropathic region (**Fig S3.10A,D vs. 3.10A,D**).

SUPPLEMENTAL FIGURES

Figures S3.1&3.2 were skipped for consistency between single-unit and multi-unit figures.

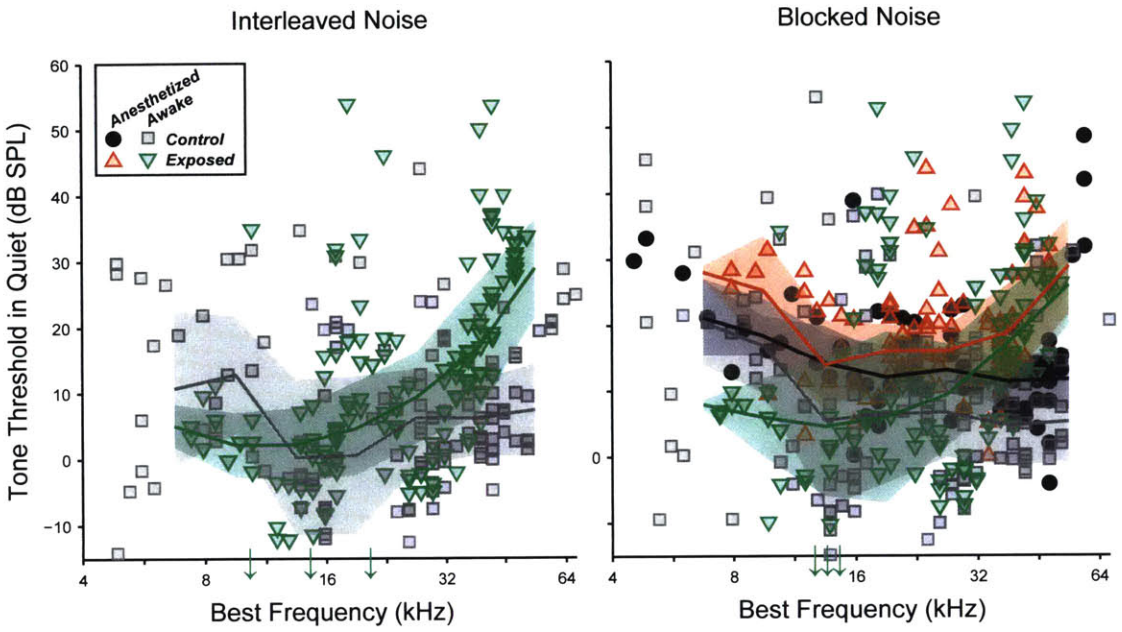

Figure S3.3 Multi-unit tone thresholds in quiet. **Left,** Thresholds collected in the interleaved noise paradigm. **Right,** Thresholds collected in the blocked noise paradigm. Multi-units in which tone frequency was within 0.1 octaves of best frequency are shown.

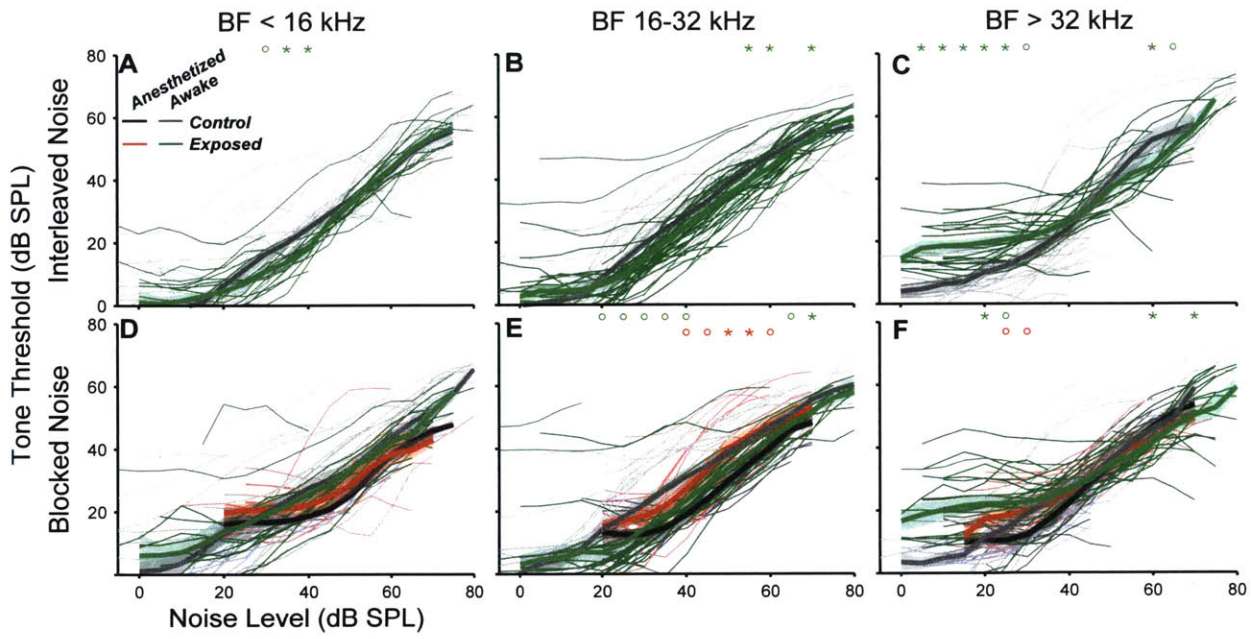

Figure S3.4. Multi-unit tone thresholds in noise. **A-C**, tone thresholds under the interleaved noise paradigm. **D-F**, thresholds under the blocked noise paradigm. Circles and stars indicate significant effects of exposure ($p<0.05$ and $p<0.01$, respectively). For this and all subsequent figures, only multi-units in which tone frequency was at best frequency are shown.

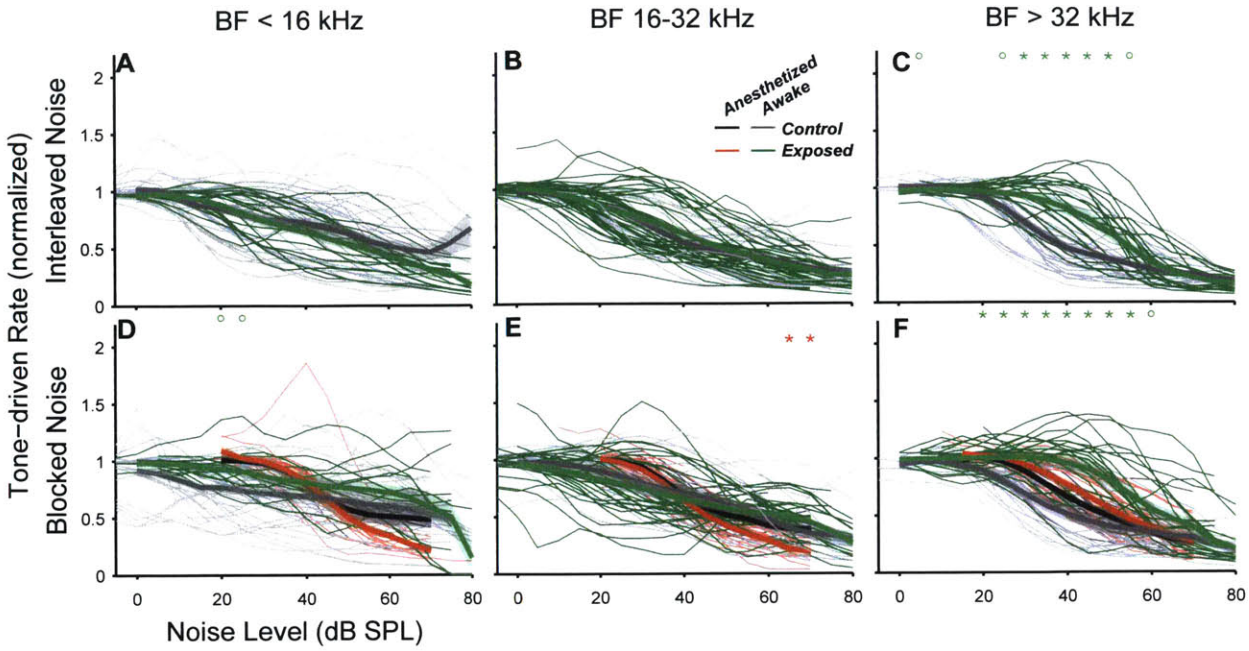

Figure S3.5. Contrary to single-units, relative tone-driven rate is unaffected by exposure in 16-32 kHz multi-units of awake mouse multi-units. **A-C**, interleaved noise paradigm. **D-F**, blocked noise paradigm. Line and star conventions are as in **Figure S3.4**.

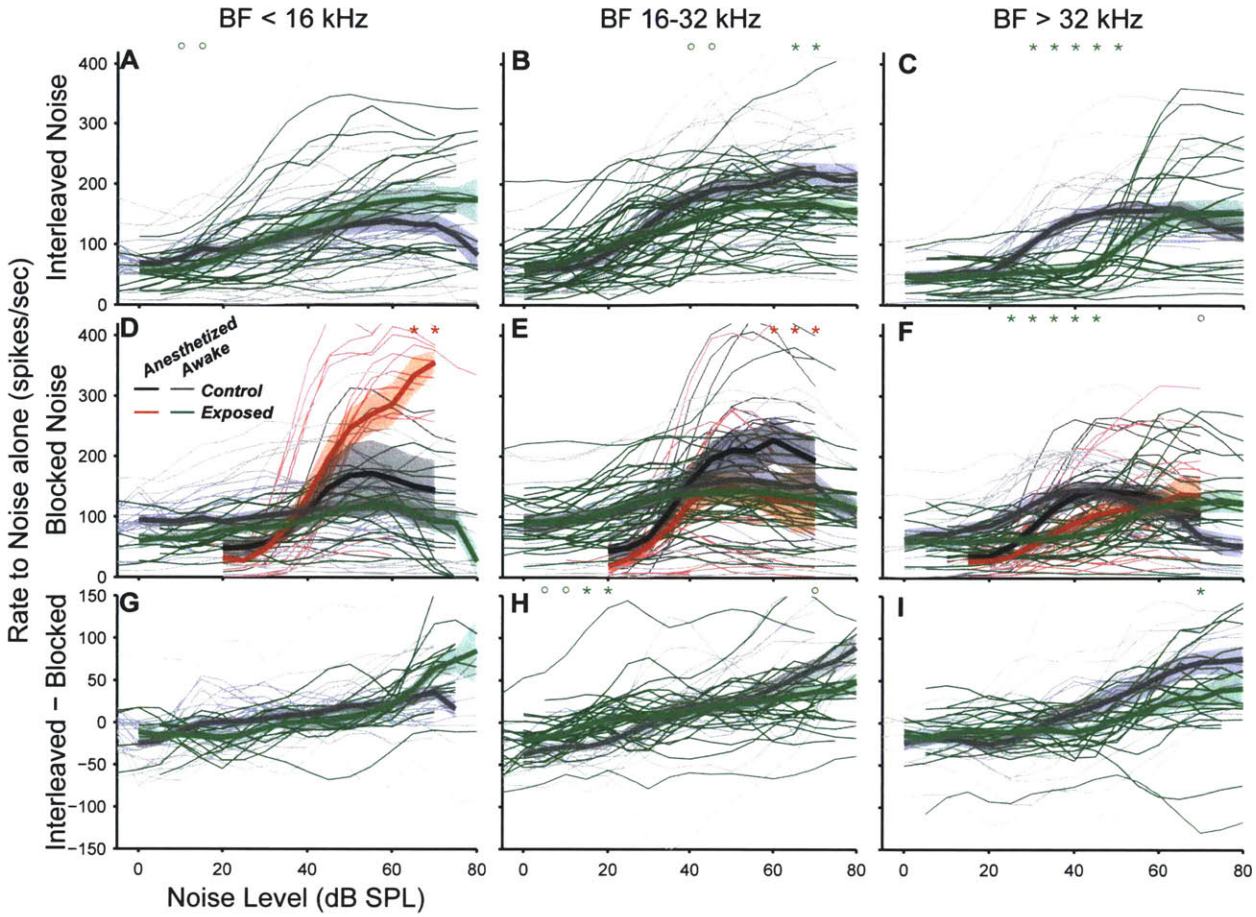

Figure S3.6. Response to noise alone in multi-units. **A-C**, interleaved noise paradigm. **D-F**, blocked noise paradigm. **G-I**, difference between the interleaved and blocked conditions. Line and star conventions are as in **Figure S3.4**.

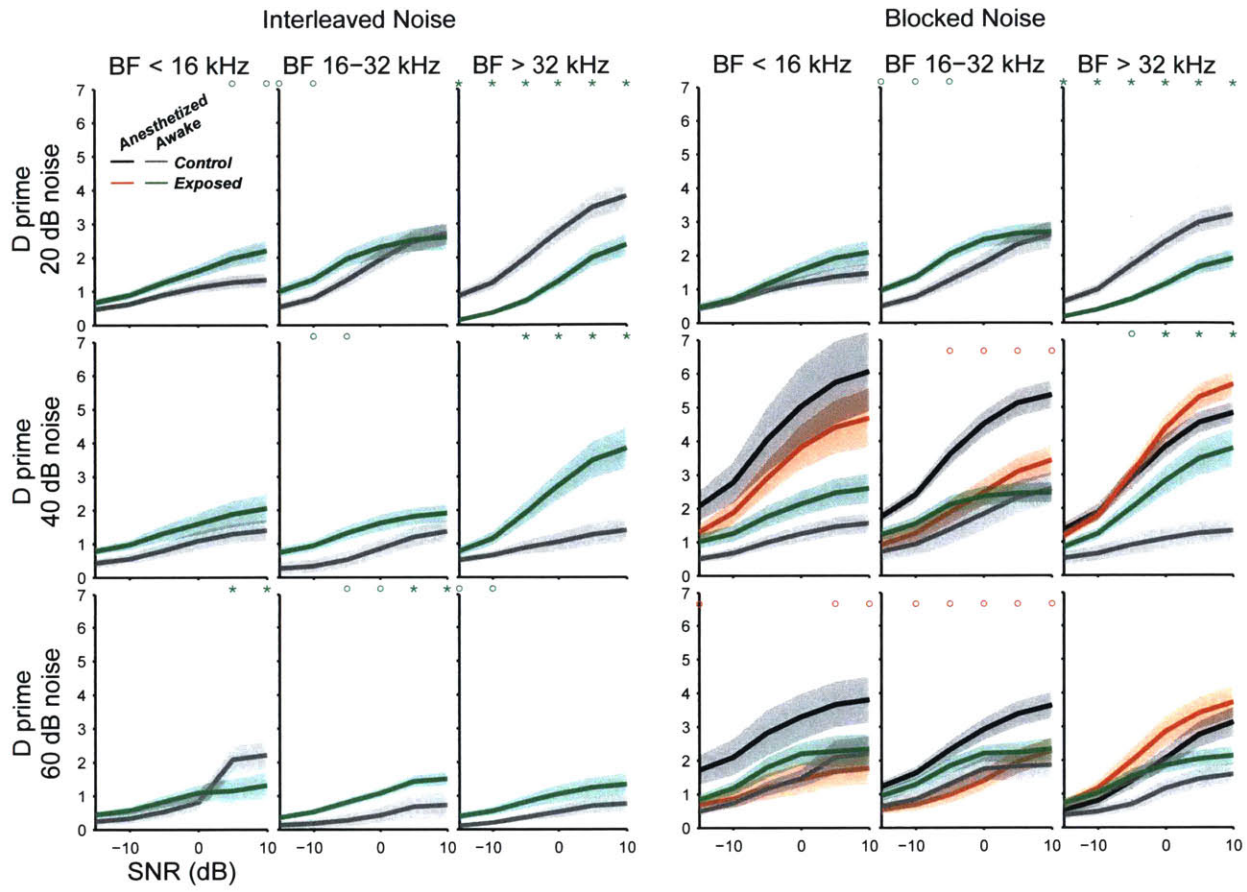

Figure S3.7. Neural detection of low-SNR tones in multi-units. **Left columns**, interleaved noise paradigm. **Right columns**, blocked noise paradigm. Line and star conventions are as in **Figure S3.4**.

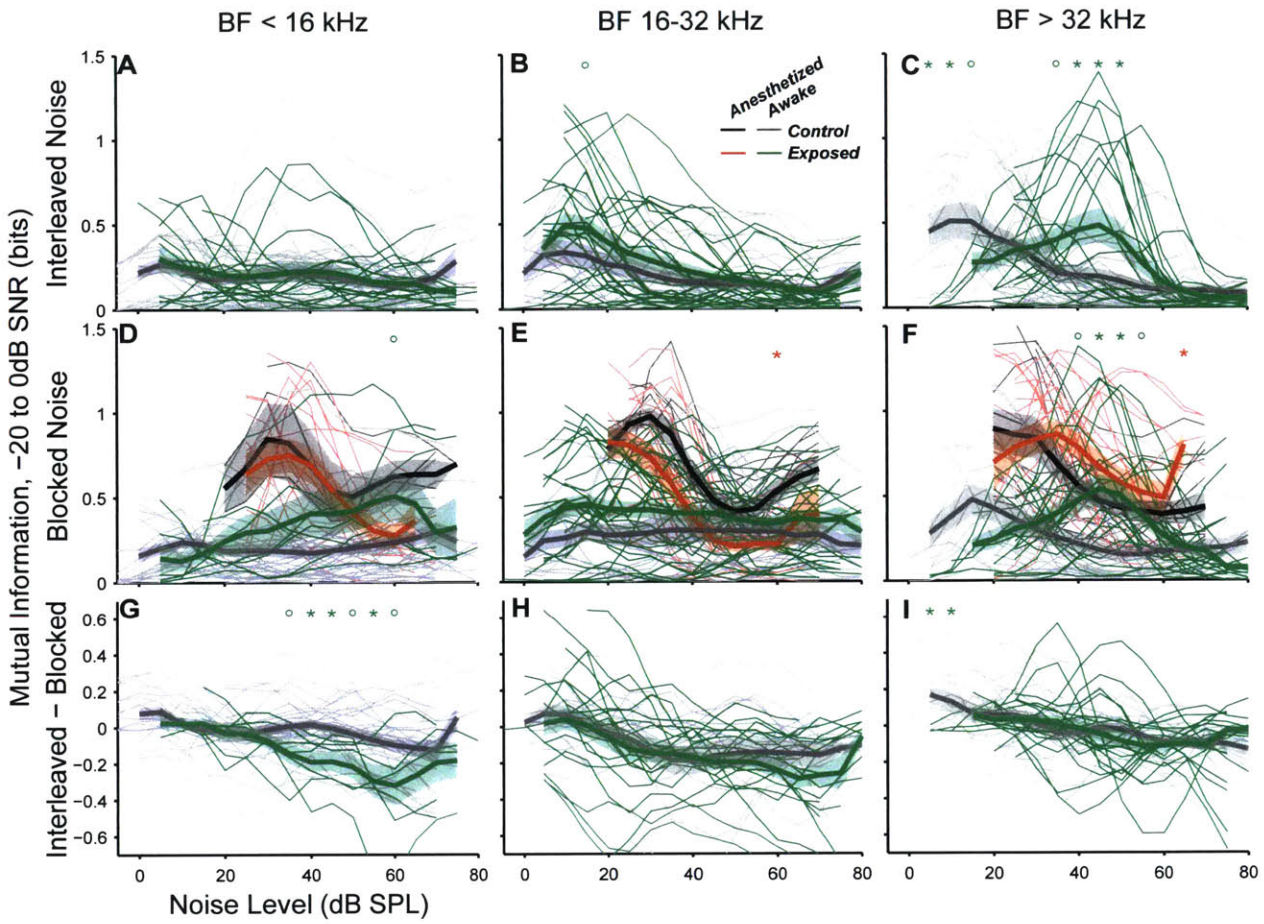

Figure S3.8. Mutual information at low SNRs in multi-units. **A-C**, interleaved noise paradigm. **D-F**, blocked noise paradigm. **G-I**, difference between the interleaved and blocked conditions. Line and star conventions are as in **Figure S3.4**.

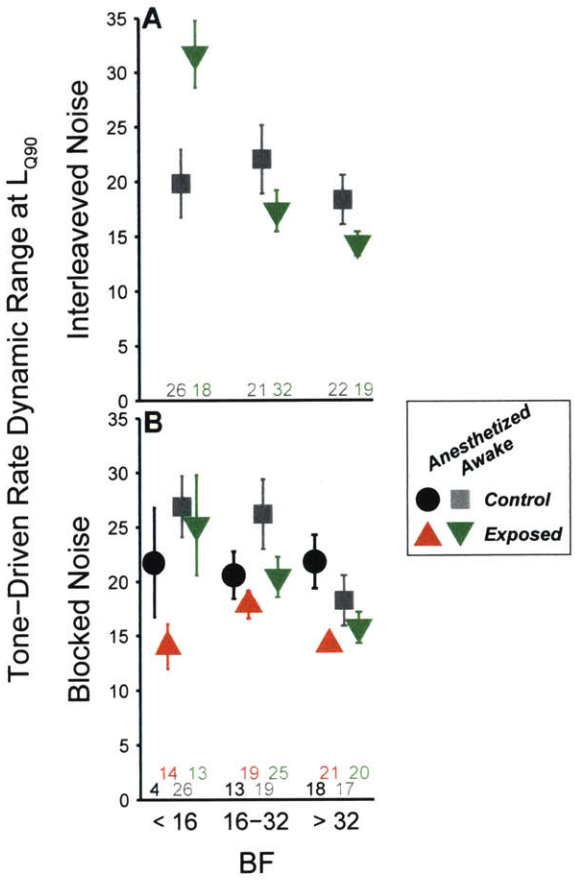

Figure S3.9. Tone-Driven Rate Dynamic Range at L_{Q90} is unchanged in exposed mice. **A**, interleaved noise paradigm. **B**, blocked noise paradigm. The dynamic range was calculated for each neuron as the range of levels encompassing 10% to 90% of the tone-driven rate-vs.-noise level function. Point and bars are mean ± SEs. Post-hoc tests did not reveal any significant effects of exposure.

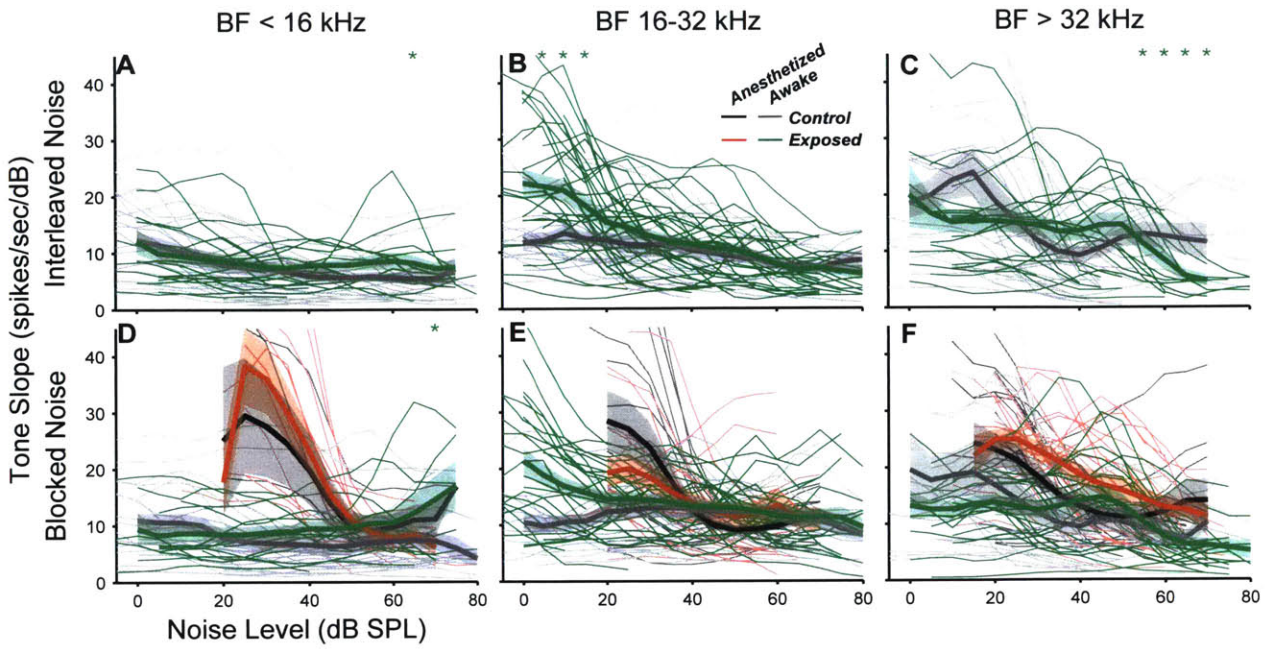

Figure S3.10. Contrary to single-units, tone slope in noise is unchanged in the non-neuropathic region of exposed multi-units. **A-C**, tone slopes under the interleaved noise paradigm. **D-F**, slopes under the blocked noise paradigm. Line and star conventions are as in **Figure S3.4**.

General Discussion

Progress on understanding the impact of cochlear neuropathy to human auditory perception is limited by the absence of a definitive test of neuropathy. In Chapter 1, I compare two methods for quantifying neuropathy using evoked electrical responses, the ABR and the EFR. I found that the EFR was comparatively more robust than the ABR, especially when parameters were optimized to maximize the contribution of AN fibers to the response. Over the course of doing this work, two other techniques for quantifying neuropathy were developed: 1) by measuring changes to the middle ear muscle reflex (Valero et al., 2016), and 2) by measuring the change in ABR latency caused by the addition of background noise (Mehraei et al., 2016). Like EFRs, these techniques were both selected because they may be especially sensitive to loss of high-threshold AN fibers. Ultimately, deciding which of these tests is most sensitive to neuropathy in humans will require a side-by-side comparison in the same population. Since neuropathy cannot be quantified directly in humans, the value of these techniques may be quantified by their ability to predict suprathreshold perceptual deficits. However, a degraded peripheral signal likely causes compensatory changes in the central auditory system, and the magnitude of compensation likely varies across individuals. While in some cases compensation may affect physiological measures, it almost certainly affects perceptual measures. While knowledge of the overall ability of the system is useful in other ways, a reliable quantification of the exact etiology of perceptual deficits is crucial for informing treatment plans such as neural regeneration via inner ear delivery of neurotrophins (Wan et al., 2014; Suzuki et al., 2016). Therefore, development of an optimized test for neuropathy may also require experiments in animal models with hearing closer to that of humans. The framework outlined in Chapter 1 should prove useful in developing an optimized test of neuropathy in both human and animal studies.

In Chapters 2 and 3, I describe a series of experiments quantifying changes to central auditory coding following neuropathy. Surprisingly, spontaneous rates were not elevated following exposure and still not elevated when the exposure was made unilateral or more intense. While these findings clearly show that neither neuropathy nor threshold shift are sufficient to cause elevated spontaneous rates, their relationship to subjective tinnitus remains unclear. The most persistent findings were changes indicative of a reduction in inhibition. This was most directly observed as an elevation of slopes in response to on-CF tones and a reduction in inhibition by off-CF tones, but reduction in inhibition may have also contributed to slope increases in noise and increased synchrony to near-threshold SAM tones. We found that coding of tones in noise was impaired when the noise changed every 600 milliseconds, but was unaffected when it changed every 70 seconds. This indicates that different adaptation systems may be operating at these two timescales, and neuropathy may cause a change only to the faster system, which can be compensated for when noise changes on a long timescale. Interpretation of these results is complicated because changes are likely caused both by direct effects of neuropathy and by compensatory changes in the central auditory system. Future studies should seek to untangle these effects, perhaps by recording from the same set of neurons over the course of recover

from exposure. Furthermore, changes may be blurred due to the heterogeneity of responses in the inferior colliculus. While recording from the same set of neurons would be challenging, it could mitigate this problem, allowing for within-neuron quantification of the effects of neuropathic exposure.

Despite the limitations the data do provide evidence of impairments following neuropathy, both in coding of tones in a noise and in coding of temporal envelopes. Both of these abilities are essential contributors to the understanding of speech in noisy environments, an ability that degreases with both age and noise exposure history, even when thresholds are unchanged (Harris et al., 2009). While the central auditory system may be able to compensate for neuropathy when performing these tasks in isolation, this ability may be more limited when the signal and noise are more complex. Thus, more substantial changes may also be found by quantifying neural changes to the coding of more spectrally or temporally complex signals in the face of background noise. The experiments described here provide a basic understanding of the changes in midbrain auditory coding following cochlear neuropathy, will help guide future endeavors.

References

Ahlf S, **Tziridis K**, **Korn S**, **Strohmeyer I**, **Schulze H**. Predisposition for and Prevention of Subjective Tinnitus Development. *PLOS ONE* 7: e44519, 2012.

Anderson S, **White-Schwoch T**, **Choi HJ**, **Kraus N**. Training changes processing of speech cues in older adults with hearing loss. *Front. Syst. Neurosci.* 7: 97, 2013.

Auerbach BD, **Rodrigues PV**, **Salvi RJ**. Central gain control in tinnitus and hyperacusis. *Neuro-Otol.* 5: 206, 2014.

Azarias G, **Kruusmägi M**, **Connor S**, **Akkuratov EE**, **Liu X-L**, **Lyons D**, **Brismar H**, **Broberger C**, **Aperia A**. A specific and essential role for Na,K-ATPase α3 in neurons co-expressing α1 and α3. *J. Biol. Chem.* 288: 2734–2743, 2013.

Bauer CA, **Turner JG**, **Caspary DM**, **Myers KS**, **Brozoski TJ**. Tinnitus and inferior colliculus activity in chinchillas related to three distinct patterns of cochlear trauma. *J. Neurosci. Res.* 86: 2564–2578, 2008.

Benzeghiba M, **De Mori R**, **Deroo O**, **Dupont S**, **Erbes T**, **Jouvet D**, **Fissore L**, **Laface P**, **Mertins A**, **Ris C**, **Rose R**, **Tyagi V**, **Wellekens C**. Automatic speech recognition and speech variability: A review. *Speech Commun.* 49: 763–786, 2007.

Bharadwaj HM, **Masud S**, **Mehraei G**, **Verhulst S**, **Shinn-Cunningham BG**. Individual Differences Reveal Correlates of Hidden Hearing Deficits. *J. Neurosci.* 35: 2161–2172, 2015.

Bharadwaj HM, **Verhulst S**, **Shaheen L**, **Liberman MC**, **Shinn-Cunningham BG**. Cochlear neuropathy and the coding of supra-threshold sound. *Front. Syst. Neurosci.* 8: 26, 2014.

Bourien J, **Tang Y**, **Batrel C**, **Huet A**, **Lenoir M**, **Ladrech S**, **Desmadryl G**, **Nouvian R**, **Puel J-L**, **Wang J**. Contribution of auditory nerve fibers to compound action potential of the auditory nerve. *J. Neurophysiol.* 112: 1025–1039, 2014.

Bramhall N, **Ong B**, **Ko J**, **Parker M**. Speech Perception Ability in Noise is Correlated with Auditory Brainstem Response Wave I Amplitude. *J. Am. Acad. Audiol.* 26: 509–517, 2015.

Brozoski TJ, **Bauer CA**. The effect of dorsal cochlear nucleus ablation on tinnitus in rats. *Hear. Res.* 206: 227–236, 2005.

Brozoski TJ, **Bauer CA**, **Caspary DM**. Elevated fusiform cell activity in the dorsal cochlear nucleus of chinchillas with psychophysical evidence of tinnitus. *J. Neurosci.* 22: 2383–2390, 2002.

Brozoski TJ, **Wisner KW**, **Sybert LT**, **Bauer CA**. Bilateral Dorsal Cochlear Nucleus Lesions Prevent Acoustic-Trauma Induced Tinnitus in an Animal Model. *J. Assoc. Res. Otolaryngol.* 13: 55–66, 2012.

Bruin NMWJ de, **Ellenbroek BA**, **Cools AR**, **Coenen AML**, **Luijtelaar ELJM van**. Differential effects of ketamine on gating of auditory evoked potentials and prepulse inhibition in rats. *Psychopharmacology (Berl.)* 142: 9–17, 1999.

Burianova J, **Ouda L**, **Profant O**, **Syka J**. Age-related changes in GAD levels in the central auditory system of the rat. *Exp. Gerontol.* 44: 161–169, 2009.

Buzsáki G, **Anastassiou CA**, **Koch C**. The origin of extracellular fields and currents — EEG, ECoG, LFP and spikes. *Nat. Rev. Neurosci.* 13: 407–420, 2012.

Cai S, **Ma W-L**, **Young E**. Encoding Intensity in Ventral Cochlear Nucleus Following Acoustic Trauma: Implications for Loudness Recruitment. *J. Assoc. Res. Otolaryngol.* 10: 5–22, 2009.

Campbell F, **Atkinson J**, **Francis M**, **Green D**. Estimation of auditory thresholds using evoked potentials. *Clin. Screen. Test Progr Clin Neurophysiol* 2: 68–78, 1977.

Cant NB. Projections from the Cochlear Nuclear Complex to the Inferior Colliculus. In: *The Inferior Colliculus*, edited by Winer JA, Schreiner CE. Springer New York. 115–131, 2005.

Carvalho TP, **Buonomano DV**. Differential Effects of Excitatory and Inhibitory Plasticity on Synaptically Driven Neuronal Input-Output Functions. *Neuron* 61: 774–785, 2009.

Caspary DM, **Ling L**, **Turner JG**, **Hughes LF**. Inhibitory neurotransmission, plasticity and aging in the mammalian central auditory system. *J. Exp. Biol.* 211: 1781–1791, 2008.

Chambers AR, **Hancock KE**, **Maison SF**, **Liberman MC**, **Polley DB**. Sound-evoked olivocochlear activation in unanesthetized mice. *J. Assoc. Res. Otolaryngol. JARO* 13: 209–217, 2012.

Chambers AR, **Resnik J**, **Yuan Y**, **Whitton JP**, **Edge AS**, **Liberman MC**, **Polley DB**. Central Gain Restores Auditory Processing following Near-Complete Cochlear Denervation. *Neuron* 89: 867–879, 2016.

Chung Y, **Hancock KE**, **Nam S-I**, **Delgutte B**. Coding of Electric Pulse Trains Presented through Cochlear Implants in the Auditory Midbrain of Awake Rabbit: Comparison with Anesthetized Preparations. *J. Neurosci.* 34: 218–231, 2014.

Clinard CG, **Tremblay KL**, **Krishnan AR**. Aging alters the perception and physiological representation of frequency: Evidence from human frequency-following response recordings. *Hear. Res.* 264: 48–55, 2010.

Coomber B, **Berger JI**, **Kowalkowski VL**, **Shackleton TM**, **Palmer AR**, **Wallace MN**. Neural changes accompanying tinnitus following unilateral acoustic trauma in the guinea pig. *Eur. J. Neurosci.* 40:2427-2441, 2014.

Cooper NP, **Robertson D**, **Yates GK**. Cochlear nerve fiber responses to amplitude-modulated stimuli: variations with spontaneous rate and other response characteristics. *J. Neurophysiol.* 70: 370–386, 1993.

Costalupes JA. Representation of tones in noise in the responses of auditory nerve fibers in cats. I. Comparison with detection thresholds. *J. Neurosci.* 5: 3261–3269, 1985.

Costalupes JA, **Young ED**, **Gibson DJ**. Effects of continuous noise backgrounds on rate response of auditory nerve fibers in cat. *J. Neurophysiol.* 51: 1326–1344, 1984.

Daniel E. Noise and Hearing Loss: A Review. *J. Sch. Health* 77: 225–231, 2007.

Darrow KN, **Benson TE**, **Brown MC**. Planar multipolar cells in the cochlear nucleus project to medial olivocochlear neurons in mouse. *J. Comp. Neurol.* 520: 1365–1375, 2012.

Davis KA, **Ramachandran R**, **May BJ**. Single-Unit Responses in the Inferior Colliculus of

Decerebrate Cats II. Sensitivity to Interaural Level Differences. *J. Neurophysiol.* 82: 164–175, 1999.

Dean I, **Harper NS**, **McAlpine D**. Neural population coding of sound level adapts to stimulus statistics. *Nat. Neurosci.* 8: 1684–1689, 2005.

Dean I, **Robinson BL**, **Harper NS**, **McAlpine D**. Rapid Neural Adaptation to Sound Level Statistics. *J. Neurosci.* 28: 6430–6438, 2008.

Dehmel S, **Pradhan S**, **Koehler S**, **Bledsoe S**, **Shore S**. Noise Overexposure Alters Long-Term Somatosensory-Auditory Processing in the Dorsal Cochlear Nucleus—Possible Basis for Tinnitus-Related Hyperactivity? *J. Neurosci.* 32: 1660–1671, 2012.

D'haenens W, **Dhooge I**, **Maes L**, **Bockstael A**, **Keppler H**, **Philips B**, **Swinnen F**, **Vinck BM**. The clinical value of the multiple-frequency 80-Hz auditory steady-state response in adults with normal hearing and hearing loss. *Arch. Otolaryngol. Head Neck Surg.* 135: 496–506, 2009.

Dimitrijevic A, **John MS**, **Picton TW**. Auditory steady-state responses and word recognition scores in normal-hearing and hearing-impaired adults. *Ear Hear.* 25: 68–84, 2004.

Dobie RA, **Wilson MJ**. Analysis of Auditory Evoked Potentials by Magnitude-Squared Coherence. *Ear Hear.* 10: 2–13, 1989.

Dubno JR, **Dirks DD**, **Morgan DE**. Effects of age and mild hearing loss on speech recognition in noise. *J. Acoust. Soc. Am.* 76: 87–96, 1984.

Durrant JD, **Wang J**, **Ding DL**, **Salvi RJ**. Are inner or outer hair cells the source of summating potentials recorded from the round window? *J. Acoust. Soc. Am.* 104: 370–377, 1998.

Eggermont JJ, **Roberts LE**. The neuroscience of tinnitus. *Trends Neurosci.* 27: 676–682, 2004.

Egorova M, **Ehret G**, **Vartanian I**, **Esser K-H**. Frequency response areas of neurons in the mouse inferior colliculus. I. Threshold and tuning characteristics. *Exp. Brain Res.* 140: 145–161, 2001.

Engineer ND, **Riley JR**, **Seale JD**, **Vrana WA**, **Shetake JA**, **Sudanagunta SP**, **Borland MS**, **Kilgard MP**. Reversing pathological neural activity using targeted plasticity. *Nature* 470: 101–104, 2011.

Fendt M, **Li L**, **Yeomans JS**. Brain stem circuits mediating prepulse inhibition of the startle reflex. *Psychopharmacology (Berl.)* 156: 216–224, 2001.

Florentine M, **Buus S**, **Mason CR**. Level discrimination as a function of level for tones from 0.25 to 16 kHz. *J. Acoust. Soc. Am.* 81: 1528–1541, 1987.

Frisina DR, **Frisina RD**. Speech recognition in noise and presbycusis: relations to possible neural mechanisms. *Hear. Res.* 106: 95–104, 1997.

Frisina RD, **Smith RL**, **Chamberlain SC**. Encoding of amplitude modulation in the gerbil cochlear nucleus: I. A hierarchy of enhancement. *Hear. Res.* 44: 99–122, 1990.

Furman AC, **Kujawa SG**, **Liberman MC**. Noise-induced cochlear neuropathy is selective for fibers with low spontaneous rates. *J. Neurophysiol.* 110: 577–586, 2013.

Gorga MP, **Kaminski JR**, **Beauchaine KA**, **Jesteadt W**. Auditory brainstem responses to tone bursts in normally hearing subjects. *J. Speech Hear. Res.* 31: 87–97, 1988.

Greenwood DD, **Joris PX**. Mechanical and "'temporal'" filtering as codeterminants of the response by cat primary fibers to amplitude□modulated signals. *J. Acoust. Soc. Am.* 99: 1029–1039, 1996.

Gu JW, **Halpin CF**, **Nam E-C**, **Levine RA**, **Melcher JR**. Tinnitus, Diminished Sound-Level Tolerance, and Elevated Auditory Activity in Humans With Clinically Normal Hearing Sensitivity. *J. Neurophysiol.* 104: 3361–3370, 2010.

Gu JW, **Herrmann BS**, **Levine RA**, **Melcher JR**. Brainstem Auditory Evoked Potentials Suggest a Role for the Ventral Cochlear Nucleus in Tinnitus. *J. Assoc. Res. Otolaryngol.* 13: 819–833, 2012.

Guinan JJ. Physiology of the Medial and Lateral Olivocochlear Systems. In: *Auditory and Vestibular Efferents*, edited by Ryugo DK, Fay RR. Springer New York, 39–81, 2011.

Hafidi A, **Beurg M**, **Dulon D**. Localization and developmental expression of BK channels in mammalian cochlear hair cells. *Neuroscience* 130: 475–484, 2005.

Hall JW. *New Handbook for Auditory Evoked Responses*. 1 edition. Boston, Mass: Pearson, 2006.

Harris KC, **Dubno JR**, **Keren NI**, **Ahlstrom JB**, **Eckert MA**. Speech Recognition in Younger and Older Adults: A Dependency on Low-Level Auditory Cortex. *J. Neurosci.* 29: 6078–6087, 2009.

Heil P, **Neubauer H**, **Irvine DRF**. An Improved Model for the Rate–Level Functions of Auditory-Nerve Fibers. *J. Neurosci.* 31: 15424–15437, 2011.

Hentschke H, **Stüttgen MC**. Computation of measures of effect size for neuroscience data sets. *Eur. J. Neurosci.* 34: 1887–1894, 2011.

Herdman AT, **Lins O**, **Roon PV**, **Stapells DR**, **Scherg M**, **Picton TW**. Intracerebral Sources of Human Auditory Steady-State Responses. *Brain Topogr.* 15: 69–86, 2002.

Hickox AE, **Liberman MC**. Is noise-induced cochlear neuropathy key to the generation of hyperacusis or tinnitus? *J. Neurophysiol.* 111: 552–564, 2014.

Hill DN, **Mehta SB**, **Kleinfeld D**. Quality Metrics to Accompany Spike Sorting of Extracellular Signals. *J. Neurosci.* 31: 8699–8705, 2011.

Holgers K, **Pettersson B**. Noise exposure and subjective hearing symptoms among school children in Sweden. *Noise Health* 7: 27, 2005.

Irving R, **Harrison JM**. The superior olivary complex and audition: A comparative study. *J. Comp. Neurol.* 130: 77–86, 1967.

Ito T, **Bishop DC**, **Oliver DL**. Functional organization of the local circuit in the inferior colliculus. *Anat. Sci. Int.* 91: 22-34, 2016.

Jahn AF, **Santos-Sacchi J**. *Physiology of the Ear*. 2 edition. San Diego, Calif: Singular, 2001.

Jensen JB, **Lysaght AC**, **Liberman MC**, **Qvortrup K**, **Stankovic KM**. Immediate and Delayed Cochlear Neuropathy after Noise Exposure in Pubescent Mice. *PLOS ONE* 10: e0125160, 2015.

Johnson DH. The relationship between spike rate and synchrony in responses of auditory-nerve fibers to single tones. *J. Acoust. Soc. Am.* 68: 1115–1122, 1980.

Johnson TA, **Brown CJ**. Threshold prediction using the auditory steady-state response and the tone burst auditory brain stem response: a within-subject comparison. *Ear Hear.* 26: 559–576, 2005.

Joris PX, **Schreiner CE**, **Rees A**. Neural Processing of Amplitude-Modulated Sounds. *Physiol. Rev.* 84: 541–577, 2004.

Joris PX, **Yin TC**. Responses to amplitude-modulated tones in the auditory nerve of the cat. *J. Acoust. Soc. Am.* 91: 215–232, 1992.

Kalappa BI, **Brozoski TJ**, **Turner JG**, **Caspary DM**. Single-unit hyperactivity and bursting in the auditory thalamus of awake rats directly correlates with behavioral evidence of tinnitus. *J. Physiol.* 592: 5065-5078, 2014.

Kawase T, **Delgutte B**, **Liberman MC**. Antimasking effects of the olivocochlear reflex. II. Enhancement of auditory-nerve response to masked tones. *J. Neurophysiol.* 70: 2533–2549, 1993.

Khimich D, **Nouvian R**, **Pujol R**, **Tom Dieck S**, **Egner A**, **Gundelfinger ED**, **Moser T**. Hair cell synaptic ribbons are essential for synchronous auditory signalling. *Nature* 434: 889–894, 2005.

Kidd RC, **Weiss TF**. Mechanisms that degrade timing information in the cochlea. *Hear. Res.* 49: 181–207, 1990.

King A, **Hopkins K**, **Plack CJ**. The effects of age and hearing loss on interaural phase difference discriminationa). *J. Acoust. Soc. Am.* 135: 342–351, 2014.

Kiren T, **Aoyagi M**, **Furuse H**, **Koike Y**. An experimental study on the generator of amplitude-modulation following response. *Acta Oto-Laryngol. Suppl.* 511: 28–33, 1994.

Kobler JB, **Guinan JJ**, **Vacher SR**, **Norris BE**. Acoustic reflex frequency selectivity in single stapedius motoneurons of the cat. *J. Neurophysiol.* 68: 807–817, 1992.

Koehler SD, **Shore SE**. Stimulus Timing-Dependent Plasticity in Dorsal Cochlear Nucleus Is Altered in Tinnitus. *J. Neurosci.* 33: 19647–19656, 2013.

Kreuzer PM, **Landgrebe M**, **Schecklmann M**, **Staudinger S**, **Langguth B**. Trauma-Associated Tinnitus: Audiological, Demographic and Clinical Characteristics. *PLOS ONE* 7: e45599, 2012.

Krishna BS, **Semple MN**. Auditory Temporal Processing: Responses to Sinusoidally Amplitude-Modulated Tones in the Inferior Colliculus. *J. Neurophysiol.* 84: 255–273, 2000.

Kujawa SG, **Liberman MC**. Acceleration of Age-Related Hearing Loss by Early Noise Exposure: Evidence of a Misspent Youth. *J. Neurosci.* 26: 2115–2123, 2006.

Kujawa SG, **Liberman MC**. Adding Insult to Injury: Cochlear Nerve Degeneration after "Temporary" Noise-Induced Hearing Loss. *J. Neurosci.* 29: 14077–14085, 2009.

Kuwada S, **Anderson JS**, **Batra R**, **Fitzpatrick DC**, **Teissier N**, **D'Angelo WR**. Sources of the Scalp-Recorded Amplitude Modulation Following Response. *J. Am. Acad. Audiol.* 13: 188, 2002.

Kuwada S, **Batra R**, **Maher VL**. Scalp potentials of normal and hearing-impaired subjects in response to sinusoidally amplitude-modulated tones. *Hear. Res.* 21: 179–192, 1986.

Lang H, **Li M**, **Kilpatrick LA**, **Zhu J**, **Samuvel DJ**, **Krug EL**, **Goddard JC**. Sox2 Up-regulation and Glial Cell Proliferation Following Degeneration of Spiral Ganglion Neurons in the Adult Mouse Inner Ear. *J. Assoc. Res. Otolaryngol.* 12: 151–171, 2011.

Li S, **Choi V**, **Tzounopoulos T**. Pathogenic plasticity of Kv7.2/3 channel activity is essential for the induction of tinnitus. *PNAS* 110: 9980-9985, 2013.

Liberman M, **Rosowski J**, **Lewis R**. Cochlear function and dysfunction. In: *Pathology of the Ear,* edited by Merchant SN, Nadol JB. *PMPH-USA* Connecticut. 104-126, 2010.

Liberman MC. Auditory-nerve response from cats raised in a low-noise chamber. *J. Acoust. Soc. Am.* 63: 442–455, 1978.

Liberman MC. Morphological differences among radial afferent fibers in the cat cochlea: An electron-microscopic study of serial sections. *Hear. Res.* 3: 45–63, 1980.

Liberman MC. Central projections of auditory-nerve fibers of differing spontaneous rate. I. Anteroventral cochlear nucleus. *J. Comp. Neurol.* 313: 240–258, 1991.

Liberman MC. Central projections of auditory nerve fibers of differing spontaneous rate, II: Posteroventral and dorsal cochlear nuclei. *J. Comp. Neurol.* 327: 17–36, 1993.

Liberman MC, **Dodds LW**. Single-neuron labeling and chronic cochlear pathology. III. Stereocilia damage and alterations of threshold tuning curves. *Hear. Res.* 16: 55–74, 1984.

Liberman MC, **Dodds LW**, **Pierce S**. Afferent and efferent innervation of the cat cochlea: quantitative analysis with light and electron microscopy. *J. Comp. Neurol.* 301: 443–460, 1990.

Lin H, **Furman A**, **Kujawa S**, **Liberman M**. Primary Neural Degeneration in the Guinea Pig Cochlea After Reversible Noise-Induced Threshold Shift. *J. Assoc. Res. Otolaryngol.* 12: 605–616, 2011.

Lobarinas E, **Salvi R**, **Ding D**. Insensitivity of the audiogram to carboplatin induced inner hair cell loss in chinchillas. *Hear. Res.* 302: 113–120, 2013.

Longenecker RJ, **Galazyuk AV**. Development of Tinnitus in CBA/CaJ Mice Following Sound Exposure. *J. Assoc. Res. Otolaryngol.* 12: 647–658, 2011.

Ma W-LD, **Hidaka H**, **May BJ**. Spontaneous activity in the inferior colliculus of CBA/J mice after manipulations that induce tinnitus. *Hear. Res.* 212: 9–21, 2006.

Maison SF, **Pyott SJ**, **Meredith AL**, **Liberman MC**. Olivocochlear suppression of outer hair cells in vivo: evidence for combined action of BK and SK2 channels throughout the cochlea. *J. Neurophysiol.* 109: 1525–1534, 2013a.

Maison SF, **Usubuchi H**, **Liberman MC**. Efferent Feedback Minimizes Cochlear Neuropathy from Moderate Noise Exposure. *J. Neurosci.* 33: 5542–5552, 2013b.

Makary C, **Shin J**, **Kujawa S**, **Liberman M**, **Merchant S**. Age-Related Primary Cochlear Neuronal Degeneration in Human Temporal Bones. *J. Assoc. Res. Otolaryngol.* 12: 711–717, 2011.

Malmierca MS, **Merchán MA**, **Henkel CK**, **Oliver DL**. Direct Projections from Cochlear Nuclear Complex to Auditory Thalamus in the Rat. *J. Neurosci.* 22: 10891–10897, 2002.

Mansbach RS, **Geyer MA**. Parametric determinants in pre-stimulus modification of acoustic startle: interaction with ketamine. *Psychopharmacology (Berl.)* 105: 162–168, 1991.

Manzoor NF, **Licari FG**, **Klapchar M**, **Elkin RL**, **Gao Y**, **Chen G**, **Kaltenbach JA**. Noise-induced hyperactivity in the inferior colliculus: its relationship with hyperactivity in the dorsal cochlear nucleus. *J. Neurophysiol.* 108: 976–988, 2012.

Matsubara A, **Laake JH**, **Davanger S**, **Usami S**, **Ottersen OP**. Organization of AMPA receptor subunits at a glutamate synapse: a quantitative immunogold analysis of hair cell synapses in the rat organ of Corti. *J. Neurosci.* 16: 4457–4467, 1996.

Mehraei G, **Hickox AE**, **Bharadwaj HM**, **Goldberg H**, **Verhulst S**, **Liberman MC**, **Shinn-Cunningham BG**. Auditory Brainstem Response Latency in Noise as a Marker of Cochlear Synaptopathy. *J. Neurosci.* 36: 3755–3764, 2016.

Meikle MB. Electronic Access to Tinnitus Data: The Oregon Tinnitus Data Archive. *Otolaryngol. -- Head Neck Surg.* 117: 698–700, 1997.

Melcher JR, **Kiang NYS**. Generators of the brainstem auditory evoked potential in cat III: identified cell populations. *Hear. Res.* 93: 52–71, 1996.

Meredith AL, **Thorneloe KS**, **Werner ME**, **Nelson MT**, **Aldrich RW**. Overactive Bladder and Incontinence in the Absence of the BK Large Conductance Ca2+-activated K+ Channel. *J. Biol. Chem.* 279: 36746–36752, 2004.

Mulders WHAM, **Robertson D**. Hyperactivity in the auditory midbrain after acoustic trauma: dependence on cochlear activity. *Neuroscience* 164: 733–746, 2009.

Mulders WHAM, **Robertson D**. Progressive centralization of midbrain hyperactivity after acoustic trauma. *Neuroscience* 192: 753–760, 2011.

Mulders WHAM, **Robertson D**. Development of hyperactivity after acoustic trauma in the guinea pig inferior colliculus. *Hear. Res.* 298: 104–108, 2013.

Müller M, **Hünerbein K von**, **Hoidis S**, **Smolders JWT**. A physiological place–frequency map of the cochlea in the CBA/J mouse. *Hear. Res.* 202: 63–73, 2005.

Nikiforidis GC, **Koutsojannis CM**, **Varakis JN**, **Goumas PD**. Reduced variance in the latency and amplitude of the fifth wave of auditory brain stem response after normalization for head size. *Ear Hear.* 14: 423–428, 1993.

Noreña AJ, **Moffat G**, **Blanc JL**, **Pezard L**, **Cazals Y**. Neural changes in the auditory cortex of awake guinea pigs after two tinnitus inducers: salicylate and acoustic trauma. *Neuroscience* 166: 1194–1209, 2010.

Obrien WJ, **Lingrel JB**, **Wallick ET**. Ouabain Binding Kinetics of the Rat Alpha Two and Alpha Three Isoforms of the Sodium-Potassium Adenosine Triphosphate. *Arch. Biochem. Biophys.*

310: 32–39, 1994.

Oliver D, **Taberner AM**, **Thurm H**, **Sausbier M**, **Arntz C**, **Ruth P**, **Fakler B**, **Liberman MC**. The role of BKCa channels in electrical signal encoding in the mammalian auditory periphery. *J. Neurosci.* 26: 6181–6189, 2006.

Ollo C, **Schwartz IR**. The superior olivary complex in C57BL/6 mice. *Am. J. Anat.* 155: 349–373, 1979.

Palmer AR, **Shackleton TM**, **Sumner CJ**, **Zobay O**, **Rees A**. Classification of frequency response areas in the inferior colliculus reveals continua not discrete classes. *J. Physiol.* 591: 4003–4025, 2013.

Pang XD, **Guinan JJ**. Effects of stapedius-muscle contractions on the masking of auditory-nerve responses. *J. Acoust. Soc. Am.* 102: 3576–3586, 1997.

Park TJ, **Pollak GD**. GABA shapes sensitivity to interaural intensity disparities in the mustache bat's inferior colliculus: implications for encoding sound location. *J. Neurosci.* 13: 2050–2067, 1993.

Parthasarathy A, **Bartlett E**. Two-channel recording of auditory-evoked potentials to detect age-related deficits in temporal processing. *Hear. Res.* 289: 52–62, 2012.

Parthasarathy A, **Datta J**, **Torres JAL**, **Hopkins C**, **Bartlett EL**. Age-related changes in the relationship between auditory brainstem responses and envelope-following responses. *J. Assoc. Res. Otolaryngol.* 15: 649–661, 2014.

Pauli-Magnus D, **Hoch G**, **Strenzke N**, **Anderson S**, **Jentsch TJ**, **Moser T**. Detection and differentiation of sensorineural hearing loss in mice using auditory steady-state responses and transient auditory brainstem responses. *Neuroscience* 149: 673–684, 2007.

Pethe J, **Von Specht H**, **Mühler R**, **Hocke T**. Amplitude modulation following responses in awake and sleeping humans--a comparison for 40 Hz and 80 Hz modulation frequency. *Scand. Audiol. Suppl.* : 152–155, 2001.

Ping J, **Li N**, **Du Y**, **Wu X**, **Li L**, **Galbraith G**. Auditory evoked responses in the rat: Transverse mastoid needle electrodes register before cochlear nucleus and do not reflect later inferior colliculus activity. *J. Neurosci. Methods* 161: 11–16, 2007.

Plack CJ, **Barker D**, **Prendergast G**. Perceptual Consequences of "Hidden" Hearing Loss. *Trends Hear.* 18: 2331216514550621, 2014.

Plomp R, **Mimpen AM**. Speech□reception threshold for sentences as a function of age and noise level. *J. Acoust. Soc. Am.* 66: 1333–1342, 1979.

Pyott SJ, **Meredith AL**, **Fodor AA**, **Vázquez AE**, **Yamoah EN**, **Aldrich RW**. Cochlear Function in Mice Lacking the BK Channel α, β1, or β4 Subunits. *J. Biol. Chem.* 282: 3312–3324, 2007.

Rabang CF, **Parthasarathy A**, **Fisher ZL**, **Gardner SM**, **Bartlett EL**. A computational model of inferior colliculus responses to amplitude modulated sounds in young and aged rats. *Front. Neural Circuits* 6: 77, 2012.

Rabinowitz NC, **Willmore BDB**, **King AJ**, **Schnupp JWH**. Constructing Noise-Invariant Representations of Sound in the Auditory Pathway. *PLoS Biol* 11: e1001710, 2013.

Ramachandran R, **Davis KA**, **May BJ**. Single-Unit Responses in the Inferior Colliculus of Decerebrate Cats I. Classification Based on Frequency Response Maps. *J. Neurophysiol.* 82: 152–163, 1999.

Ramachandran R, **Davis KA**, **May BJ**. Rate Representation of Tones in Noise in the Inferior Colliculus of Decerebrate Cats. *J. Assoc. Res. Otolaryngol.* 1: 144–160, 2000.

Rees A, **Møller AR**. Stimulus properties influencing the responses of inferior colliculus neurons to amplitude-modulated sounds. *Hear. Res.* 27: 129–143, 1987.

Rees A, **Palmer AR**. Rate□intensity functions and their modification by broadband noise for neurons in the guinea pig inferior colliculus. *J. Acoust. Soc. Am.* 83: 1488–1498, 1988.

Rhode WS, **Smith PH**. Characteristics of tone-pip response patterns in relationship to spontaneous rate in cat auditory nerve fibers. *Hear. Res.* 18: 159–168, 1985.

Rickards FW, **Clark GM**. Field potentials in cat auditory nuclei in response to frequency and amplitude modulated sound. In: *Proceedings of the Australian Physiological and Pharmacological Society*. 201, 1972.

Roberts LE, **Eggermont JJ**, **Caspary DM**, **Shore SE**, **Melcher JR**, **Kaltenbach JA**. Ringing Ears: The Neuroscience of Tinnitus. *J. Neurosci.* 30: 14972–14979, 2010.

Robertson D, **Bester C**, **Vogler D**, **Mulders WHAM**. Spontaneous hyperactivity in the auditory midbrain: Relationship to afferent input. *Hear. Res.* 295: 124–129, 2013.

Ropp T-JF, **Tiedemann KL**, **Young ED**, **May BJ**. Effects of Unilateral Acoustic Trauma on Tinnitus-Related Spontaneous Activity in the Inferior Colliculus. *J. Assoc. Res. Otolaryngol.* 15: 1007-1022, 2014.

Rouiller EM, **Cronin-Schreiber R**, **Fekete DM**, **Ryugo DK**. The central prod ections of intracellularly labeled auditory nerve fibers in cats: An analysis of terminal morphology. *J. Comp. Neurol.* 249: 261–278, 1986.

Ruggles D, **Bharadwaj H**, **Shinn-Cunningham BG**. Normal hearing is not enough to guarantee robust encoding of suprathreshold features important in everyday communication. *Proc. Natl. Acad. Sci.* 108: 15516–15521, 2011.

Rüttiger L, **Singer W**, **Panford-Walsh R**, **Matsumoto M**, **Lee SC**, **Zuccotti A**, **Zimmermann U**, **Jaumann M**, **Rohbock K**, **Xiong H**, **Knipper M**. The Reduced Cochlear Output and the Failure to Adapt the Central Auditory Response Causes Tinnitus in Noise Exposed Rats. *PLoS ONE* 8: e57247, 2013.

Sachs MB, **Abbas PJ**. Rate versus level functions for auditory-nerve fibers in cats: tone-burst stimuli. *J. Acoust. Soc. Am.* 56: 1835–1847, 1974.

Salvi RJ, **Saunders SS**, **Gratton MA**, **Arehole S**, **Powers N**. Enhanced evoked response amplitudes in the inferior colliculus of the chinchilla following acoustic trauma. *Hear. Res.* 50: 245–257, 1990.

Sanes DH, **Woolley SMN**. A Behavioral Framework to Guide Research on Central Auditory Development and Plasticity. *Neuron* 72: 912–929, 2011.

Saunders GH, **Haggard MP**. The clinical assessment of "Obscure Auditory Dysfunction" (OAD)

2. Case control analysis of determining factors. *Ear Hear.* 13: 241–254, 1992.

Sausbier U, **Sausbier M**, **Sailer CA**, **Arntz C**, **Knaus H-G**, **Neuhuber W**, **Ruth P**. Ca2+-activated K+ channels of the BK-type in the mouse brain. *Histochem. Cell Biol.* 125: 725–741, 2006.

Schaette R. Tinnitus in men, mice (as well as other rodents), and machines. *Hear. Res.* 311: 63–71, 2014.

Schaette R, **McAlpine D**. Tinnitus with a Normal Audiogram: Physiological Evidence for Hidden Hearing Loss and Computational Model. *J. Neurosci.* 31: 13452–13457, 2011.

Schmiedt RA, **Okamura H-O**, **Lang H**, **Schulte BA**. Ouabain application to the round window of the gerbil cochlea: A model of auditory neuropathy and apoptosis. *J. Assoc. Res. Otolaryngol.* 3: 223–233, 2002.

Schofield BR. Superior Olivary Complex and Lateral Lemniscal Connections of the Auditory Midbrain. In: *The Inferior Colliculus*, edited by Winer JA, Schreiner CE. Springer New York. 132–154, 2005.

Schuknecht HF, **Woellner RC**. An Experimental and Clinical Study of Deafness from Lesions of the Cochlear Nerve. *J. Laryngol. Otol.* 69: 75–97, 1955.

Schwaber MK, **Hall JW**. A simplified technique for transtympanic electrocochleography. *Am. J. Otol.* 11: 260–265, 1990.

Seki S, **Eggermont JJ**. Changes in spontaneous firing rate and neural synchrony in cat primary auditory cortex after localized tone-induced hearing loss. *Hear. Res.* 180: 28–38, 2003.

Seluakumaran K, **Mulders WHAM**, **Robertson D**. Unmasking effects of olivocochlear efferent activation on responses of inferior colliculus neurons. *Hear. Res.* 243: 35–46, 2008.

Sergeyenko Y, **Lall K**, **Liberman MC**, **Kujawa SG**. Age-Related Cochlear Synaptopathy: An Early-Onset Contributor to Auditory Functional Decline. *J. Neurosci.* 33: 13686–13694, 2013.

Shaheen LA, **Valero MD**, **Liberman MC**. Towards a Diagnosis of Cochlear Neuropathy with Envelope Following Responses. *J. Assoc. Res. Otolaryngol.* 16: 727–745, 2015.

Shannon RV, **Zeng FG**, **Kamath V**, **Wygonski J**, **Ekelid M**. Speech recognition with primarily temporal cues. *Science* 270: 303–304, 1995.

Shera CA, **Bergevin C**. Obtaining reliable phase-gradient delays from otoacoustic emission data. *J. Acoust. Soc. Am.* 132: 927–943, 2012.

Skinner LJ, **Enée V**, **Beurg M**, **Jung HH**, **Ryan AF**, **Hafidi A**, **Aran J-M**, **Dulon D**. Contribution of BK Ca2+-Activated K+ Channels to Auditory Neurotransmission in the Guinea Pig Cochlea. *J. Neurophysiol.* 90: 320–332, 2003.

Sroka JJ, **Braida LD**. Human and machine consonant recognition. *Speech Commun.* 45: 401–423, 2005.

Stamataki S, **Francis HW**, **Lehar M**, **May BJ**, **Ryugo DK**. Synaptic alterations at inner hair cells precede spiral ganglion cell loss in aging C57BL/6J mice. *Hear. Res.* 221: 104–118, 2006.

Stapells DR, **Makeig S**, **Galambos R**. Auditory steady-state responses: threshold prediction using phase coherence. *Electroencephalogr. Clin. Neurophysiol.* 67: 260–270, 1987.

Strait DL, **Kraus N**. Biological impact of auditory expertise across the life span: Musicians as a model of auditory learning. *Hear. Res.* 308: 109–121, 2014.

Strelcyk O, **Dau T**. Relations between frequency selectivity, temporal fine-structure processing, and speech reception in impaired hearing. *J. Acoust. Soc. Am.* 125: 3328–3345, 2009.

Suzuki J, **Corfas G**, **Liberman MC**. Round-window delivery of neurotrophin 3 regenerates cochlear synapses after acoustic overexposure. *Sci. Rep.* 6: 24907, 2016.

Taberner AM. Using knockout mice to study the molecular mechanisms that shape auditory nerve responses. Massachusetts Institute of Technology. 2005.

Taberner AM, **Liberman MC**. Response properties of single auditory nerve fibers in the mouse. *J. Neurophysiol.* 93: 557–569, 2005.

Torterolo P, **Falconi A**, **Morales-Cobas G**, **Velluti RA**. Inferior colliculus unitary activity in wakefulness, sleep and under barbiturates. *Brain Res.* 935: 9–15, 2002.

Tsuzuku T. 40-Hz Steady State Response in Awake Cats After Bilateral Chronic Lesions in Auditory Cortices or Inferior Colliculi. *Auris. Nasus. Larynx* 20: 263–274, 1993.

Turner JG, **Brozoski TJ**, **Bauer CA**, **Parrish JL**, **Myers K**, **Hughes LF**, **Caspary DM**. Gap detection deficits in rats with tinnitus: a potential novel screening tool. *Behav. Neurosci.* 120: 188–195, 2006.

Tziridis K, **Ahlf S**, **Jeschke M**, **Happel MFK**, **Ohl FW**, **Schulze H**. Noise trauma induced neural plasticity throughout the auditory system of Mongolian gerbils: differences between tinnitus developing and non-developing animals. *Neuro-Otol.* 6: 22, 2015.

Valero MD, **Hancock KE**, **Liberman MC**. The middle ear muscle reflex in the diagnosis of cochlear neuropathy. *Hear. Res.* 332: 29–38, 2016.

Viana LM, **O'Malley JT**, **Burgess BJ**, **Jones DD**, **Oliveira CACP**, **Santos F**, **Merchant SN**, **Liberman LD**, **Liberman MC**. Cochlear neuropathy in human presbycusis: Confocal analysis of hidden hearing loss in post-mortem tissue. *Hear. Res.* 327: 78–88, 2015.

Viemeister NF. Auditory intensity discrimination at high frequencies in the presence of noise. *Science* 221: 1206–1208, 1983.

Viemeister NF. Intensity coding and the dynamic range problem. *Hear. Res.* 34: 267–274, 1988.

Wan G, **Gómez-Casati ME**, **Gigliello AR**, **Liberman C**, **Corfas G**. Neurotrophin-3 regulates ribbon synapse density in the cochlea and induces synapse regeneration after acoustic trauma. *eLife* 3: e03564, 2014.

Wang J, **Salvi RJ**, **Powers N**. Plasticity of response properties of inferior colliculus neurons following acute cochlear damage. *J. Neurophysiol.* 75: 171–183, 1996.

Watkins PV, **Barbour DL**. Specialized neuronal adaptation for preserving input sensitivity. *Nat. Neurosci.* 11: 1259–1261, 2008.

Wen B, **Wang GI**, **Dean I**, **Delgutte B**. Dynamic Range Adaptation to Sound Level Statistics in the Auditory Nerve. *J. Neurosci.* 29: 13797–13808, 2009.

Wen B, **Wang GI**, **Dean I**, **Delgutte B**. Time course of dynamic range adaptation in the auditory nerve. *J. Neurophysiol.* 108: 69–82, 2012.

Wier CC, **Jesteadt W**, **Green DM**. Frequency discrimination as a function of frequency and sensation level. *J. Acoust. Soc. Am.* 61: 178–184, 1977.

Winslow RL, **Sachs MB**. Single-tone intensity discrimination based on auditory-nerve rate responses in backgrounds of quiet, noise, and with stimulation of the crossed olivocochlear bundle. *Hear. Res.* 35: 165–189, 1988.

Xie R, **Gittelman JX**, **Pollak GD**. Rethinking Tuning: In Vivo Whole-Cell Recordings of the Inferior Colliculus in Awake Bats. *J. Neurosci.* 27: 9469–9481, 2007.

Xiong XR, **Liang F**, **Li H**, **Mesik L**, **Zhang KK**, **Polley DB**, **Tao HW**, **Xiao Z**, **Zhang LI**. Interaural Level Difference-Dependent Gain Control and Synaptic Scaling Underlying Binaural Computation. *Neuron* 79: 738–753, 2013.

Yang L, **Pollak GD**, **Resler C**. GABAergic circuits sharpen tuning curves and modify response properties in the mustache bat inferior colliculus. *J. Neurophysiol.* 68: 1760–1774, 1992.

Ye Y, **Machado DG**, **Kim DO**. Projection of the marginal shell of the anteroventral cochlear nucleus to olivocochlear neurons in the cat. *J. Comp. Neurol.* 420: 127–138, 2000.

Young ED, **Barta PE**. Rate responses of auditory nerve fibers to tones in noise near masked threshold. *J. Acoust. Soc. Am.* 79: 426–442, 1986.

Yuan Y, **Shi F**, **Yin Y**, **Tong M**, **Lang H**, **Polley DB**, **Liberman MC**, **Edge ASB**. Ouabain-induced cochlear nerve degeneration: synaptic loss and plasticity in a mouse model of auditory neuropathy. *J. Assoc. Res. Otolaryngol.* 15: 31–43, 2014.

Zhu L, **Bharadwaj H**, **Xia J**, **Shinn-Cunningham B**. A comparison of spectral magnitude and phase-locking value analyses of the frequency-following response to complex tones. *J. Acoust. Soc. Am.* 134: 384–395, 2013.

Acknowledgments

The work of my thesis would not have been possible without the tremendous hearing science community of Boston.

First, I'd like to thank Charlie Liberman, who has provided constant, steady guidance through the whole PhD. I am grateful for the freedom he gave me to explore my own ideas, and for his support in developing those ideas into useful results. Charlie's work has a unique clarity and focus that is invaluable when exploring new research areas. This is especially true of his writing and public speaking, both of which have had a dramatic positive effect on my own communication abilities. I'd also like to thank members of the lab for fruitful discussions, help with experiments, and good camaraderie: Michelle Valero, Yanbo Yin, Stephané Maison, Lavinia Sheets, Tyler Hickman, Jun Suzuki, Leslie Liberman, and Ann Hickox.

My first research endeavors at EPL were done under the guidance of Bertrand Delgutte, who taught me how to plan an experiment and to make sense of the results. His keen wit was crucial in maturing my scientific thought process.

I'd like to thank the members of my committee: Bertrand Delgutte, Dan Polley, Jennifer Melcher, and Barbara Shinn-Cunningham for their valuable insights in both planning this research and in understanding the results. It was a true privilege to work with advisors that were experts in their fields, yet down-to earth and approachable.

I'd also like to recognize the many teachers I've had while at EPL. The teachers of the core classes did a tremendous job at giving us a thorough understanding of the speech and auditory systems. Further, I'd like to thank the many people that have taught me specific research techniques: Grace Wang, Yoojin Chung, Michael Slama, Mitch Day, Ann Hickox, Leslie Liberman, Wei Guo, and Ross Williamson. Each of these people taught me valuable skills that I will continue to use in future projects.

None of this work would have been possible without the help of the EPL technical community. I'm grateful to Evan Foss and Ishmael Stefanov-Wagner for their help creating mechanical and electrical hardware used to conduct this research. I'd also like to thank Ken Hancock, who created the data acquisition software, and tirelessly revised it as my needs changed. Ken was also a great resource for patient explanations of both technical and scientific concepts. And thanks to both Leslie Liberman and Michelle Valero for their expert work in cochlear micro-dissection and immunostaining. And finally, thanks to Dianna Sands and the EPL administrative staff for their support and good humor.

I'd like to thank the SHBT students for their friendship and support over the years, in particular my classmates: Jonathan Whitton, Jonathan Sellon, Golbarg Mehraei, David Chhan, and Samiya Alkhairy.

Finally, I'd like to thank my friends and family for their support. And of course, a huge thanks to my wife Michelle, who has been a constant source of both support and inspiration.

This work was supported by NIH grants R01 DC00188, P30 DC05209 and T32 DC00038, and the Amelia Peabody Charitable Fund.